Institut für Molekulare Mechanismen bei Krankheiten
der Vetsuisse-Fakultät Universität Zürich

Direktor: Prof. Dr. med. vet. et phil. II Michael Hottiger

Musculoskeletal Research Unit (MSRU)
Leiterin: Prof. Dr. med. vet. Brigitte von Rechenberg

Arbeit unter wissenschaftlicher Betreuung von
Dr. med. vet. Karina Klein, DVM-PhD, Musculoskeletal Research Unit (MSRU)

Variable Fixation Locking Screw (VFLS): Investigation of Bone Healing with a Device Intended to Optimize Strain and Micromotion for each Phase of Fracture Healing

Inaugural-Dissertation

zur Erlangung der Doktorwürde der
Vetsuisse-Fakultät Universität Zürich

vorgelegt von

Katrin Planzer

Tierärztin
von Bürglen UR, Schweiz

genehmigt auf Antrag von

Prof. Dr. med. vet. Brigitte von Rechenberg, Referentin

Prof. Dr. Stephen Ferguson, Korreferent

2019

Institut für Molekulare Mechanismen bei Krankheiten
der Vetsuisse-Fakultät Universität Zürich

Direktor: Prof. Dr. med. vet. et phil. II Michael Hottiger

Musculoskeletal Research Unit (MSRU)
Leiterin: Prof. Dr. med. vet. Brigitte von Rechenberg

Arbeit unter wissenschaftlicher Betreuung von
Dr. med. vet. Karina Klein, DVM-PhD, Musculoskeletal Research Unit (MSRU)

Variable Fixation Locking Screw (VFLS): Investigation of Bone Healing with a Device Intended to Optimize Strain and Micromotion for each Phase of Fracture Healing

Inaugural-Dissertation

zur Erlangung der Doktorwürde der
Vetsuisse-Fakultät Universität Zürich

vorgelegt von

Katrin Planzer

Tierärztin
von Bürglen UR, Schweiz

genehmigt auf Antrag von

Prof. Dr. med. vet. Brigitte von Rechenberg, Referentin

Prof. Dr. Stephen Ferguson, Korreferent

2019

den Schafen dieser Studie

Zusammenfassung

In dieser experimentellen Studie wurde die Frakturheilung bei interner Fixation mittels der „Variable Fixation Locking Screw“ (VFLS) evaluiert und mit der Lockingschraube (LS) von DePuy Synthes verglichen. Das Schraubendesign der VFLS ermöglicht eine Mikromotion nach 2-3 Wochen um die Knochenheilung zu stimulieren. Für den Versuch wurde ein Schafmodell mit einer Tibiaosteotomie (3 mm Defekt fixiert mit 6-Loch LCP) gewählt. Die operierten Beine der 12 Schafe wurden postoperativ geröntgt, gecastet und die Schafe wurden für 3 Wochen ins Netz gehängt. Danach folgten wöchentliche Röntgenaufnahmen und Castwechsel. Fluoreszenzfarbstoff wurde in Woche 3 und 6, sowie 48-72h vor der Schlachtung injiziert. Nach der Schlachtung wurden die Tibiae makroskopisch und radiologisch untersucht, sowie mittels µCT, biomechanischen Tests und Histologie analysiert. Die Resultate haben aufgezeigt, dass die VFLS eine biokompatible und sichere Schraube ist. Histologie- und Fluoreszenzergebnisse zeigten, dass die VFLS durch Micromotion ein starkes Remodeling über die ganze Tibia ausüben kann. Die VFLS wies signifikant mehr endostalen Kallus ($p=0.012$) zwischen dem 3. und 4. Schraubenloch auf. In den biomechanischen Tests erlangte die VFLS leicht bessere Ergebnisse. Es liegt die Vermutung nahe, dass die VFLS wegen des starken Remodelings bei Patienten mit einer Frakturheilungsstörung ein besseres Endergebnis erzielen könnte.

Summary

In this experimental study, fracture healing was evaluated by using the Variable Fixation Locking Screw (VFLS) and comparing it to the Locking Screw (LS) of DePuy Synthes. The special screw design of the VFLS allows micromotion after 2-3 weeks to stimulate bone healing. A standardized tibia osteotomy model in sheep (90°, 3mm fracture gap, fixed with 6-hole LCP) was selected for this study. The sheep were suspended for 3 weeks. Radiographs were performed post-surgery and weekly after three weeks in combination with cast changes. Fluorescent dyes were administered subcutaneously in week 3 and 6, as well as 48-72h prior to sacrifice. After sacrifice, a radiological and macroscopical examination as well as μCT, biomechanical testing and histology analysis was performed.

The results showed that the VFLS is a biocompatible and safe screw. Histological and fluorescence results showed that VFLS could provide a strong remodeling across the whole tibia due to its micro motion. The VFLS showed a significantly ($p=0.012$, histology) higher amount of endosteal callus between the 3rd and 4th screw hole. In the biomechanical tests, the VFLS performed slightly better.

The VFLS could achieve a better outcome in patients predisposed for fracture failure mainly due to the strong remodeling.

1 Introduction

1.1 Healthcare Expenditure

Osteosynthesis failure has a tremendous impact on healthcare expenditure per patient in all countries. Epidemiological data about delayed and non-unions in the literature vary from 1-6% of patients with long-bone fractures[1-4] to 5-15% of bone fractures as a whole[5]. SUVA (schweizerische Unfallversicherung) collects information about occurrence and treatment costs for fractures in Switzerland. The most expensive 10% of the cases are finally responsible for 63% of the total insurance costs[6]. Therefore, it is evident that any effort aiming at decreasing the average costs of treating the most expensive 10% patients, namely those patients with complications and comorbidities, would have a substantial impact on the average treatment costs.

Population ageing is taking place in nearly all countries of the world and the incidence of bone fractures is known to significantly increase after the middle of the lifespan[7]. By 2050 the number of persons aged 80 years or older will be more than three times higher than today[8]. Beside the normal effect of ageing on the bone tissue, the increasing incidence of conditions impairing bone healing like diabetes[9,10], obesity[11] and several other metabolic diseases significantly contributes to an already substantial problem[12].

1.2 Clinical problem

The significant problem beside infections and screws cut out is represented by patients with delayed unions (healing after 3 months according to FDA 1988) or non-unions (no union after 8-9 months according to FDA 1988)[13-16].

Clinicians identified potential risk factors that could be responsible for this failed fracture healing response. While patient related factors (genetics and systemic disorders), environment related factors (smoking, medication and alcohol), and injury related factors (trauma impact, soft tissue involvement) are given patient conditions, surgeons have an important influence on bone healing, defining the fracture treatment modalities through choosing the best implant, surgical technique and post-operative treatment[12].

The entire bone healing process is driven by gradual changes in the strain of the forming tissue and for each of the four phases of secondary fracture healing the ideal strain levels are slightly different[13,17]. Plates and screws that are used today, are not completely able to reproduce those changes in bone callus boundary conditions known

to activate the mechano-metabolic signals boosting fracture healing. In fact, current locking systems feature constant mechanical properties during the entire fracture treatment, thus providing a constant strain to the forming callus during the whole fracture healing period. If the allowed strain is not in the right range, the fracture will not properly heal.

1.3 Purpose of the study

The variable fixation locking screw (VFLS) is a medical device especially designed to take the different strain conditions into account, known to promote fracture healing during its different phases. A resorbable sleeve is fixed under the screw head in a position such that it is fully inserted in the cis cortex of a bone once implanted. Starting from very stable conditions, this sleeve progressively decreases its mechanical properties and dimensions. After an initial period of stability, the fixation of each implanted sleeve decreases, leading to a progressive increase in interfragmentary motion.

The primary goal of this study is to test the safety and efficacy of this new screw, especially developed to address the risk of delayed and non-unions.

The secondary goal is to compare the performances of this new device with respect to those of the standard locking screw (DePuy Synthes).

Finally, we aim at understanding if keeping the healing tissue in conditions known to promote its maturation has potential to boost the entire healing process. Our long-term goal is to allow a larger number of patients to return to their everyday life earlier and thus decrease the number of extremely expensive patients with complications.

2 Literature overview

2.1 Fracture healing

Fractures can heal in two ways: through primary/direct or secondary/indirect bone healing. Diaphyseal bone fractures often show secondary or indirect bone healing via an external callus, which assists as support for the stabilization of the fracture. This secondary bone healing includes four phases[18,19]:

2.1.1 Phase I: Inflammation

The inflammatory process starts immediately after fracture occurrence. It usually lasts one to seven days after a fracture occurred. Due to the rupture of blood vessels in the bone, periosteum and soft tissue, blood cells and inflammatory cells get into the fracture gap. Furthermore, a fracture hematoma develops. Within hours, an inflammatory cascade modulates the release of cytokines and growth factors. Furthermore, the cascade increases the vascularity through vasodilatation and hyperemia. Macrophages and neutrophils are stimulated to migrate and proliferate. Bone necrosis takes place at the fracture fragment (near the fracture gap) and is removed later by osteoclasts. During the building of the hematoma, a network of fibrin, reticulin and collagen fibrils slowly forms a granulation tissue. This granulation tissue slowly replaces the fracture hematoma and bridges the ends of the fracture.

2.1.2 Phase II: Soft callus formation

After one week, callus formation will start. The progenitor cells in the endosteum and periosteum play an important role. The differentiation from the progenitor cells to osteoblasts is stimulated by the mechano-construction of the fracture. Callus formation starts in the periphery (proximal and distal of the fracture gap) and moves towards the fracture line. Near the fracture gap, there are mesenchymal progenitor cells. They can differentiate into fibroblasts and produce fibrous tissue or they are also able to differentiate into chondrocytes and create cartilage. The fibrous tissue and cartilage replace the granulation tissues from phase I. Furthermore, vessels grow in and form the soft callus.

2.1.3 Phase III: Hard callus formation

Phase III starts when the soft callus of phase II links the fracture ends together. It takes 3-4 months until the soft callus is converted by endochondral ossification into an osseous callus (hard callus) or woven bone respectively.

2.1.4 Phase IV: Remodeling

Once the fracture gap is bridged by hard callus, the biomechanical load decreases and osteoclasts remove the woven bone. Lamellar bone replaces the woven bone by osteonal remodeling. This process could take between a few months and several years.

2.2 Interfragmentary strain and micromotion – the most important parameters

2.2.1 The interfragmentary strain

In the past few years in fracture bone healing research, scientists found out that for fracture healing it is important to not only consider fracture mobility (stability), since tissue deformation (namely strain) is as important as fracture mobility[20]. Perren et al. summarized 50 years of research on fracture healing, stating that biomechanical conditions are the basics for every fracture healing. Furthermore, every fracture healing success depends on a huge range of biomechanical conditions. Comparing different clinical and experimental cases, they conclude that the mobility of a fracture may not be the main reason that determines the outcome[20,21]. They propose thinking of strain and not only considering fracture mobility, respectively stability like many researchers did before[22-24]. The theory of strain helps to understand the fracture healing and to improve the treatment, because biomechanical stimuli are the inductors in the fracture healing[20].
The entire bone healing process is driven by gradual changes in the strain of the forming tissue and for each of the four phases of secondary fracture healing the ideal strain levels are slightly different[17]. Liu et al concluded that during the early phases of fracture repair a loading (respectively strain) might impede stabilization, whereas loading during the matrix deposition and remodeling phase promotes cartilage formation and bone formation, which enhances the fracture stabilization. An early loading during the inflammatory phase will delay the clearance of the hematoma and bone matrix deposition. In summary, they concluded that loading in early stages of fracture healing can lead the osteochondroprogenitor cells to a cartilage phenotype, whereas loading during the bone matrix formation phase pushes the osteochondroprogenitor cells to a

bone phenotype[17]. In other studies, where the dependence on strain rate and timing was examined, this theory was confirmed[25,26]. In clinical observations, Lujan et al. confirmed this theory too, noticing an asymmetric and inconsistent callus formation in patients treated for distal femoral fractures using locking plates. Apparently, the callus formation was inhibited at the cis cortex but well supported at the trans cortex. The interfragmentary movement is more pronounced far from the plate (trans cortex) when using locking plates. This situation confirms that different strain levels can promote or inhibit fracture-healing[13]. The interfragmentary movement generates a strain on the healing tissue in every phase of fracture healing[27]. Perren et al. defined strain as follows in an article in 1979: "The Strain (ε, %) is defined as the ratio of the fragment relative motion (d" = displacement, mm) to the original gap (G = gap width, mm) between the bone fragments"[28].

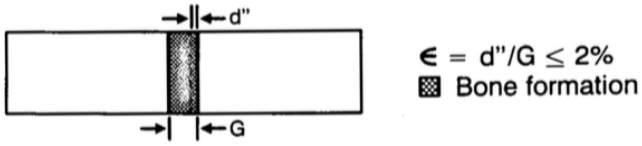

Fig. 2.1: The Strain is the displacement of the fragments (d") divided through the gap width (G)[29].

The strain is dependent on the distance of the fracture ends respectively the size of the fracture gap (G). If the size of the original gap (G) gets larger, the strain gets smaller as "the strain is inversely proportional to the size of the fracture gap (G)"[28,29]. Despite the fact that defining absolute values is often very challenging in biology, currently researcher think that when the strain is lower than 2% and the bone fragments are not in contact, fracture healing doesn't occur (non-union). When it is less than 2% (absolute stability) and the ends of the bone segments are well in contact, primary bone healing is stimulated. When strain is kept between 2% and 10% (relative stability) secondary bone healing can develop but closer to the extremes of this range fracture healing is delayed. When strain is over 10% the formation of the tissue cannot start and the mineralization process cannot be completed. The callus permanently organizes itself as fibrocartilaginous tissue (pseudo arthrosis)[30].

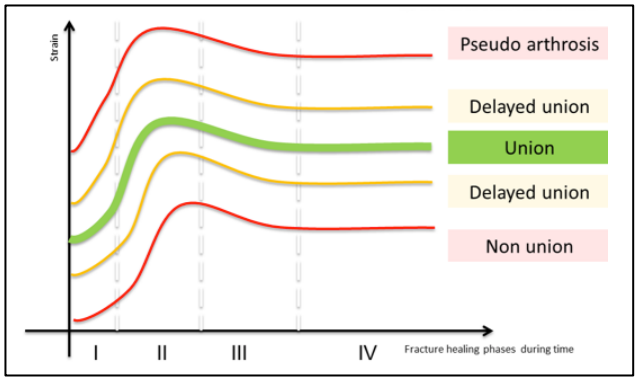

Fig. 2.2: Studies have shown that each phase of fracture healing requires a different level of strain to bring the fracture healing to the next phase (source: Biomech Innovations AG).

2.2.2 Micromotion or Interfragmentary Movement (IFM)

Secondary bone healing is stimulated by micromotion in the millimeter range[31-33]. Callus formation occurs in a given range of interfragmentary instability. The interfragmentary movement (IFM) is needed to give the cells the necessary strain. The cell reacts to an alteration in biomechanical environment like IFM respectively strain. This results in an increased proliferation rate and matrix synthesis. If the IFM is in a physiological tolerance range, the callus formation is faster[20,34]. The ideal size of the IFM is a range between the minimum, which induces callus formation and the maximum, which induces a bony bridging. In one study of Hente et al, it was discovered that a gap width of 2 mm and a daily compression respectively distraction of 1 mm on one fracture side for over two weeks induces bending stiffness[35]. IFM of 0.2-1 mm boosts bone fracture healing[36]. In a study with four different groups of IFM (0.0, 0.2, 0.4, 0.8 mm) they found out, that the best IFM is 0.4 mm, but without significance[32,37]. Axial motion, bending, torsional and translational shears together result in the IFM. Axial stiffness plus shear stiffness together improve the fracture healing, whereas translational shear movement leads to delayed or non-union[34].

In summary, depending on the strain, which is given through the IFM, the cells in the callus behave differently. A very low strain or no strain does not stimulate the cells enough to produce callus, and then a non-union occurs. If the range of strain is adequate, meaning an optimal fracture mobility and gap width, the cells produce a nice callus and they can remodel and calcify that callus. High strain condition leads the cells to deposit fibrocartilage only, which results in pseudoarthrosis[20,21].

What was found out so far?

More and more scientists reported that with less rigid implants a better secondary bone healing was visible. 1985 Goodship et al. was convinced that the micromotion created by less rigid implants, boosts fracture healing without losing the advantages of locking plates[31]. In 1991 Kenwright and Goodship published a study with external skeletal fixation, where they found out that clinical and mechanical healing were enhanced in groups with micromovement[38]. Titanium plates are more flexible than stainless steel plates and enhance callus formation[13].

Gardner et al. showed us in 2009 how the surgeon could decrease the risk of fixation failure with a simple modification. They proposed to mill bigger slots than needed in the cis cortex. With a bigger slot than necessary the screw shaft is able to move and reduce the axial stiffness. Their experiments showed that reducing the axial stiffness has no influence on the fixation stability, since there was no implant failure[39]. Stoffel et al suggested omitting screw holes to boost the flexibility of the plate. By omitting one or two screws per fracture fragment respectively, spontaneous fracture healing should occur faster. They found a second option for decreasing the construct stability by increasing the bone to plate space by 4 mm (from 2 mm to 6 mm)[40].

2.3 Medical Devices

Non-operative treatments include the usage of external bone stimulation devices like ultrasonic, pulsed electric magnetic field (PEMF), and combined magnetic field (CMF) stimulators[41,42].

Operative treatments include performing an additional surgery with new implantable devices aiming at slightly destabilizing the bone fragments hoping to gain callus bridging and/or the use of bone grafts and bone morphogenetic proteins in combination with different fixation techniques[43-45]. In any case, the occurrence of delayed and non-healing significantly prolongs the treatment duration and exposes patients to the onset of comorbidities. Therefore, it is all the more important to have good devices on the market that promote bone healing.

2.3.1 Standard LS

Fig. 2.3: The 5 mm standard locking screw from DePuy Synthes with its typical locked screw head[46].

The standard locking screw (LS) self-tapping (self-drilling also possible) has a very fine thread in the screw head compared to the conventional screw. This fine thread locks into the screw hole of the locking plate. The locking plate with the LS is also called internal fixator. The rigid construct consisting of screw hole and screw head takes over all loads, so that no pressure is exerted on the periosteum compared to conventional plates, which is better for the blood supply. Furthermore, when pulling out the locking plate, the thread of the LS works evenly in all of the LS and is firmly anchored, which is not the case using the conventional screw[46,47].

2.3.2 DLS (Dynamic Locking Screw)

Fig. 2.4: The DLS consist of two parts, a shell and a pin which allows micromotion and is connected to the locking head[48].

The DePuy Synthes DLS is a hollow threaded shell hosting a locking head welded pin having a maximum of 0.2 mm motion to displace. The DLS claims to allow modulating the rigidity of the locking plate. The load distribution will be better and the fracture site motion will be nearly parallel. This factors should boost fracture bone healing[48,49].

Döbele et al found out, that with this special design the axial stiffness is reduced and thus the IFM increased significantly, without losing the benefits of the locking plate like angular stability and strength[50]. The study by Richter et al showed that fractures treated with DLS had greater uniform callus formation and a significantly higher callus amount on the cis cortex. In addition, DLS performed better than LS in the biomechanical test[51].

In the year 2015 the FDA (U. S. Food and Drug Administration) recalled the DLS because of „pin breakage during planned implant removal, after uneventful and successful healing of the fracture“[52].

2.3.3 FCL (Far Cortical Locking) Screw / Zimmer® MotionLoc® Screw

Fig. 2.5: FCL or MotionLoc® Screw has a cortical thread which is anchored in the far cortices, therefore the middle part with the reserve cutting thread is able to move[53].

The Far Cortical Locking Screw (FCL) or MotionLoc® (designed from Zimmer®) is a screw with a trans cortical thread which anchors into the far cortices or trans cortex of a diaphysis respectively. The proximal shaft is smooth and smaller compared to the distal part. This threadless part of the screw allows some micromotion while the screw head and the trans cortical thread are anchored. The middle distal part has a reverse cutting thread for a problemless implant removal[53].

Bottlang et al proved in different studies that the FCL formed more callus through the flexible fixation, the reduced stiffness and the IFM respectively[54,55]. In addition, the FCL performed better compared to the LS in biomechanical tests[55].

2.3.4 VFLS (Variable Fixation Locking Screw)

Fig. 2.6: The VFLS (Variable Fixation Locking Screw) has a degradable sleeve (white) around the non-degradable core. The sleeve has a well-tuned degradation profile and allows a decrease of the construct stiffness and IFM. The distal portion of the screw is designed to purchase into the cortical bone; the head of the screw can be fully constrained in the locking plate hole; between the distal portion and the sleeve, the screw features forward and backward cutting flutes allowing insertion and removal of the screw.

The VFLS by Biomech Innovations AG is a standard metallic locking screw featuring biologically degradable materials fixed on the shaft of the screw. A well-tuned degradation profile of the sleeve material allows for gaining a controlled decrease in the resistance to compression perpendicular to the screw major axis offered by the proximal portion of the screw. The sleeve provides thus an important key: variability in fixation over time. Variable fixation means that the strain during the fracture-healing phase is variable. In the first healing phase (up to approximately three weeks) the sleeve is still present and does not reduce the stiffness of the plate and therefore does not induce micromotion. This gradual decrease in mechanical properties aims at driving bone healing causing a progressive and controlled increase in the strain provided to the healing tissue. Hereafter a pictorial explanation on the function provided by the combination of materials during the fracture healing period (source: Biomech Innovations AG).

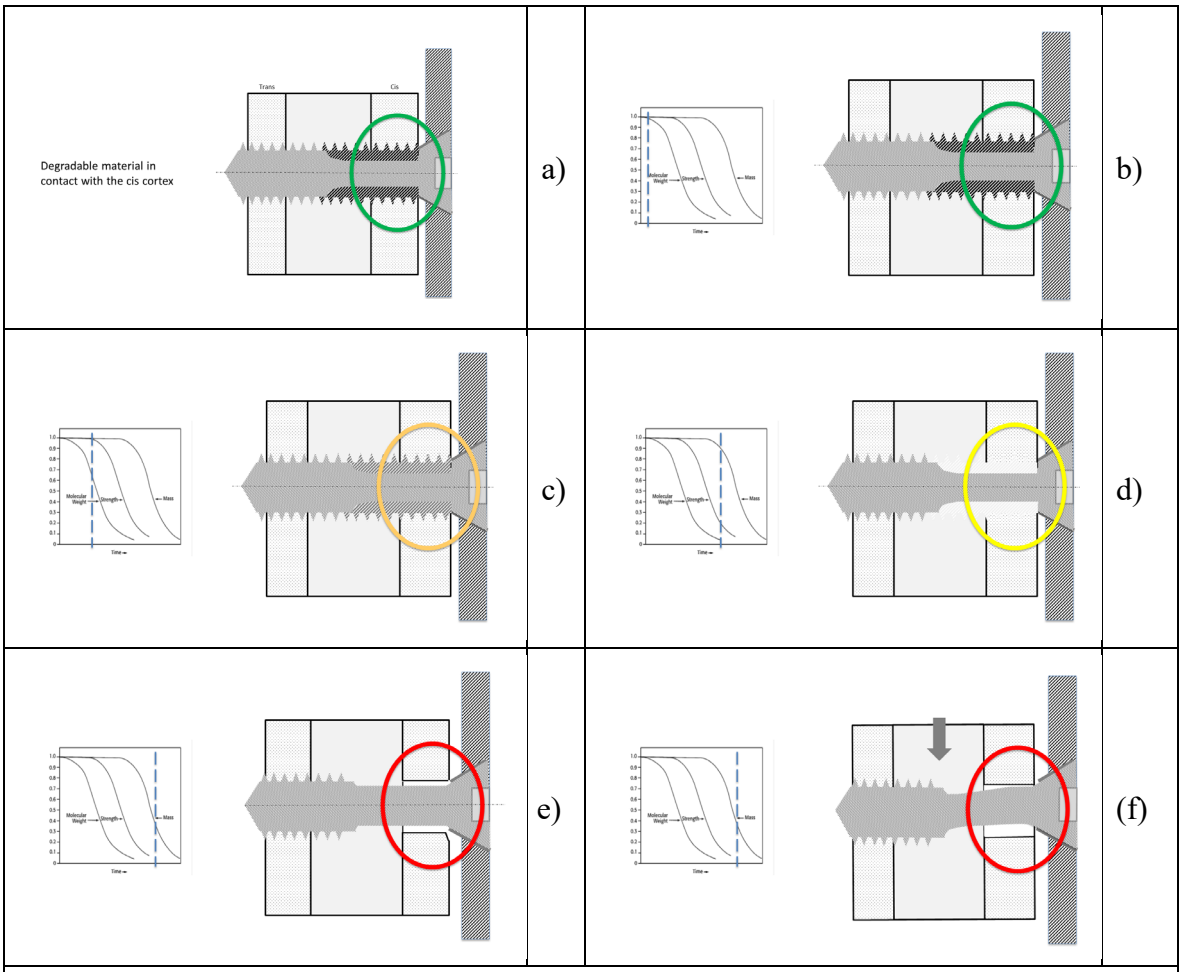

Fig. 2.7: When implanted, the metallic portion of the cortical VFLS purchases in the trans cortex while the degradable part is in direct contact with the cis cortex (a). At the beginning of the treatment the mechanical properties of the degradable material are at their maximum, providing the required high degree of stability. As time goes by the mechanical properties of the degradable sleeve start progressively (c) decreasing (d). The resistance to compression offered by the sleeve decreases with time in unloading (e) and loading conditions (f).

In comparison to the Standard locking screw and MotionLoc® screw, the VFLS has a variable strain magnitude and not a constant strain. The VFLS is developed using the strain levels provided by the medical device already on the market as predicate "maximum and minimum boundary" conditions. Namely the stiffness of the standard locking screw is the reference for the initial condition, phase I of fracture healing (higher stiffness = lower strain, boundary condition "minimum"). This has been chosen because it is known that the resorbing hematoma and the forming tissue need a relatively low level of strain to allow the healing process to proceed to the following phase. On the other side, the stiffness of the DLS and FCL/MotionLoc® Screw is the reference for phase II of fracture healing (lower stiffness = higher strain, boundary condition "maximum"). This has been chosen because experimental work has proven that the additional strain provided by these screws promotes callus formation[50,51].

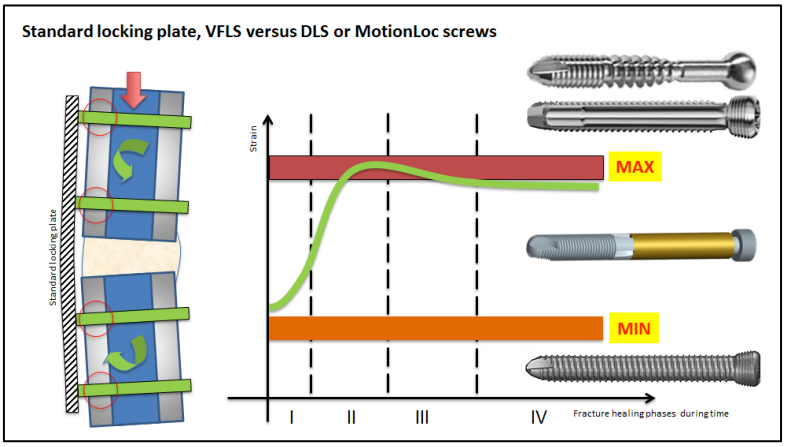

Fig. 2.8: Pictorial example showing the reference minimum and maximum boundary conditions used to develop the VFLS. In this picture the expected differential boosting effect provided by the VFLS can be appreciated in phase II. A maximum constant strain level is given by the DLS and by the MotionLoc® and a minimum constant strain level by the Locking Screw (source: Biomech Innovations AG).

2.4 Animal as human model

The functionality of the VFLS is evaluated in a large animal model. Observation of defect healing simulating a fracture gap in such an animal model is mandatory to evaluate the safety and efficacy of the proposed method prior to application in humans. Sheep represent a well-proven animal model featuring bone size and body weight comparable to humans[51,55-57]. The size of the animals means that the same instruments and implants can be implanted as for human subjects receiving clinical treatment[58]. Furthermore, bone mineral composition does not significantly differ between humans and sheep[59]. Although it has been observed that some animals regenerate bone better than humans, the sheep's ability to do so appears comparable to humans[58,60]. The results obtained from sheep experimentation can be extrapolated to humans without further testing on other animals. Sheep bred for experimental purposes are not available to our knowledge. Therefore local, mature, female Swiss Alpine sheep, similar in weight and size were used.

3 Materials and Methods

3.1 Structure of the Study

3.1.1 Study design and experimental animals

For this study, 14 (12 + 2 reserve) adult female Swiss alpine sheep with a mean age of 35.4 months (29-36 months) and a mean body weight of 75.8 kg (70.3-83.5 kg) were used (see appendix, page 65, Tab. 7.1). All animal experiments were conducted at the Musculoskeletal Research Unit (MSRU), Winterthurerstrasse 260, 8057 Zurich, Switzerland according to the Swiss laws of animal protection and welfare (Tierschutzverordnung / Tierschutzgesetz, 455). The planned experiment was authorized by the cantonal ethical committee (license no ZH 071/17).

Using a transverse tibia osteotomy model in sheep with internal fixation and a 3 mm interfragmentary gap, internal fixation was achieved using a locking compression plate and two different types of locking screws were compared. One set of screws was standard locking screws (Reference Item, RI) and the other set newly coated locking screws (Test Item, TI). After surgery, the operated limbs of all animals were casted and the animals were kept in suspension during the first 3 weeks after surgery. Cast changes and radiographs in three projections were performed weekly beginning in week 3 until sacrifice. After 9 weeks of follow up, the sheep were sacrificed. After sacrifice of the animals, fracture healing was tested radiologically, biomechanically and histologically. All animals were randomly selected and allocated to the treatment groups during the acclimatization period. Fig. 3.1 and Tab. 3.1 give a short overview of the in-life phase and study design:

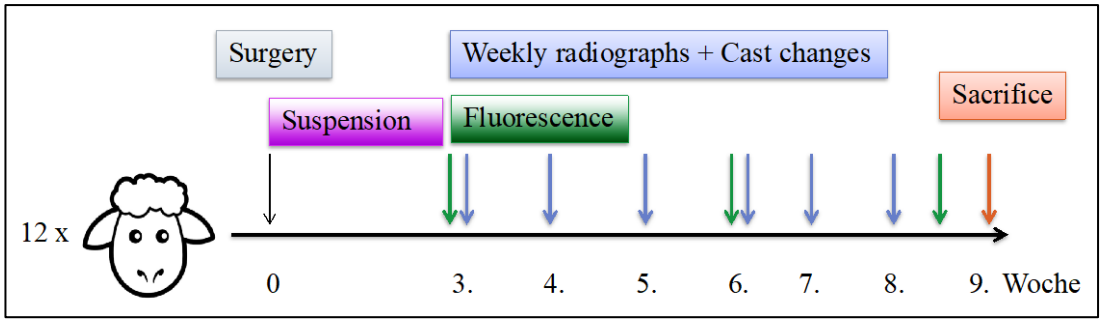

Fig. 3.1: Short overview of the in-life phase

Analysis	Purpose	Time points
CT evaluation	Status quo after surgery of bone volume density using a clinical CT scanner, as well as after sacrifice using a µCT scanner.	Post OP under anesthesia as CT, after sacrifice as µCT
Radiographic evaluation	Radiologic healing was studied focusing on callus of the cis- and trans cortex as well as bone marrow over time. Radiographs of the osteotomies were taken at different angles to allow better visualization of the callus formation at the cis cortex.	Post op, weekly beginning at week 3 till sacrifice
Fluorescence labeling	Determination of new bone formation in the fracture gap at different time points by means of fluorescence marker injection	3w. post OP: calcein green 6w. post OP: xylenol orange 48h prior to sacrifice: oxytetracycline
Macroscopical examination at sacrifice	Local draining lymph nodes were collected and callus formation, mechanical stability and inflammation were documented	At sacrifice
Biomechanical testing post mortem	Destructive methods for testing of torsional stiffness and energy to failure	Immediately after sacrifice
Histology of undecalcified bone samples	Evaluation was performed qualitatively (for type of bone healing, predominant cell types, vessel formation) and quantitatively (histomorphometrical analysis for percentage of new bone)	After sacrifice

Tab. 3.1: Overview of the study design

3.2 Characterization of Devices

Test Items (TI) and Reference Items (RI) were stored at room temperature, under monitoring of temperature and humidity. RI's were cleaned and sterilized according to routine while TI's were delivered sterile double packed.

3.2.1 Characterization of Test Item (TI) and Reference Item (RI)

As TI, a 5 mm variable fixation locking screw (VFLS, Biomech Innovations AG, Aarbergstrasse, Nidau, Schweiz) with a length of 32-34 mm length was used. The VFLS is a standard metallic locking screw featuring biologically degradable materials fixed on the shaft of the screw. An optimal degradation profile of the sleeve material allows for gaining a controlled decrease in the resistance to compression perpendicular to the screw axis offered by the proximal portion of the screw. The sleeve thus provides an important key: variability in fixation over time. This gradual decrease in mechanical

properties aims at driving bone healing causing a progressive and controlled increase in the strain provided to the healing tissue.

The TI's were delivered in single sterile packages. Drill sleeves were cleaned and sterilized according to routine.

The RI consisted of a standard 5 mm locking screw with hexagonal drive self-tapping (TAN 413.332 + 413.334: 32 mm and 34 mm length, titan, DePuy Synthes).

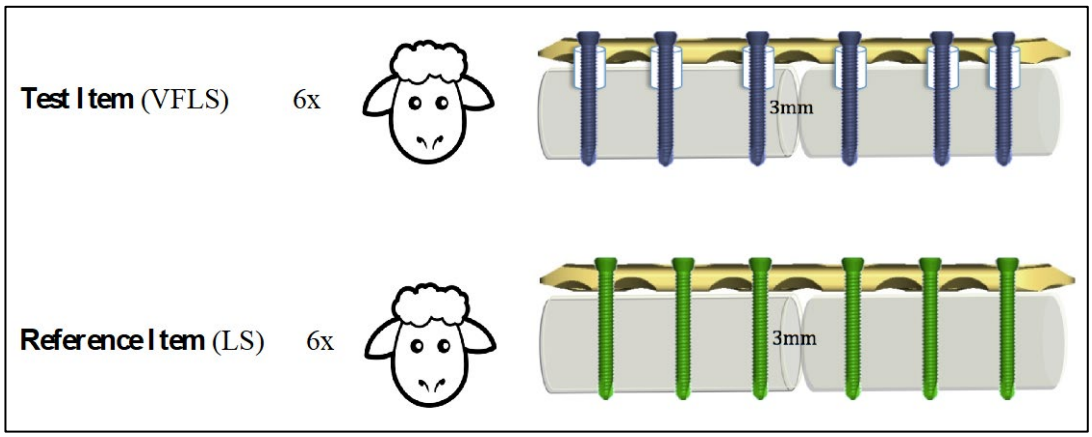

Fig. 3.2: The TI group with the VFLS and the RI group with the LS, N=6 for each group.

3.3 Animal Management

The experimental animals (white Swiss Alpine Sheep) were brought to the MSRU stables at least seven days prior to surgery. The animal management contained vaccination against pasteurella and clostridia and deworming according to standard operation procedures.

The exact room number was documented in the raw data. At the day of arrival of the animals, a standardized health check was performed using a physical examination form. During the acclimatization period the weight was recorded once, and every animal received a blood screening (haematology and chemistry). Only healthy sheep without any signs of illness and normal blood results were included in this study. Food was withdrawn 24 h before induction of anesthesia, while water was available ad libitum.

3.3.1 Animal Identification

All the animals were labelled with an eartag (Allflex®) and a subcutaneous transponder (DATAMARS®, Datamars AG, Via ai Prati 6930 Bedano, Switzerland) on the left side of the neck.

3.3.2 Anesthesia

After 24 hours of fasting and 30 minutes prior to induction of anesthesia, the animals were premedicated with buprenorphine (0.01 mg/kg BW im, Temgesic®, Reckitt Benckiser AG, Wallisellen, Schweiz) and xylazine (0.1 mg/kg BW im, Xylazin Streuli ad us. vet., Streuli Pharma AG, Uznach, Schweiz). A catheter was placed into the jugular vein and prophylactic antibiotics (penicillin 30'000 IU/kg BW iv, Penicillin natrium Streuli ad us vet, Streuli Pharma AG, Uznach, Schweiz; gentamicin 4 mg/kg BW iv, Vetagent® ad us. vet., MSTD Animal Health GmbH, Luzern, Schweiz), as well as a pre-emptive analgesic drug, carprofen (4 mg/kg BW iv, Rimadyl®, Zoetis Schweiz GmbH, Zürich) were given intravenously. A booster against tetanus (3'000 IU/sheep sc, Tetanus Serum Intervet, MSTD Animal Health GmbH, Luzern) was administered subcutaneously.

Anesthesia was induced with midazolam (0.1 mg/kg BW iv, Midazolam Sintetica, Sintetica AG, Mendrisio, Schweiz), ketamine (3-5 mg/kg BW iv, Ketanarkon® 100 ad us. vet., Streuli Pharma AG, Uznach, Schweiz) and propofol (0.4-0.6 mg/kg BW iv, or more if needed, Propofol 1% MCT Fresenius, Fresenius Kabi AG, Oberdorf, Schweiz), the latter administered to effect. After laryngeal desensitization with lidocaine spray, the trachea was intubated, and correct placement was confirmed by expired carbon dioxide monitoring (FetCO2). Anesthesia was maintained with a balanced anesthetic protocol employing the administration of isoflurane (1%–3%, Attane™, Isoflurane ad us. vet., Provet AG, Lyssach, Schweiz) in oxygen via an adult F-circuit, a variable rate infusion of propofol (0.5–1 mg/kg/h) and ketamine (20-50 µg/kg/h).

Monitoring parameters included: electrocardiogram (ECG), heart rate, pulse rate and invasively measured blood pressures (systolic, mean and diastolic arterial) via an arterial catheter in an auricular artery. Furthermore, inspired and expired concentrations of carbon dioxide, oxygen and isoflurane, as well as esophageal temperature and saturation of arterial blood (SpO2) were monitored. All parameters were constantly measured and recorded in 10-minute intervals. Intraoperatively, Ringer's lactate solution was administered at a rate of 5-10 mL/kg/h.

3.4 Surgery

3.4.1 Surgical procedure

Anesthetized sheep were placed in lateral recumbency with the upper limb in flexion, retracted craniodorsally and fixed to the surgery table. The lower limb was exposed on its medial side up to above the stifle joint. The limb was firmly supported through an inflatable tablemat routinely used during surgeries.

The entire limb was clipped prior to surgery and the surgical site scrubbed and cleansed according to surgical routine with the limb in suspension. The animal was draped according to routine with the limb draped separately, such that it could be moved during surgery without violating sterility.

An approximately 15 cm incision was performed at the medial aspect of the tibia shaft extending from 1 cm above the tarsus to the metaphysis of the proximal tibia (see annex Fig. 7.1, page 77, picture 1). Bleeding was controlled with electrocautery. Soft tissue and fascia were incised and dissected down to the bone. At the proximal end of the tibia, the muscles at the caudal aspect were slightly incised at their insertion to the bone and retracted caudally exposing the full tibia shaft (see annex Fig. 7.1, picture 2).

A broad 6-hole 5 mm locking compression plate (DePuy Synthes 426.561 LCP 4.5/5.0, broad, 6 holes, length 115.8 mm, width 17.5mm, height 6 mm, Titanium alloy) was adapted to the medial aspect of the tibia shaft with the most distal hole about 1.5-2 cm above the tibiotarsal joint. The plate was slightly contoured to fit the tibial shaft. A specially developed cutting guide, with four rubber rings (O-Ring VMQ 13 x 2 mm, Angst+Pfister, Embrach) in place (two proximal, two distal), was temporarily fixed to the bone using Kirschner wires (2.0 mm; DePuy Synthes 292.000.201) at both ends (see annex Fig. 7.1, picture 3). In addition, the usage of the drill sleeve spacer (Biomech Innovations i100010N) served to keep a bone to plate distance. Using 3.2 mm LCP drill guides (DePuy Synthes 324.176) and a 3.2 mm LCP drill, the cutting guide was temporarily fixed to the intact tibia with four monocortical 4 mm diameter screws (L16-18 mm, steel, DePuy Synthes 02.204.016-18, two proximal and two distal, starting with screw position 1 and 6, thereafter 2 and 5) (see annex Fig. 7.1, picture 4).

An oscillating saw (DePuy Synthes, saw blade 519.150, 70/49*14*0.6/0.4 mm) was used to perform the osteotomy through the guiding slots under constant irrigation with 0.9% saline solution (see annex Fig. 7.1, picture 5). After removal of the template, the fragments were repositioned and fixed with the six-hole LCP, utilizing the 3 mm

distance holder to ensure a standardized parallel gap (see annex Fig. 7.1, picture 6). The already drilled holes were fixed again using the monocortical screws starting with screw position 2 and 5 followed by 1 and 6 (see annex Fig. 7.1, picture 7). Afterwards screw positions 3 and 4 were drilled using the 5 mm drill sleeve with a 4.3 mm drill bicortically (see annex Fig. 7.1, picture 8). Afterwards the monocortical screws were removed and replaced by 5 mm bicortical screws (see annex Fig. 7.1, picture 9). All six drill holes were made using a 4.3 mm drill bit, and 5.0 mm bicortical screws (either TI or RI) were implanted in the order: 2, 5, 1, 6. Screws were locked to the plate using a 4 Nm torque-limited screwdriver. After fixation of the plate, the rubber rings were cut, stretched, and removed, with protection of the periosteum. The 3 mm distance holder was removed (see annex Fig. 7.1, picture 10). Routine closure of the fascia and subcutaneous tissue was performed using resorbable suture material (vicryl® 2-0) (see annex Fig. 7.1, picture 11), and the skin was closed using a continuous suture technique with non-resorbable suture material (supramid® 2-0) (see annex Fig. 7.1, picture 12). See also Fig. 7.2 and Fig. 7.3 surgery protocol in the appendix, page 78.

3.5 Postoperative Management

3.5.1 Diagnostic imaging

The still anesthetized sheep was brought to the large animal CT (Somatom Sensation open, Siemens Medical Solutions, Erlangen, Deutschland, Syngo CT 2009E, 08872017, serial number: 494434, received: 2005) and a CT scan of the treated tibia was performed. After the CT scan, radiographs were taken in mediolateral (270°) and anteroposterior (0°) directions to confirm correct implantation.

Starting three weeks post-surgery, radiographs were taken weekly in three different projections until sacrifice: anteroposterior (0°) and two angled planes: anterolateral (275°) and posterolateral (265°) (see appendix, page 80, Fig. 7.6). The radiographs were made with a digital radiographic plate (FDR D-Evo II D35, Fujifilm (Switzerland) AG, Dielsdorf, Switzerland, serial number: 67151100, Received: 14.10.2017) in combination with a portable x-ray apparatus (Orange 8016HF, inserted x-ray tube: Model: Superior SXR-80-14/10P, Focal spot 1.0 mm x 1.0 mm, Raymed Imaging AG, medical x-ray, Düdingen, Switzerland).

3.5.2 Cast and suspension system

After radiographic examination, a cast (including stifle joint and claws) was applied at the operated limb, and full weight bearing while standing was allowed immediately after surgery. However, in order to decrease the risk of postoperative tibia fractures, each sheep was kept in a suspension system for three weeks after surgery. This system allows the animal all physiological functions full weight bearing while standing and to rest far from the ground.

Starting three weeks post-surgery, weekly cast changes were performed in combination with radiographic imaging.

3.5.3 Medication

3.5.3.1 Peri-, intra- and postoperative routine analgesia

Buprenorphine (0.01 mg/kg BW, im Temgesic®, Reckitt Benckiser AG, Wallisellen, Schweiz) was applied as pre-emptive analgesia and additional sedative 30 minutes before induction of anesthesia and every 4-6 hours after recovery on the day of surgery and as deemed necessary for up to three days after surgery depending on pain assessment.

Carprofen (4 mg/kg BW, SID, iv Rimadyl®, Zoetis Schweiz GmbH, Zürich) was given as pre-emptive analgesia prior to induction of anesthesia and for five days after surgery depending on pain assessment.

For cast changes and radiographic examination two sheep (84.07 and 84.14) had to be sedated with medetomidine (0.02 mg/kg BW, im Medetor®, Virbac AG, Opfikon, Schweiz). After the procedure the antidote atipamezol (2/3 of the given medetomidine, im Revertor®, Virbac AG, Opfikon, Schweiz) was given.

3.5.3.2 Prophylactic antibiotic therapy

Prophylactic antibiotic therapy was administered for five days starting on the day of surgery: penicillin (30’000 IU/kg BW, BID, iv, Penicillin natrium Streuli ad us vet, Streuli Pharma AG, Uznach, Schweiz)) and gentamycin (4 mg/kg/BW, SID, iv, Vetagent® ad us. vet., MSTD Animal Health GmbH, Luzern, Schweiz).

Tetanus serum (3’000 IU/sheep sc, Tetanus Serum Intervet, MSTD Animal Health GmbH, Luzern) was given on the day of surgery.

3.5.4 Fluorescence dyes

The fluorescence dyes were freshly prepared in our laboratory. The fluorescence dyes were injected at different time points post surgery to document new bone deposition and remodeling during the early stages of healing:

3 weeks post-surgery:	calcein green; 5 mg/kg BW, sc
6 weeks post-surgery:	xylenol orange; 90 mg/kg BW, sc
48-72 h prior to sacrifice:	oxytetracycline, 20 mg/kg BW, sc

All three fluorescence dyes were injected in four different application regions to have maximally 20 ml in one region.

3.6 In-life observations and examinations

Using standardized protocols, veterinarians, veterinary engineers and specially trained animal caretakers under supervision performed all in-life observations and examinations of the animals. Medical records were kept for each animal and the observations like general health check at acquisition, blood examination, body weight, anesthesia health check and clinical signs were recorded.

At the day of surgery (before and after sedation), a general health check of cardiovascular and respiratory function of every animal was performed prior to induction of anesthesia. Moreover, the sheep received a labelled ear tag and a subcutaneous transponder for identification purposes.

The postoperative recovery period lasted two hours starting at the end of surgery. During which time, all sheep were observed intensely. Afterwards they were observed routinely twice a day.

They were housed in the MSRU stables (room numbers were documented in the raw data) during the whole experimental period. Group housing was in pens with at least 1.2 square meters for each animal. The animals were monitored for clinical signs of pain and discomfort including cast checks twice daily. Hay and mineral supplements were provided ad libitum. Representative diet samples were routinely analyzed for contaminants and results listed in the raw data.

Before every cast change, the animals were fasted for at least 18-24 hours to prevent bloating.

Environmental conditions were continuously monitored using a data logger for temperature and humidity (temperature range 10-35 °C, relative humidity range 10-95%). There was daylight cycle.

3.7 Post-mortem sample preparation

3.7.1 Tissue harvest after sacrifice

After 9 weeks, the animals were sacrificed and both hind limbs were immediately harvested. The non-operated tibiae were cleaned from surrounding tissue and put in a plastic bag labeled with the sheep number and ‘left’ or ‘right’.

Radiographs of the threated tibia were performed with the digital radiographic plate in the same three projections as during the in-life phase for evaluation of the healing process, hardware failures and/or screw loosening.

Local draining lymph nodes (lnn. poplitei and inguinales) were macroscopically examined and changes of lymph nodes like size, color, consistency and any other observations were recorded. The lymph nodes were collected and fixed in 4% formalin solution for histological evaluation.

Both tibiae were cleansed from surrounding tissue and macroscopic examination of the whole tibia, implantation sites and surrounding tissue was conducted (see appendix, page 79, Fig. 7.4 and Fig. 7.5). For representative implant-related macroscopic findings additional photographs were taken of the ROI with and without plate.

The macroscopic examination included the control of screw locking using a torque screw driver and the micromotion at the trans cortex by hand. The removal torque was measured with the WinWedge RS232 data capture system (Gedore Dial Measuring torque wrench ADS 8; serial number OER015722; torque range 1.6 - 8 Nm; accuracy +/- 3% of reading) for the animals 84.01-84.12 and another torque screw driver (CEDAR Digital torque screw driver/tester; DIS-RL10, 0.1 - 10.0 Nm; 0.5% FS accuracy) for sheep 84.13 and 84.14. Data have been continuously acquired at 12Hz. The presence of callus/ossification over the implant, fibrosis around the screw hole and metallosis were scored:

- \- not present
- \+ minimal amount
- ++ moderate amount
- +++ high amount

The sleeve degradation was checked and additional notes before and after the implant removal were taken.

After macroscopic evaluation, screw and plate removal, the treated tibiae of each animal were put in plastic bags labeled with sheep number and ‘left’ or ‘right’. Additionally, plate and screws were stored in jars with 70% ethanol.

Macroscopic findings	Score
Screw locked in plate	yes/no
Micromotion in transcortex	yes/no/not measurable
Removal torque	in Nm
Callus/ossification over implant	(-,+,++,+++)
Fibrosis around screw hole	(-,+,++,+++)
Metallosis	(-,+,++,+++)
In TI: Sleeve still present	yes/no
Additional notes before and after implant removal	

Tab. 3.1: Macroscopic evaluation for each screw position one to six

3.7.2 Sample preparation for transport

Both tibiae of each sheep were enwrapped in wet gauzes soaked with saline solution and put in labelled plastic bags for transport. The operated tibiae were transported immediately to test location one (SCANCO Medical AG, Fabrikweg 2, CH-8306 Brüttisellen, Switzerland) for extreme-CT examination. Afterwards, they were transported to test location two (Institute of Biomechanics ETHZ, Prof. Ferguson, Zürich) for the biomechanical testing, where the non-treated tibiae had already been transported and tested.

3.7.3 Sample preparation for histological analysis

After biomechanical testing the samples were cut with an oscillating saw (Proxxon MBS 230/0 Oberrüti, Switzerland) between the first and second and the fifth and sixth screw holes. The three pieces (1. screw hole, 2. - 5. screw hole and 6th screw hole) were placed in labeled jars separately and fixed in 40% ethanol for at least 1 week, followed by a series of ethanol dehydration (50-100%).

- 3x2 days in 50% ethanol
- 2x2 days in 70% ethanol
- 2x2 days in 80% ethanol
- 2x2 days in 90% ethanol
- 2x2 days in 96% ethanol
- 4x2 days in 100 % ethanol

• 2x3 days in xylol as an intermedium to MMA (Methylmethacrylate)

After the complete dehydration, all samples were degreased in xylene and subsequently infiltrated in liquid MMA. Polymerization was carried out in glass molds closed with a lid that were kept at 4°C for at least 18 days, thereafter in a water bath at room temperature until polymerization occurred. Finally, the glass molds were placed in an uncovered incubator (37,5°C) to complete hardening of the samples. The whole process took at least 4 weeks until the tibia blocks were fully polymerized and ready to cut.

For MMA preparation methacrylacid-methylester (Sigma-Aldrich, Buchs, Switzerland), dibutylphthalat (Sigma-Aldrich, Buchs, Switzerland) and Perkadox 16 (Dr. Grogg Chemie AG, Stettlen-Deisswil, Switzerland) was needed. They were mixed in a ratio of 1 l - 200 ml - 5 g ratio respectively and homogenized for 30 minutes with a magnetic stirrer (Heidloph MR 3001 D, Laborbedarf, Schaffhausen, Switzerland). The pharmacy of the canton of Zurich produced xylol (Xyolol KA, Kantonsapotheke, Zürich, Switzerland) and ethanol (Ethanol KA, Kantonsapotheke, Zürich, Switzerland).

The glass around the polymerized block was broken to pieces to get the block out. The polymerized block was washed up with tap water and depending on the sample orientation in the block, it had to be cut and sanded (Struers Labor POL 5, Struers Gmbh, Birmensdorf, Switzerland) for an exact labeling of the cutting line with a waterproof pen and a ruler.

The polymerized bone blocks were cut lengthwise (longitudinally) to the screw axis in the midline of the bone sample using an Exact® 310 saw (EXAKT® Band System 300/301, Exakt Apparatebau GmbH & Co KG, Norderstedt, Germany). These non-decalcified samples were used for histomorphometrical and fluorescence analysis. Therefore, 600-800 µm ground sections were cut. The samples were cleaned with 70% alcohol. For drying, they were put in a cellulose tissue and smoothened under metal weights.

Microradiographs of all ground sections were taken with a faxitron (27 KV, 11s, Cabinet x-ray-faxitron series, model: 43855A, Faxitron X-ray System, Hewlett Packard®, McMinnville, OR, USA) and X-ray plate (Fuji Photo Film Co., Ltd. Tokyo, Japan) prior to mounting the slices on Acropal slides and surface staining.

One of the ground sections was used for fluorescence evaluation. For this, the section was fixed with a quick adhesive (Cementit® Ca 12, Merz + Benteli AG, Niederwangen, Switzerland) on a glass slide, labelled and enwrapped in aluminum foil. The second ground section was used for the toluidine blue staining. The section was fixed on an

opaque acrylic glass carrier (Perspex GS Acrylglas Opal 1013, Wachendorf AG, Basel, Switzerland), grinded using a sanding machine (Exakt Mikroschleifsytem 400 CS, Exakt Apparatebau GmbH, Norderstedt, Germany) and then surface stained with toluidine blue solution.

The solution was prepared as follows: the sections were etched with 0.7% formic acid (Sigma-Aldrich, Buchs, Switzerland) and then cleaned under tap water. 0.1% Toluidinblau-O-solution (Sigma-Aldrich, Buchs, Switzerland) with phosphate puffer pH 8.0 was sprinkled over the sections. After 15 minutes the sections were rinsed under tap water and deionized water. One hour later they could be used for the analysis.

Thin sections (including the defect area and both screws close to the defect) were used for histological evaluation on cellular level and the evaluation focused on the cellular reactions of the tissue. Thin sections (5µm) were produced of the remaining bone blocks after preparing the ground sections and were cut with a microtome (Leica RM 2155, Leica Instruments GmbH, Nussloch, Germany). To fit the areas of interest on a slide, each sample had to be divided into two sections (N=24 sections, Fig. 3.3).

Section 1 (medial): Cis cortex including half of the screw holes, defect area and bone marrow cavity

Section 2 (lateral): Trans cortex including half of the screw holes, defect area and the other half of the bone marrow cavity

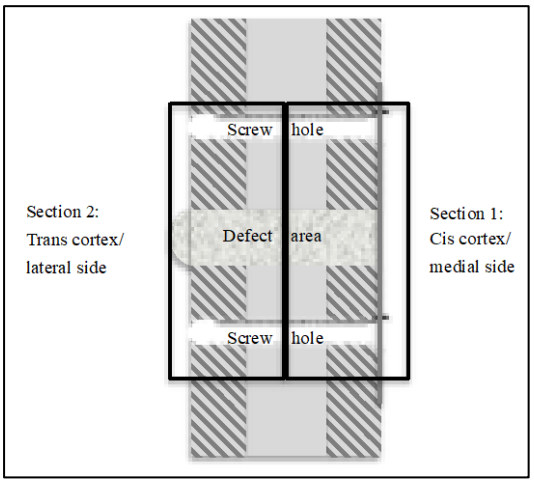

Fig. 3.3: Thin section preparation: Section 1 (medial): Cis cortex including half of the screw holes, defect area and bone marrow cavity; Section 2 (lateral): Trans cortex including half of the screw holes, defect area and the other half of the bone marrow cavity

In total, 72 sections were stained using toluidine blue (N=24), von Kossa (N=24) and Hematoxylin-Eosin (HE) (N=24) according to routine.

3.8 Evaluative procedures

3.8.1 Radiologic evaluation

3.8.1.1 Semiquantitative radiographic evaluation

The semiquantitative evaluation of all radiographs (week 3 to week 9) was performed by two independent reviewers (a board certified radiologist and a board certified surgeon) using a specially designed scoring sheet (see appendix, page 66, Tab. 7.2).
The scoring sheet was structured into three parts: callus formation, callus opacity and bone activation.
The first part "callus formation" included all three projections (anteroposterior (0°), anterolateral (275°) and posterolateral (265°)). For cortical callus formation, bridging of the defect was scored. The RUST score (Radiographical Union Scale in Tibial fractures) is a scoring system for human tibiae radiologic evaluation, developed by Wehlan et al.. As a tool for the assessment of fractures, it should help to standardize the radiographic assessment of tibia fractures. The RUST score evaluates cortical bridging formation. It has been shown, that the bridging formation correlates with the biomechanical strength of the fracture site. Leow et al. evaluated the scoring system as a "reliable and repeatable outcome measure for assessing tibial fracture healing"[61]. Scores for cis cortex and trans cortex were assigned depending how much callus was reaching into the defect and whether the fracture line was visible in the callus. Additionally, in the cranial and caudal projection the callus within the osteotomy gap respectively cortical gap was examined by its occurrence in the fracture gap.
The second and third part ("callus opacity" and "bone activation") was evaluated in the anteroposterior projection. Callus opacity was determined in comparison to the soft tissue opacity with a scoring system. Bone activation was defined as the irritation callus formation around the screw tips.

3.8.1.2 Quantitative radiographic evaluation

Quantitative analysis of all radiographs (week 3-9) was performed using specialized computer imaging software (OsiriX) measuring the total callus area (see appendix, page 80, Fig. 7.7).

3.8.1.3 Micro-CT evaluation

The samples were measured with a commercially available cone-beam CT, µCT (XtremeCT II, SCANCO Medical AG, Brüttisellen, Switzerland). µCT examinations were non-destructive; the samples remained available for other examination techniques afterwards. It operated with a cone beam originating from a 60 µm focal-spot X-ray tube. The photons were detected by a CCD-based area detector and the projection data were reconstructed into a 1654 x 1654 image matrix. The region of interest for scanning was defined from ~5 mm proximally of the proximal k-wire hole to ~5 mm distally of the distal k-wire hole. The k-wire positions were identified visually and the image processed only in between these. The scans were visually inspected for artefacts, etc. and repeated if necessary.

The image was first roughly segmented (native bone > 1000 mgHA/ccm, callus 250-1000 mgHA/ccm) to generate seeding masks. Then the final bone and callus masks were refined from the seeding masks using a series of transformations: 1. Opening (1 voxel, discard speckles of < 50 voxels), 2. Closing (3 voxels) and 3. Bone masked off callus.

Bone volume and density were computed from the grayscale image within their respective masks. Moments of inertia were computed slice wise in XY planes along Z and exported to histograms. Bone biomechanical properties were estimated by calculating the polar moment of inertia representing bone torsional strength (pMOI), resistance to bending calculated across the bone along the maximal centroid-edge (Imax/Cmax) and along the minimal centroid-edge (Imin/Cmin).

The grayscale data was exported as DICOM. A 3D rendering of each model was generated. Finally, longitudinal and sagittal sections were extracted from the center of each scan for visualization.

3.8.1.4 Microradiographic evaluation

Microradiographs were performed using a faxitron machine (Model: 43855A, Faxitron x-ray System, Hewlett Packard, McMinnville, OR, USA) and stored digitally.

3.8.2 Biomechanical testing

The biomechanical testing took place at ETH Hönggerberg in Zurich with an Instron® E10000 electrodynamic testing machine under laboratory conditions (see appendix, page 80, Fig. 7.8). To avoid losing the elasticity of the bones, they were enwrapped in

wet gauzes soaked with saline (0.9% NaCl-Solution) and were packed in labelled plastic bags in a transportation box. The proximal and distal ends of each tibia were embedded in PMMA (polymethylmethacrylate), providing the same exposed section (150 to 160 mm in length) for each pair of tibiae. For having better hold in the PMMA, both ends of each tibia were additionally fixated with four screws. The embedding forms were greased with commercial hand cream to facilitate the leaching of the PMMA. To fit into the embedding forms 8 to 12 mm of the tuberositas tibiae and 10 to 15 mm of the lateral condyle had to be cut. Torsional testing was performed in angular displacement control. The loading was adjusted in internal rotation, with a constant angular velocity of 5°/min until failure. The contralateral, intact tibia served as control. Torsional stiffness was calculated by interpolating the linear portion of the torque/angular displacement curve. The energy to failure was calculated as the integral under the torque/displacement curve.

3.8.3 Histological evaluation

3.8.3.1 Histomorphometry of ground sections

Quantitative histomorphometrical evaluation was conducted using computer-based histomorphometric measurements. First, the sections were captured with a microscope in various magnifications (Leica Z6 APOA, Leica DFC 420C, Glattbrugg, Switzerland) as digital images in TIF-format. Thereafter, the images were prepared for measurements to quantify the percentage of old and new bone, and non-bone (non-bone containing tissue like fibrous tissue, fat, bone marrow tissue) in the predefined ROI. The ROI was the osteotomy area including the 3rd and 4th screw.

The tissues of interest were manually color-highlighted interactively with Adobe Photoshop Elements 10 (Adobe Systems, San Jose, CA).

Total section evaluation

For total section evaluation, the amount of old and new bone plus non-bone tissue was measured in each ground section sample. Using a standardized pixel-detecting tool of Adobe Photoshop the samples were color highlighted as followed:

- old bone: light blue (R: 0; G: 210; B: 255; #00d2ff)
- new bone: dark green (R: 34; G: 79; B: 7; #224f07)
- non-bone: pink (R: 242; G: 40; B: 211; #f228d3)
- background: beige (R: 198; G: 156; B: 96; #c69c60)

Sectoral evaluation

For the sectoral section evaluation the callus was split in three parties: cis- and trans cortex and endosteal area. Using a standardized pixel-detecting tool of Adobe Photoshop the samples were color highlighted as followed:

- callus in the cis cortex area: light blue (R: 0; G: 210; B: 255; #00d2ff)
- callus in the endosteal area: dark green (R: 34; G: 79; B: 7; #224f07)
- callus in the trans cortex area: pink (R: 242; G: 40; B: 211; #f228d3)
- background: beige (R: 198; G: 156; B: 96; #c69c60)

Afterwards, the colored images were analyzed using a specialized image analysis software program (Fiji, ImageJ, version 2.0,0-rc-46/1.50g, build 179d1b4146, date 2016-03-04, open source image processing software, copyright 2010-2018, http://imagej.net/Contributors, this image from ESO/J. Emerson/VISTA Cambridge Astronomical Survey Unit) and the colored fractions were automatically detected and measured in number of pixels. Afterwards the pixels within the area of interest (exclusion of background) were set as 100% and the percentage of the different tissues was quantified.

3.8.3.2 Semiquantitative analysis of the local tissue effects (thin sections)

The semiquantitative evaluations of biocompatibility (inflammation and tissue response), bone remodeling (osteoclasts, bone activity, defect unity) and additional observations (traumatic necrosis, foreign debris) were performed according to ISO 10993-Part 6 Annex E (Third edition 01.12.2016) on thin sections (N=72) using a light microscope (microscope Leica DMR system). The evaluation was performed by two independent observers.

Assessment of biocompatibility parameters of the TI screws in comparison to the RI screws was evaluated in the area of the screw holes (cis and trans cortex) including bone marrow cavity and were characterized by inflammation and tissue reaction (see Fig. 3.4). Additionally, traumatic necrosis and foreign debris were evaluated in the same area. Bone remodeling evaluation was performed only in the defect area (see Fig. 3.4).

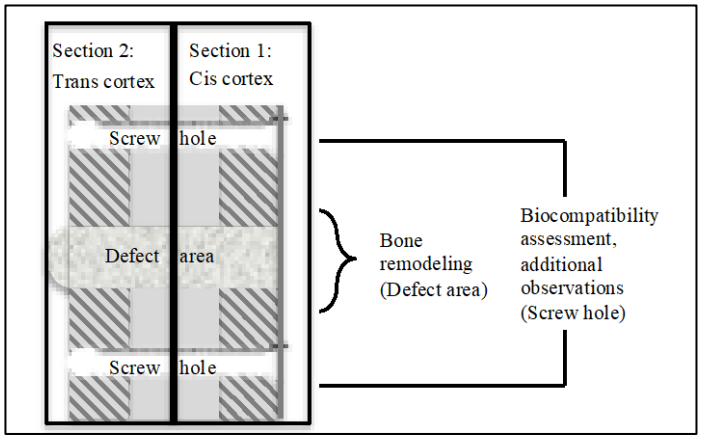

Fig. 3.4: Thin section evaluation including biocompatibility and additional observations (only evaluated in screw hole) plus bone remodeling (only evaluated in defect area).

Biocompatibility scoring contained 1. Inflammation and 2. Tissue response and was separately performed in the implant surrounding area (screw hole) at the cis and the trans cortex (see appendix, page 67, Tab. 7.3).

Inflammation was characterized by cellular components:

- polymorphonuclear cells
- eosinophils
- lymphocytes
- plasma cells
- macrophages
- giant cells
- necrosis and osteolysis

Tissue response was described by remodeling reaction including:

- neovascularization
- fibrous capsule formation/fibrosis
- fatty infiltration (at the cis and trans cortex area only)

Due to the greater importance of inflammatory cell infiltrates and necrosis, these parameters were multiplied by a factor two to provide a weighted value as compared to tissue remodeling parameters, which describe a more secondary effect and healing response. The values were summarized, and then an average score for TI and RI was calculated.

The average score for the control treatment was subtracted from the TI average to determine a reactivity grade based on the following scale:

- minimal or no reaction (0.0 to 2,9)
- slight reaction (3.0 to 8,9)
- moderate reaction (9.0 -15.0)
- severe reaction (≥15.1)

Additional observations in screw hole

Additional observations contained traumatic necrosis due to the surgical procedure, foreign debris (metallosis or other free particles, cell associated particles or both). The used scoring scheme is shown see appendix, page 68, Tab. 7.4.

Bone remodeling in defect

Bone remodeling including osteoclasts and bone activity was evaluated using the scoring scheme shown see appendix, page 68, Tab. 7.5.

3.8.4 Fluorescence

Fluorescent sections were evaluated quantitatively and semiquantitatively for the differences of dye integration between groups and at different time points (calcein green at 3 weeks, xylenol orange at 6 weeks and oxytetracycline at 9 weeks postsurgery). Digital images of the region of interest ROI (defect area) were recorded. Therefore, 8x8 single images were taken in a 1.25 magnification and merged together using a special microscope, camera and specific merging software (Leica LAS-X standard software Leica Microscopes, “Stitching function”; Leica DM 6000B, Leica DFC 350 FX, Leica Microsystems CMS GmbH, Mannheim, Germany).

Quantitative evaluation

For quantitative evaluation, the fluorescent areas/tissues were manually color-highlighted interactively with Adobe Photoshop Elements 10 (Adobe Systems, San Jose, CA):

- calcein green: dark green (R: 34; G: 79; B: 7; #224f07)
- xylenol orange: pink (R: 242; G: 40; B: 211; #f228d3)
- oxytetracycline: light blue (R: 0; G: 210; B: 255; #00d2ff)
- background: beige (R: 198; G: 156; B: 96; #c69c60)

Afterwards, the colored images were analyzed using a specialized image analysis software program (Fiji, ImageJ) and the colored fractions were automatically detected

and measured in number of pixels. Afterwards the pixels within the ROI (exclusion of background) were set as 100% and the percentage of the different tissues was quantified.

Semiquantitative fluorescence evaluation

For semiquantitative fluorescence evaluation, the sections were evaluated by two independent observers with the following score system: callus on the cis cortex (C), trans cortex (T) and intramedullary (M) was scored in three grades:

1 no to little fluorescence detection
2 moderate fluorescence detection
3 good fluorescence detection.

3.8.5 Histological analysis of the draining lymph nodes

Local draining lymph nodes (lnn. inguinales, lnn. poplitei) were harvested and macroscopically examined at sacrifice, with a focus on the following parameters: size, color and consistency. All deviations from normal size, color and consistency were protocolled. Qualitative histological evaluation of the lymph nodes was conducted based on structure changes and cellular content (non-local cells). Particular attention was paid to inflammatory cells and the presence of foreign material in the lymph nodes. The evaluation was performed by two independent observers using the evaluation criteria in see appendix, page 69, Tab. 7.6.

3.8.6 Statistical analysis

Statistical analysis of data from radiologic evaluation, histomorphometrical measurements, semiquantitative histological evaluation, e-CT evaluations and biomechanical evaluation was performed using Independent Samples t-tests to compare statistical differences between means of TI and RI. All statistical analyses were performed using the software program SPSS (IBM SPSS statistics for Mac OS X, Version 24.0, Chicago, Illinois).

4 Results

4.1 Excluded animals

In total, 12/14 sheep completed the study as planned. Two sheep had to be excluded from the group analysis and were replaced by reserve animals. None of the exclusions were directly related to the Test Item.

In one animal (84.04, TI), the drill sleeve was attached to the 4th screw hole in an incorrect angle. Subsequently, the hole was drilled incorrectly and the 4th screw was accidentally placed in direct connection to the fracture gap. In addition, the screw could not be locked completely.

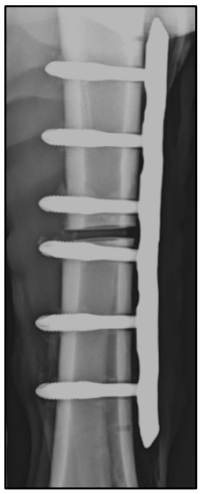

Fig. 4.1: Animal 84.04, TI, Radiograph post operative: The 4th screw is in direct connection to the fracture gap.

The second excluded animal (84.14, TI) was lying more often than all other animals of this study and therefore, developed an inflamed sternal lesion. The reduced load bearing on the operated limb led to an atypical callus formation (more callus medially) compared to all other sheep.

4.2 Surgery

In all 14 animals, neither anesthesia complications nor severe surgical complications occurred. In one sheep (84.05) increased bleeding in the bone marrow of the defect area occurred without having an impact on the study outcome.

The average surgery time was 80 min (62-98 min) in the TI group and 74.2 min (46-158 min) in the RI group. The longest surgery time (158 min) occurred in the first animal (84.01) due to a lack of the correct LC plates. A correct plate had to be picked up at a partner institute (University hospital Zurich). Therefore, the surgery was prolonged by about one hour.

In total, 61 TI screws were used. Out of these, 13 screws had to be replaced due to sleeve breakage during the implantation procedure. After removal of these, all 48 implanted screws had an intact sleeve. In 7/48 TI screw positions (6/8 sheep, except 84.02 and 84.06), the sleeve broke 1-3 times. In all cases of sleeve breakage, the surgeon was able to notice the breakage visually and acoustically as a click during breakage. Due to sleeve breakage and reinsertion of a new screw, the surgery time was prolonged. In 35 cases the sleeve was slightly displaced (shifting towards the screw head) during the implantation procedure without breakage. An overview of sleeve breakages and surgery time is illustrated in Tab. 4.1: Overview of the sleeve breakages and surgery times.

Animal	1. Screw	2. Screw	3. Screw	4. Screw	5. Screw	6. Screw	Total	Surgery Time
84.02	m	m	m	m	m	m	-	62 min
84.04	m	m	m	m	s	2x b, 1x m	2x b	84 min
84.06	m	m	s	s	m	m	-	83 min
84.07	s	3x b	s	2x b	m	m	**5x b**	**93 min**
84.09	m	s	m	2x b	m	s	2x b	**98 min**
84.12	s	m	m	2x b, 1x m	m	s	2x b	72 min
84.13	m	m	m	m	m	1x b, 1x m	1x b	72 min
84.14	m	m	m	m	1x b, 1x m	s	1x b	73 min
Total	-	**3x b**	-	**6x b**	**1x b**	**3x b**		

Legend: s = Sleeve stayed in place, m = Sleeve moved, b = Sleeve broke

Tab. 4.1: Overview of the sleeve breakages and surgery times.

4.3 Postsurgical in-life observations

None of the 14 animals revealed complications during the recovery phase or severe clinical abnormalities influencing the overall outcome of the study. The suspension system, cast changes and weekly performed radiographs were mostly well tolerated. Only two sheep (84.07, 84.14) had to be sedated (medetomidine, 0.02mg/kg BW, im Medetor®, Virbac AG, Opfikon, Schweiz) for 2-3 times due to nervous behavior being unable to sit still while radiographs were taken. Pressure injuries and chafing were immediately treated with betadine ointment and additionally padded with cotton wool. After radiologic diagnosis, one sheep (84.04) had to be excluded because the 4th screw was placed in direct connection to the fracture gap. In week 3, one other sheep (84.09) developed a fracture in the trans cortex, but it was unclear if it had to be excluded or not. Therefore, two reserve sheep were operated (84.13 and 84.14). One of these sheep (84.14) had such a big sternal wound due to often lying on the ground that prevented mechanical loading. Thus, it had to be excluded from the group analysis. For more details see chapter “4.1 Excluded animals”.

4.4 Sacrifice

In all animals, the sacrifice procedure after 9 weeks could be performed according to routine. All samples, including lymph nodes and both tibiae, could be harvested as planned. The individual results of each animal at sacrifice are shown in annex, page 70, Tab. 7.7.

Overall, the anatomical dissection performed right after sacrifice showed that in both groups, TI and RI, the tissue adjacent to the implants did not show any alteration of the normal structure. No heamatoma, edema, encapsulation, and/or other additional gross findings have been recorded. In addition, no macroscopical abnormalities were found in any of the harvested lymph nodes.

All 72 screws (TI=36, RI=36) were found to be locked in the plate. Only one TI screw of an excluded sheep (84.04) was not locked. It was the 4th screw which was placed in direct connection to the fracture gap.

The removal torque was measured with average of 2.01 Nm in the TI group and 2.79 Nm in the RI group. In two sheep of the RI group (84.03 and 84.10), the removal torque of the fifth screw were not measured due to human error. At all TI screws, the sleeve had been completely resorbed. No screw tip micro motion in the trans cortex was found in any of the sheep. In one sheep (84.13, TI) some fibrosis around all screw holes was detected. Metallosis at the screw head – plate junction was found in 11/12 sheep of both groups (TI=5, RI=6). Only in one sheep of the RI group (84.03) no metallosis could be detected. Overall, metallosis was more pronounced in the RI group than in the TI group. Callus ossification around the implants was only seen in the TI group (3/6 sheep). Three examples (2x TI and 1x RI) are shown in pictures (see annex, page 81 and 82, Fig. 7.9-7.11).

4.5 Radiologic evaluation

4.5.1 Radiographs

Radiologic analysis proved valuable to determine the osseous reaction around the screws (bone reaction, radiologically visible radiolucent zones around the screws) as well as to evaluate the grade of radiologically detectable healing of the defect area evidenced by callus formation in that area. Furthermore, an activation of the complete bone could be detected in the TI group (irritation callus around screw tips).

A semiquantitative and quantitative radiologic evaluation were performed.

Briefly summarizing the results of the semiquantitative evaluation, more callus formation reaching into the defect and bridging of the defect was scored for the RI group. Additionally, in the quantitative radiologic evaluation, the TI group showed a tendency for higher values of total callus area around the fracture gap.

4.5.1.1 Semiquantitative radiologic evaluation

The semiquantitative radiologic evaluation was performed by two independent reviewers (a board certified radiologist and a board certified surgeon) using a standardized score sheet. The results are shown in appendix, page 71, Tab. 7.8-7.15.

Overall, the RI group achieved a higher score compared to the TI group in almost all of the criteria evaluated, except for bone activation. However, note that the radiographic evaluation measured only callus formation under the anteroposterior (0°), anterolateral (275°) and posterolateral (265°) projections, which does not include the formation at the anterior and posterior side. Therefore, radiographic results are not conclusive by itself, but have to be compared to the µCT evaluation. In addition, radiographic evaluation of the endosteal callus was not performed due to superimposition of the callus formation at the anterior and posterior side of the bone. Thus, endosteal callus formation was accessed in histomorphometry. Although the RI showed higher scores in almost all variables in the later time points, in the early time points between week 3 and 4 the cortical callus formation at the cis cortex was almost identical between groups. The callus formation at the trans cortex was lower throughout the whole observation period, also during the early time points. The callus of the TI showed a larger distribution and reached partly up to and over the third and fourth screw hole. The callus area of the RI was limited to the area in and around the fracture gap and had a compact callus accumulation and higher callus density.

At three weeks postsurgery, the TI group showed higher mean score results for **cortical callus formation** compared to the RI group. At all later time points, RI showed higher mean scores compared to TI. In week 9 the RI showed significantly higher scores (p=0.043) for cortical callus compared to the TI without any significant differences in the other time points.

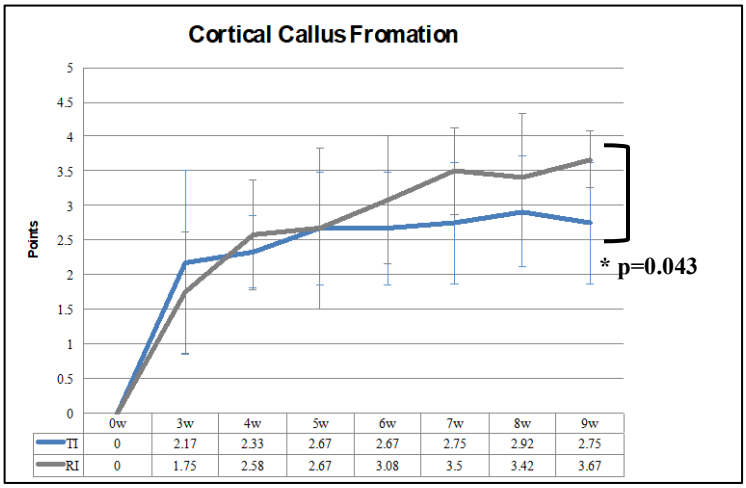

Fig. 4.2: Cortial callus formation over 9 weeks. TI blue, RI grey, w = weeks.

The **RUST score** revealed higher means for the RI group at all time points.

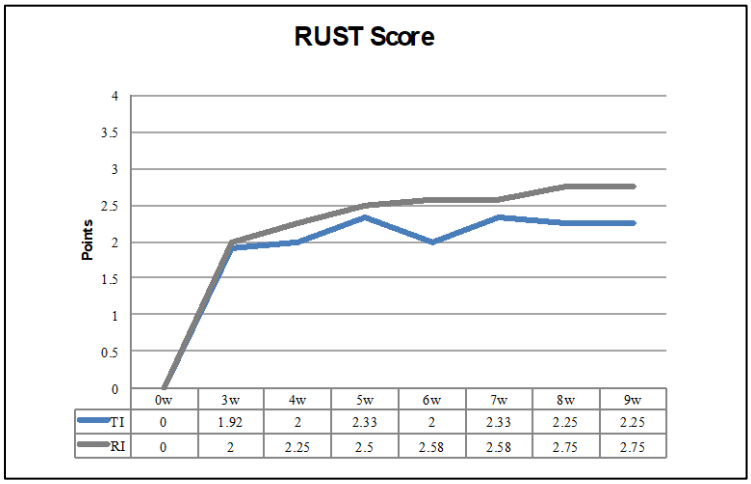

Fig. 4.3: RUST score over 9 weeks. TI blue, RI grey, w = weeks.

Scores for callus area at the **cis cortex** were slightly higher in the RI than in the TI group. The same was found for the **trans cortex**, where the RI had higher scores at all time points compared to the TI, with significant differences in week 3 (p=0.002) and week 6 (p=0.017), see Fig. 4.4.

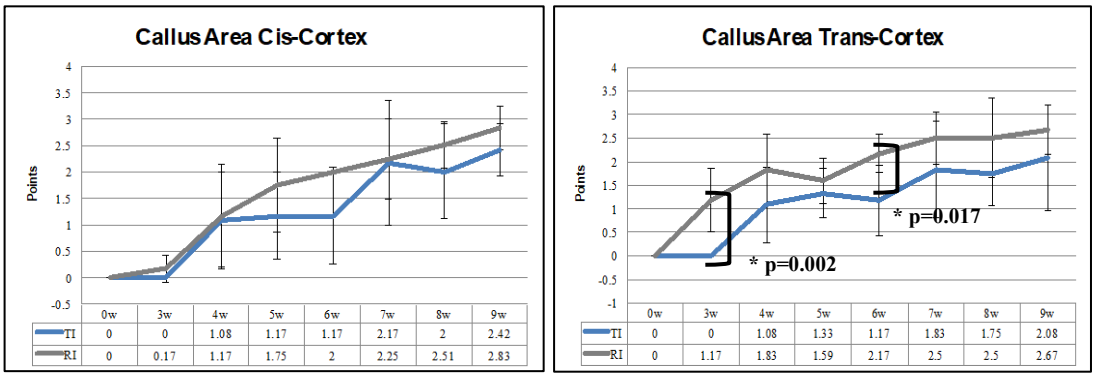

Fig. 4.4: Callus area cis- and trans-cortex. TI blue, RI grey, w = weeks.

According to the radiologist, the RI revealed more callus area **cranial** and **caudal at the gap area** compared to the TI at all time points. Significant differences were seen only in week 6 of the cranially callus area in the gap area (p=0.036), see Fig. 4.5.

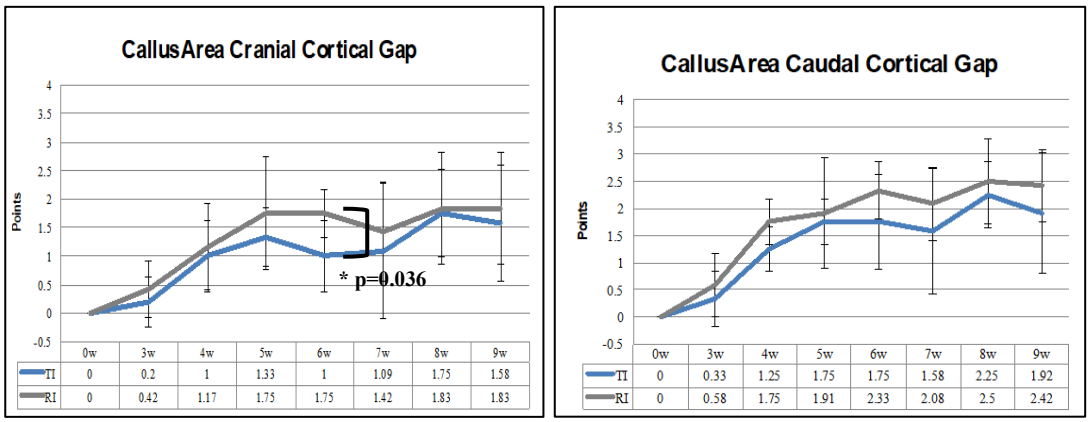

Fig. 4.5: Callus area cranial and caudal cortical gap. TI blue, RI grey, w = weeks.

The **callus opacity** revealed identical scores in week 7, but at all other time points, the opacity was higher in the RI group compared to the TI. In week 8 the RI had significant (p=0.024) higher callus opacity, see Fig. 4.6.

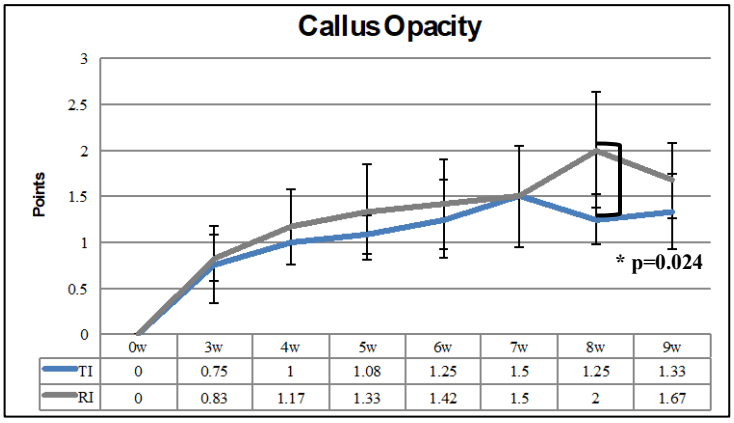

	0w	3w	4w	5w	6w	7w	8w	9w
TI	0	0.75	1	1.08	1.25	1.5	1.25	1.33
RI	0	0.83	1.17	1.33	1.42	1.5	2	1.67

Fig. 4.6: Callus opacity. TI blue, RI grey, w = weeks.

Bone activation around the screw tip was higher in the TI than in the RI group. Between week 3 to 7 the bone activation was significantly higher in the TI than in the RI group (3w p=0.024, 4w p=0.011, 5w p=0.040, 6w p=0.023, 7w p=0.009), see Fig. 4.7.

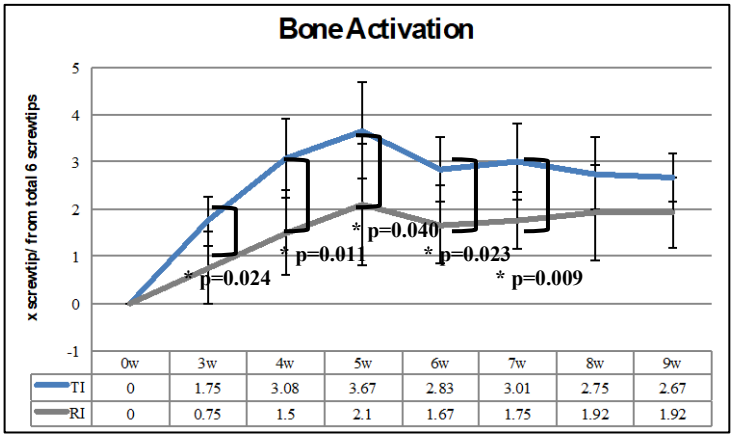

	0w	3w	4w	5w	6w	7w	8w	9w
TI	0	1.75	3.08	3.67	2.83	3.01	2.75	2.67
RI	0	0.75	1.5	2.1	1.67	1.75	1.92	1.92

Fig. 4.7: Bone activation. TI blue, RI grey, w = weeks.

At nine weeks post-surgery, a higher radio density at the endosteal area of the proximal screws was found in 5/6 sheep of the VFLS group. Out of these, in 3/5 sheep an enhanced radio dense rim was found at the 2nd screw, see Fig. 4.8. An endosteal seam around the TI was detected more often in the 2nd screw than in the other five screws.

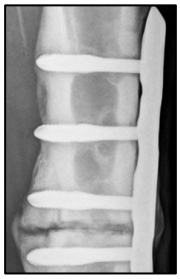

Fig. 4.8: Radiologically visible radiolucent zones in the TI group, also called endosteal seam, were often detected around the 2nd screw.

4.5.1.2 Quantitative radiologic evaluation

The quantitative radiologic evaluation was performed using OsiriX to measure the callus area at the fracture gap in all three projections (anteroposterior (ap, 0°), anterolateral (275°) and posterolateral (265°)).

In total, in the mean measurements of all three projections the TI showed more callus area compared to the RI group. Detailed results see appendix, page 72, Tab. 7.16 – 7.20.

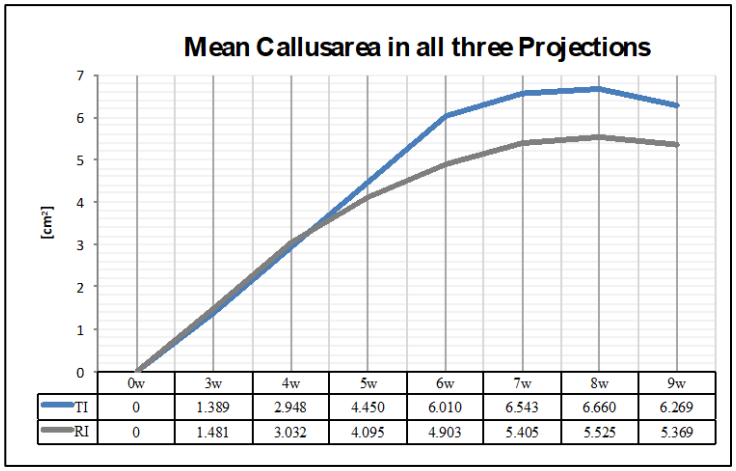

Fig. 4.9: Mean callus area in all three projections. The TI group (blue) showed more callus area compared to the RI group (grey), w = weeks.

At week 3 and 4 post-surgery, the RI group had slightly more callus area in total (TI 1.39-2.95 cm^2; RI 1.48-3.03 cm^2). In both groups periosteal callus increased continuously until week 8, at which the peak callus area was detected. The callus area in week 9 was lower than in week 8 for both groups. There were no significant differences at any time point.

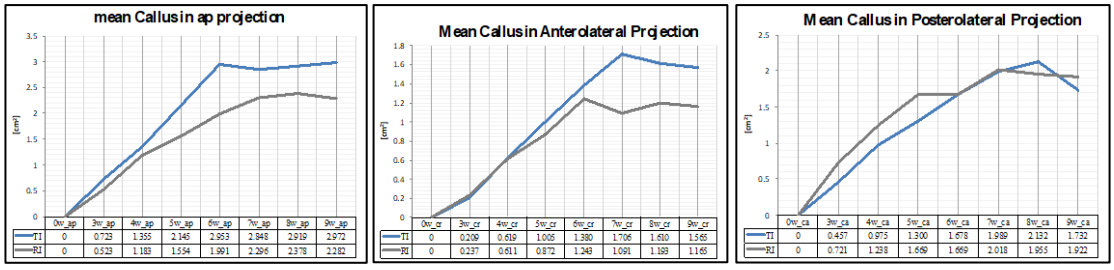

Fig. 4.10: Mean callus in anteroposterior, anterolateral and posterolateral projection. TI blue, RI grey, w = weeks.

On the anteroposterior and the anterolateral projection a bigger callus area was measured in the TI group, except in week 3. However, in week 3 the RI (0.237 cm^2) showed more callus compared to the TI group (0.209 cm^2). In the posterolateral projection, the callus area of RI was more pronounced until week 6, at all later time points the callus areas were almost the same size.

4.5.2 Micro-CT

The µCT allowed three dimensional evaluation of bone volume and density as well as callus volume and density. Additionally, the polar moment of inertia (pMOI) was measured as quantitative information about the distribution of the callus around the bone axis. In all 12 tibiae, µCT measurements were performed between the proximal k-wire insertion and the distal k-wire insertion measuring the total callus and bone area (not only the fracture gap area).

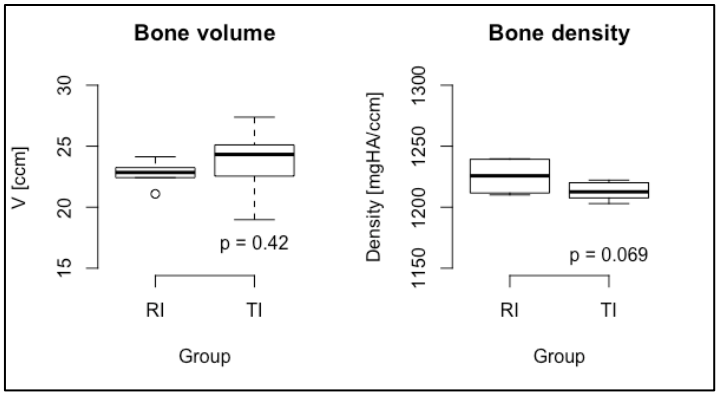

Fig. 4.11: Bone volume and bone density boxplots (source: Micro-CT report Scanco Medical)

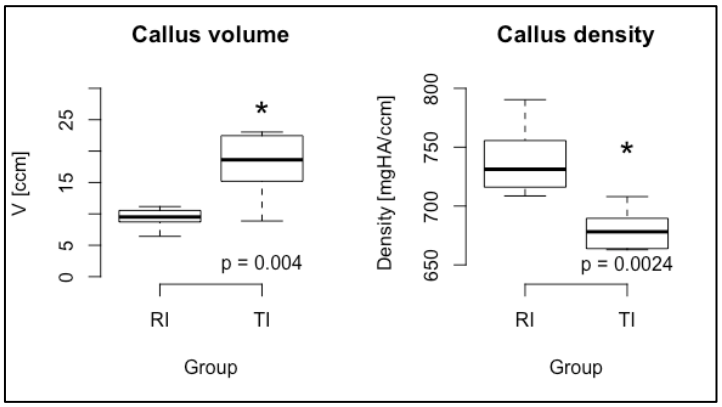

Fig. 4.12: Callus volume and callus density boxplots (source: Micro-CT report Scanco Medical)

No significant differences between groups could be found for bone volume and density (p=0.42, p=0.069). TI (23.8 ccm ± 2.8 ccm) showed slightly higher values for bone volume compared to RI (22.8 ccm ± 1.0 ccm). Bone density was slightly higher in RI (1225 mgHA/ccm ± 13 mgHA/ccm) compared to TI (1213 mgHA/ccm ± 8 mgHA/ccm). There was a significantly larger amount of callus (p=0.004) in TI samples implanted with TI (17.8 ccm ± 5.4 ccm) with respect to those implanted with RI (9.3 ccm ± 1.7 ccm). However, this tissue featured a significant lower density (p=0.0024) in the TI group (680 mgHA/ccm ± 18 mgHA/ccm) compared to the RI group (739 mgHA/ccm ± 31 mgHA/ccm).

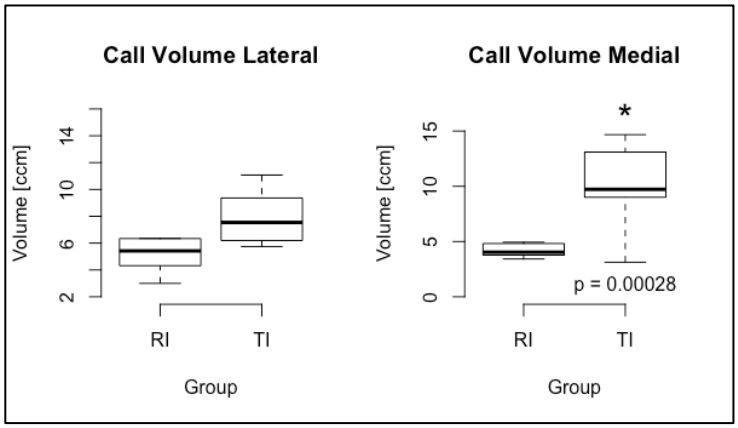

Fig. 4.13: Callus volume lateral and callus volume medial boxplots (source: Micro-CT report Scanco Medical)

Callus volume by orientation was performed by cutting the bone longitudinally into a medial and a lateral side. While the callus volume on the medial side showed significantly (p=0.00028) higher values for TI (9.89 ccm ± 4 ccm) compared to RI (4.17 ccm ± 0.6 ccm), the callus amount on the lateral side showed only a tendency for higher values for TI (7.91ccm ± 2.07ccm) compared to RI (5.14 ccm ± 1.32 ccm).

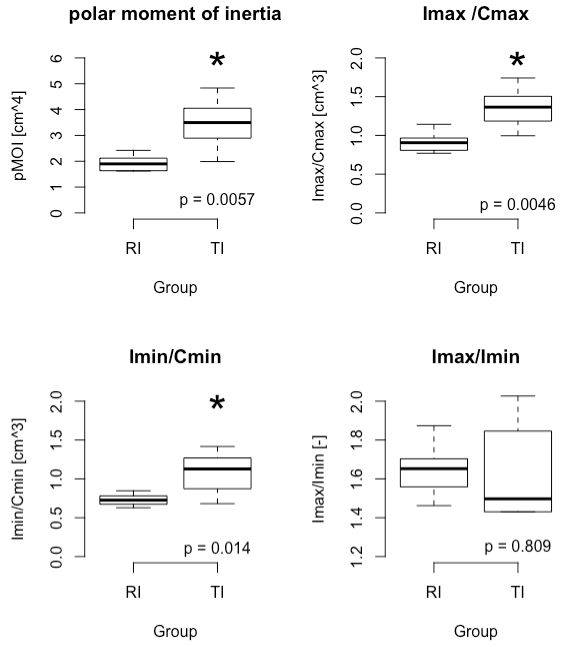

Fig. 4.14: Box plots of moments analysis (source: Micro-CT report Scanco Medical)

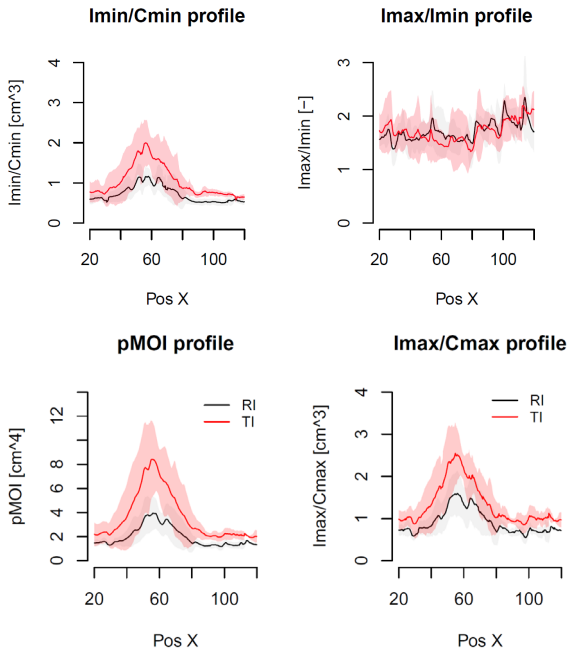

Fig. 4.15: Spatial analysis of moments (source: Micro-CT report Scanco Medical)

The polar moment of inertia was significantly (p=0.0057) higher in TI (3.46 cm^4 ± 1.02 cm^4) compared to RI (1.93 cm^4 ± 0.3 cm^4). Also the Imax/Cmax was significantly (p=0.0046) higher in TI (1.36 cm^3± 0.27 cm^3) compared to the RI group (0.92 cm^3 ± 0.13 cm^3). Furthermore, TI (1.08 cm^3 ± 0.28 cm^3) showed significantly (p=0.014) higher values in Imin/Cmin compared to RI (0.73 cm^3 ± 0.08 cm^3), but no differences in Imax/Imin (TI: 1.62 ± 0.25; RI: 1.65 ± 0.14).

The profiles of the moments of inertia illustrate the spatial distribution of callus tissue with respect to the relative bone axis. The Pos X = 60 is the middle of the fracture gap. There was a clear difference in polar moment of inertia at all cross-sections between 40 mm proximal and distal to the fracture gap (TI in red and RI groups in black). For example, at midshaft (Pos X=60), pMOI was >200% higher in TI compared to RI ($p<0.05$), I_{MAX}/C_{MAX} ~160%, I_{MIN}/C_{MIN} ~100% respectively.

Gap sub-analysis ROI

Additionally, an analysis of the gap including the 3rd and 4th screw hole (ROI) was performed (see Fig. 4.16 and Fig. 4.17).

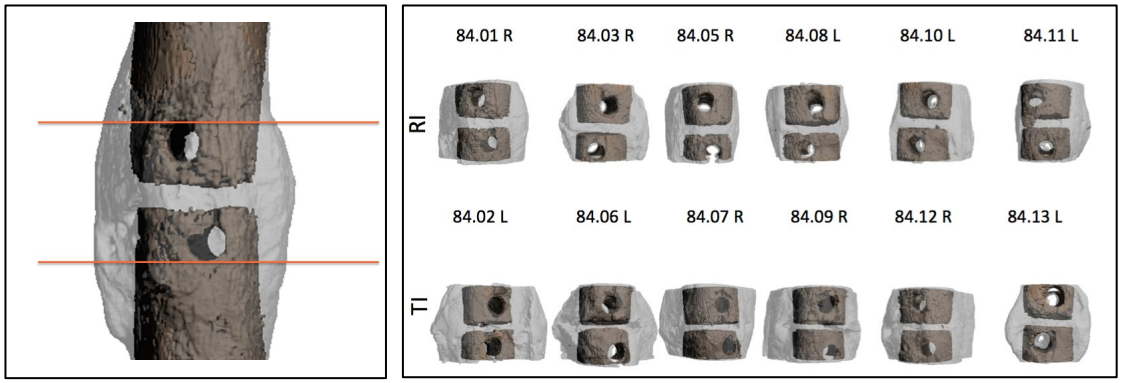

Fig. 4.16: Gap sub-analysis ROI (source: Micro-CT report Scanco Medical)

Limiting the investigation to the smaller ROI (callus volume around the gap divided into medial and lateral part) showed that:

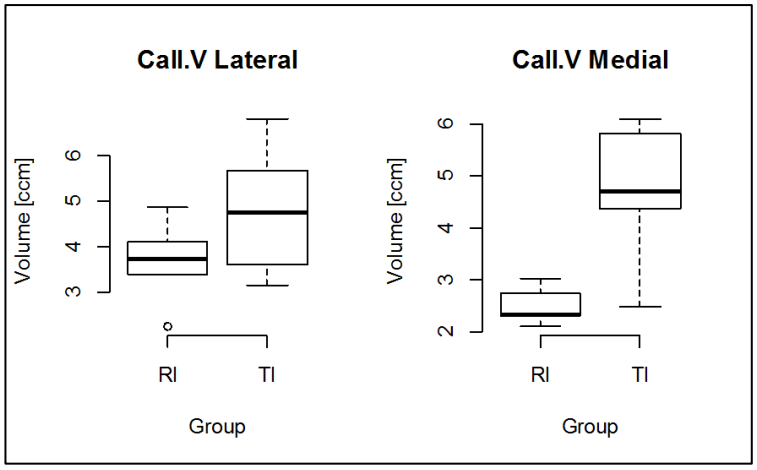

Fig. 4.17: Gap sub-analysis by orientation (source: Micro-CT Scanco Medical)

In total, the callus volume on the lateral side was higher TI (4.79 ccm ± 1.29 ccm) compared to RI (3.67 ccm ± 0.82 ccm). On the medial side TI also revealed more callus (4.7 ccm ± 1.19 ccm) compared to RI (2.48 ccm ± 0.32 ccm).

TI featured a significantly larger amount of callus on the medial side ($p=0$, TI:med-RI:med) and on the lateral side ($p<0.0001$, TI:lat-RI:lat) with respect to RI.

There was a significant ($p<0.0001$, RI:med-RI:lat) difference in the amount of medial callus compared to the lateral callus in RI.

TI featured on the medial side a significantly ($p=0.0001$, TI:med-RI:lat) larger amount of callus compared to RI on the lateral side. The medial callus amount of TI was significantly ($p=0$, RI:med-TI:lat) larger compared to the lateral amount of RI.

There is no difference between the amount of callus on the medial and on the lateral side in TI (TI:med-TI:lat).

Pair	p-value
TI:LAT-RI:LAT	0.0000198
RI:MED-RI:LAT	0.0000043
TI:MED-RI:LAT	0.0001002
RI:MED-TI:LAT	0
TI:MED-TI:LAT	0.9799711
TI:MED-RI:MED	0

Tab. 4.2: Results of gap sub analysis: Tukey post-hoc analysis

4.5.3 Microradiographs

Microradiographs revealed a radiologically completely bridged fracture gap in 5/6 sheep in both the TI and the RI group (see appendix, page 82, Fig. 7.12). Microfractures due to biomechanical testing were not included in the evaluation. The comparison between the microradiographs and the toluidine blue stained ground sections showed a high correspondence of radiopaque and blue stained structures.

4.6 Biomechanical testing

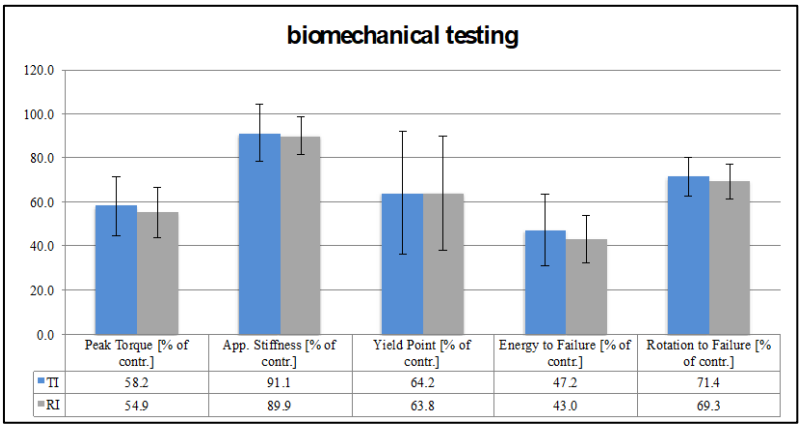

Fig. 4.18: Biomechanical testing showed slightly higher values for TI (blue) than for RI (grey).

Biomechanical testing could be performed in all 12 sheep included in the study analysis. The results are summarized in Fig. 4.18. Overall, the biomechanical evaluation revealed similar values for TI and RI.

In all biomechanical tests, the TI and RI group performed equally. TI revealed higher values for peak torque (58.2% ± 13.4) compared to RI (54.9% ± 11.3). Apparent stiffness was slightly more pronounced in TI (91.1% ± 13.0) than in RI (89.9% ± 8.4). In addition, the yield point was higher in TI (64.2% ± 27.8) than in RI (63.8% ± 25.9). Furthermore, the TI demonstrated more energy to failure (47.2% ± 16.2) compared to RI (43.0% ± 10.8). Finally, the rotation to failure value was slightly higher in TI (71.4%

± 8.7) than in RI (69.3% ± 7.9). However, statistically significant values were not found in any of the five tests, see detailed results in appendix, page 73, Tab. 7.21.

4.7 Histological evaluation

4.7.1 Histomorphometry

Twelve toluidine blue stained histological ground sections of two implant types (TI=6 and RI=6) were histomorphometrically evaluated using total and sectoral section analysis. For histological slides see appendix, page 83, Fig. 7.13.

For each sample, percentages of old bone, new bone, as well as non-bone structures (non-bone containing tissue) were measured for the total section, while for the sectoral evaluation, percentages of new bone formation (callus) in the endosteal, cis and trans area were evaluated. Overall, histomorphometrical measurements revealed a good healing of the defect area for both, TI and RI.

4.7.1.1 Total section

Results for histomorphometrical evaluation of the total section are shown in appendix, page 73, Tab. 7.22 and page 83, Fig. 7.14.

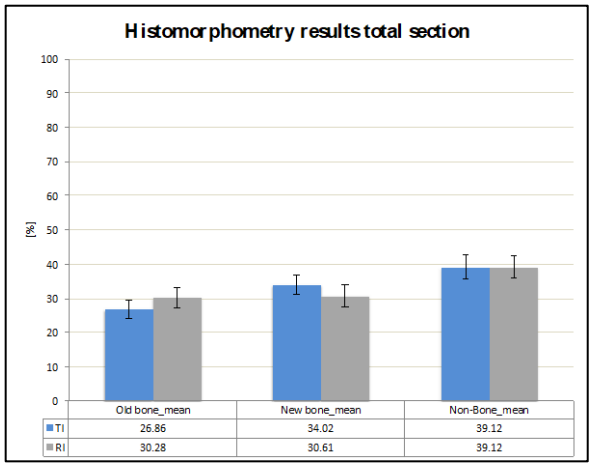

Fig. 4.19: In the TI group more old bone was resorbed (3.02%) and therefore more new bone built (3.45%) than in the RI group. Non-bone tissue was almost equal with 0.43% difference.

Overall, no significant differences were found between TI and RI for any of the values for the total section analysis. Nevertheless, the percentage of old bone matrix was slightly lower in the TI (26.86% ± 2.77) than in the RI group (30.28% ± 3.11), while slightly more new bone tissue was detected in the TI (34.02% ± 2.94) than in the RI group (30.61% ± 3.18). Non-bone tissue showed equal results in both groups, TI (39.12% ± 3.64) and RI (39.12% ± 3.22).

4.7.1.2 Sectoral section

Results for histomorphometrical evaluation of the sectoral section are shown in appendix, page 73, Tab. 7.23 and page 84, Fig. 7.15.

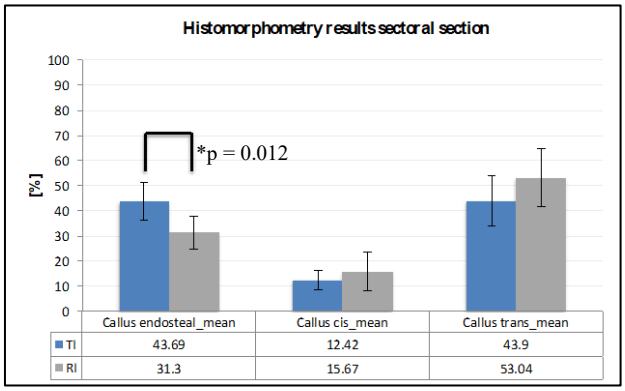

Fig. 4.20: There was a significant difference (p=0.012) in the endosteal callus amount. The TI group built 12.39 % more endosteal callus.

Significant differences were found in the sectoral evaluation for endosteal callus, with significantly (p= 0.012) higher values in the TI (43.69%) than in the RI group (31.3%). Slightly higher values for callus formation were found in the RI group at the cis cortex (15.67%) and at the trans cortex (53.04%) compared to the TI group (12.42% and 43.9%, respectively).

4.7.2 Thin section evaluation (cis/trans): quantitative and semiquantitative analysis of local tissue effects (ISO)

Assessment of biocompatibility parameters, bone remodeling and additional observations (traumatic necrosis and foreign debris) of TI and RI was performed separately in two different sections (cis and trans cortex). In the screw hole area (cortices including bone marrow cavity) only biocompatibility and additional observations were evaluated. In the defect area only bone remodeling was evaluated.

In total, 72 Hematoxylin-Eosin, toluidine blue and von Kossa stained histological sections of two implant types (TI and RI) were evaluated according to ISO-Norm 10993-6:2016(E). The evaluation was performed by two independent observers.

Individual scoring results for TI and RI are illustrated in appendix, page 74, Tab. 7.25 Anhang for the results at the cis cortex and in appendix, page 75, Tab. 7.26 for the trans cortex.

Biocompatibility (screw hole)

Under the conditions of this study, TI was considered to demonstrate a minimal reaction (ØTI - ØRI = 2.0) to the tissue at the trans cortex compared to RI. At the cis cortex

(where the LCP was placed), the TI demonstrated a slight reaction (ØTI - ØRI = 8.2) compared to RI indicating normal biodegradation and tissue remodeling.

Overall, at both cortices and in the bone marrow cavity, no polymorphonuclear cells, no eosinophils and no necrosis/osteolysis were observed in any of the samples of both groups, TI and RI.

Trans (lateral) side including bone marrow cavity:

No lymphocytes and plasma cells were found in both groups, TI and RI. Macrophages could be detected in all 6/6 TI samples and in 1/6 RI samples. They were found in the TI group in 4/6 animals in a low (score 2) and in 2/6 animals in a minimal amount (score 1). In the RI group, in one sample (84.01) a low amount (score 2) was detected. Giant cells were found in the TI group in 1/6 samples in a low amount (score 2) and in 2/6 samples in a minimal amount (score 1). In the RI group, giant cells were detected in 1/6 samples in a minimal amount (score 1). Neovascularization was found in 5/6 animals of TI and in 1/6 animals of the RI group with minimal capillary proliferation (score 1). Minimal amounts of fibrosis (score 1) were detected in 5/6 animals of the TI and in 1/6 animals of the RI group. No fatty infiltration (cortex only) was found in any of the samples of both groups. See example in appendix, page 87, Fig. 7.25.

Cis (medial) side including bone marrow cavity:

No plasma cells were found in either of both groups. Lymphocytes were detected in a minimal amount (score 1) in 2/6 animals of the TI group, whereas in the RI, no lymphocytes were found. Macrophages could be detected in all animals of both groups, TI and RI. They were found in a moderate amount (score 3) in 3/6 animals of the TI group and in 3/6 animals in a low amount (score 2). In the RI group, the amount of macrophages was low (score 2) in 3/6 animals and in 3/6 animals it was minimal (score1). Giant cells were spotted in the TI in all 6/6 animals, whereas in the RI group no giant cells were detected. Neovascularization and fibrosis was found only in a minimal amount in 1/6 animals of the RI, while in the TI group they were found in all 6/6 animals either in a minimal (score 1, 4/6 animals) or slight amount (score 2, 2/6). Low amounts of fatty infiltrates (cortex only) were found in 5/6 animals of TI group, see appendix, page 88, Fig. 7.26.

Additional observations (screw hole)

No traumatic necrosis due to the surgical procedure was detected in either group.

Metallosis was found in 5/6 TI samples and 6/6 RI samples at the cis cortex as dark brown and black stained conglomerates (see appendix, page 87, Fig. 7.24). At the trans

cortex, metallosis was only found in 3/6 RI samples. Cell associated (macrophages, giant cells) and free foreign material was detected in all evaluated TI samples (see appendix, page 86, Fig. 7.20-7.23). In the cis cortex sections, it was found in the cortex and in the bone marrow area, while in the trans cortex sections it was mostly found in the bone marrow area of the sections, described as finely stippled material.

Bone remodeling (defect area)

Trans (lateral) side including only defect area:

In the TI, osteoclasts were detected in 4/6 animals in a rare amount (score 1) and in 2/6 animals in a moderate amount (score 2), whereas all animals from the RI group showed a rare amount (score 1). Bone activity was static in 5/6 animals and in formation in 1/6 animals (84.02) in the TI group. The same level of resorption and formation (score static) was detected in 4/6 animals and only formation was seen in 2/6 animals in the RI group. 4/6 samples of TI were almost united (score 4, 76-100%), 1/6 samples was moderately united (score 3, 51-75%), 1/6 samples slightly united (score 1, <15%) (84.06). In the RI group, 4/6 samples showed a defect unity of over 76% (score 4), 1/6 samples a moderate unity (score 3, 51-75%) and 1/6 sample had no unity at all (score 0, 0%) (84.03). Sheep 84.03 and 84.06 showed a delayed-union.

Cis (medial) side including only defect area:

In the TI, no osteoclasts (score 0) were seen in 1/6 animals (84.09), in 3/6 animals a rare amount (score 1) was spotted and in 2/6 animals a moderate amount (score 2), whereas in the RI group osteoclasts were found in low numbers (score 1) in all animals. All samples from the TI showed a static bone activity, whereas in the RI in 4/6 samples a static bone activity was evaluated and in 2/6 samples in formation. The defect was in in all samples almost united or united (score 4, 76-100% defect unity).

4.7.3 Fluorescence

Fluorescence dyes are markers for bone activation (including bone activation, bone development and bone resorption) in the next 48-72 hours after injection as it binds to the calcium. See appendix page 84 and 85, Fig. 7.16- Fig. 7.19.

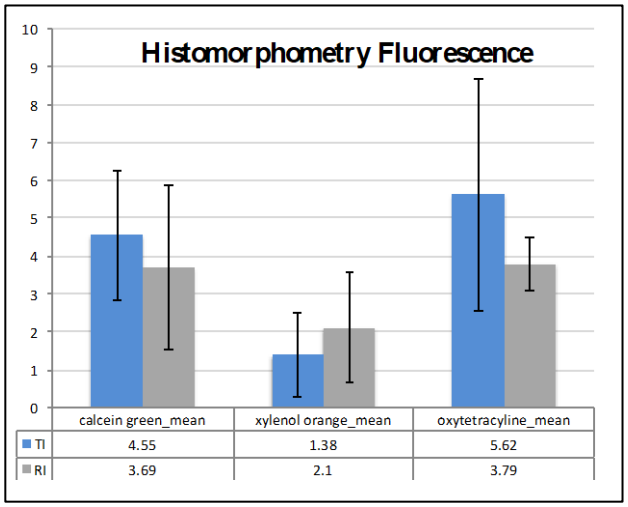

Fig. 4.21: In the different fluorescence sections there was always a slight difference between the two groups.

Quantitative evaluation at nine weeks demonstrated a dominance of calcein green (application three weeks postoperatively) in TI (4.55 ± 1.72) compared to RI (3.69 ± 2.18). Xylenol orange, which was injected six weeks postoperatively, was detected in a higher amount in RI (2.1 ± 1.46) than in TI (1.38 ± 1.11). Finally, oxytetracycline depositions (given 48 to 72 hours before sacrifice) were more prominent in TI (5.62 ± 3.08) than in RI (3.79 ± 0.7). Detailed results see appendix, page 73, Tab. 7.24.

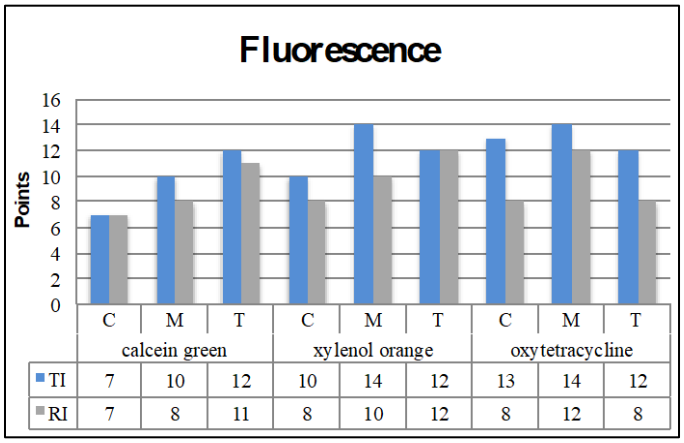

Fig. 4.22: Overall, the TI showed more fluorescence depositions compared to the RI.

The semiquantitative evaluation performed by two independent observers revealed an almost equal deposition of calcein green for TI and RI (TI: C7, M10, T12; RI: C7, M8, T11). Xylenol orange sections of TI showed more depositions at the cis cortex and intramedullary than at the trans cortex (TI: C10, M14, T12; RI: C8, M10, T12). The oxytetracycline colored slides of TI showed more fluorescence deposition in all three parts (TI: C13, M14, T12; RI: C8, M12, T8).

4.7.4 Lymph node analysis

In total, 48 lymph nodes (lnn. inguinales and poplitei treated and non-treated limb) of 12 animals were evaluated (see Fig. 4.23). Individual scoring results for TI and RI are illustrated in appendix, page 76, Tab. 7.27.

Overall, no test item related findings were detected during the lymph nodes evaluation. Minimal structure changes (score 1), characterized by slight activation of the germinative zones were found in the popliteal and inguinal lymph nodes in both groups, TI and RI. These changes were found in both limbs, treated and non-treated. In addition, only a minimal amount (score 1) of nonlocal cells (inflammatory/hypersensitivity cells) were detected in the popliteal and inguinal lymph nodes in similar amounts in both groups. Comparable scores were found for the treated and non-treated limbs.

In almost all lymph nodes of the RI and in all of the TI group, different amounts of activated foamy (epithelioid-like) macrophages were detected mostly along lymph vessels. This finding indicates non test-item related systemic reaction of unspecified origin. In 11/12 animals of both groups, no intra or extracellular foreign material could be found in either of the lymph nodes (lnn inguinales or poplitei). Only in one animal of the TI group (84.02), unidentified brownish-beige small dotlike particles were observed in the cytoplasm of foamy (epithelioid-like) macrophage aggregates detected in the right inguinal lymph node. This intracellular material was not polarizing under the microscope, and therefore could not be specified, neither as wear particles nor sleeve material (see appendix, page 88, Fig. 7.27). The Ziehl-Neelsen staining for acidophilic bacteria was negative.

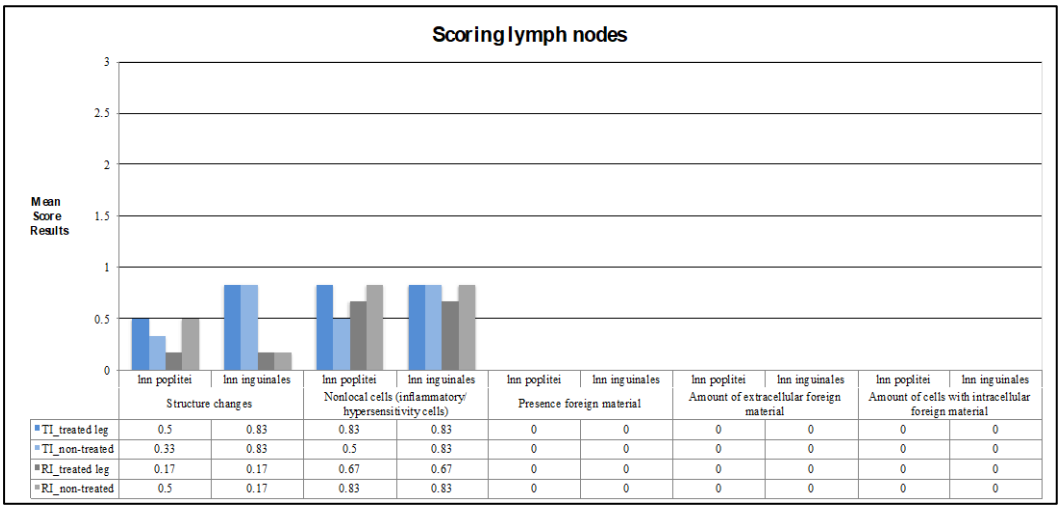

	Structure changes		Nonlocal cells (inflammatory/ hypersensitivity cells)		Presence foreign material		Amount of extracellular foreign material		Amount of cells with intracellular foreign material	
	lnn poplitei	lnn inguinales	lnn poplitei	lnn inguinales	lnn poplitei	lnn inguinales	lnn poplitei	lnn inguinales	lnn poplitei	lnn inguinales
TI_treated leg	0.5	0.83	0.83	0.83	0	0	0	0	0	0
TI_non-treated	0.33	0.83	0.5	0.83	0	0	0	0	0	0
RI_treated leg	0.17	0.17	0.67	0.67	0	0	0	0	0	0
RI_non-treated	0.5	0.17	0.83	0.83	0	0	0	0	0	0

Fig. 4.23: Results of histological scoring of 48 lymph nodes of 12 animals. TI treated leg blue, TI non-treated leg light blue; RI treated leg grey, RI non-treated leg light-grey.

5 Discussion

In this study, the VFLS has been investigated for its boosting effect on bone fracture healing through using the variable fixation technology with a suitable animal model. Perren et al. found out, that biomechanical stimuli are the inductors in fracture healing[20]. By using variable fixation technology, it should be possible to optimize biomechanical stimuli respectively strain for each phase of fracture healing. Liu et al. confirmed, that the bone healing process is driven by gradual changes in the strain and that for each of the four healing phases the ideal strain levels are slightly different[17]. The VFLS showed in this study that it has the potential to implement the theory and the present research.

Overall, the surgical procedure was optimized using cadaver surgeries and pre-operative radiographs of the sheep tibiae to measure its diameter. Only large sheep with long and straight tibiae of a wide diameter were selected for this study. A wide diameter was important as the screws for human medicine are longer (32 mm and 34 mm). The surgeries could be performed precisely and reproducibly with custom-designed drill guides. The surgery procedure was similar to a previous MSRU study[51] performed by the same surgeon.

A standardized animal model using a transverse tibia osteotomy in sheep with a 3 mm gap was needed to compare the results to those from previous studies testing new screw designs [50,51,55]. Sheep used in this study were healthy animals and did not have a predisposition for non- or delayed unions. The differences between VFLS and LS might be more evident than highlighted in this study. If only patients with a predisposition for fracture healing failures were selected for the study, the result may differ more between VFLS and LS. In the LS group less callus formation, whereas in the VFLS group a union would be expected.

Furthermore, the major differences in veterinary and human medicine are the compliances and the patient behaviour. Animals use their operated limbs right after the surgery with full weight bearing, whereas humans control their weight bearing and use crutches to protect their operated limb. To prevent a full weight bearing, sheep were kept in a suspension system for the first 3 weeks. Additionally, the operated limb was casted immediately after surgery to reduce torsional and sheer forces, as translational

sheer movement can lead to delayed or non-union[34]. However the main reason for casting was to avoid re-fracturing.

Regarding the surgery, the insertion of the VFLS was possible in all eight sheep. None of the VFLS failed after successful implantation, got loosened or elicited a problem during implant removal at sacrifice after 9 weeks. During the insertion procedure of the screws, the sleeve was often displaced and in 7/48 screws it broke one to three times. Due to that, the VFLS were inserted by hand. In some cases, the screw hole was predrilled with a VFLS without a sleeve to enlarge the hole and prevent sleeve breakage. In cadaver tests performed by our surgeon, with human and sheep tibiae, no sleeve breakage or sleeve displacement occurred while using the drilling machine. The reason for that could be that by using the drilling machine, the cis cortex had no time to contract. The sleeve often broke in the 4th screw. Anatomically, the tibia has a smaller diameter in the region where the 4th screw was implanted than in the remaining part. Due to that, the sleeve could have touched the trans cortex during insertion, slipped and then broke.
One sheep (84.04) with the 4th screw in direct connection to the gap was excluded, because the fracture healing could have been boosted by this 4th screw, in order of more bone activation and remodeling.

All evaluation methods for this study could be applied precisely, reproducibly and successfully to evaluate bone healing by using the VFLS.

At the day of sacrifice, the RI screw showed a higher value in removal torque compared to the TI screw. All screws of both groups were locked. The thread of the RI screw was in contact with the cis and trans cortex, while threads of the TI screw were only fixed in the trans cortex. In contrast to the Far Locking Screw system the VFLS did not have a problem with removal at the cis cortex. In preclinical tests with the FLS the osseointegration in the cis cortex had been far advanced, such that difficulties with threads from the trans cortex occurred during removal. Thus, the design of the final screw required adaptation such that the lag screw part was widened and even shows thread-like structures which allow for removal without complication. With the VFLS the polymer seems to keep the distance. That could be the reason why the removal torque was lower in the TI without negative consequences for the locking system. It

may be concluded that the TI is easier to remove than the RI at least after 9 weeks. This is a very relevant point as, for example, the DLS has been recalled by the FDA in 2015 due to pin breakage during removal[52].

Radiographically, the two reviewers were able to agree on the same mean score for every radiograph (semiquantitative radiographic evaluation). It was debatable, if the callus at the trans cortex of the VFLS was considered as irritation callus, as there was often a callus around the screw tip. Irritation callus might be the consequence of micro-instability[16], which in patients with predisposition to bone healing failure could be a problem. On the other hand, it could also stimulate bone healing in those people, where bone healing activity parameters are a major problem. That means, TI is able to activate the bone tissue, eliciting a reaction far from the fracture gap as well as the whole organ itself.

Exceeding callus at the cortex is not always desired and does not always mean that the bone heals properly. In the early time points between three and four weeks after surgery both groups had almost similar scores. The reason for that could be, that the sleeve resorption starts around that time and at earlier time points the VFLS acts like the LS. As for phase I of fracture healing the LS gives the reference point. Liu et al. found out that the ideal strain levels are slightly different in all four phases of bone healing[17]. The VFLS takes the different strain conditions into account to promote fracture healing. After four weeks, the TI group showed less periosteal callus compared to the RI group. Taking the histomorphometry results into account, it could be shown that the TI developed significantly more endosteal callus compared to the RI group. This increased endosteal callus formation over time provides higher stability right within the longitudinal axis of the bone. Therefore, callus formation at the trans cortex was less promoted, since the endosteal callus already ensured sufficient stability.

Furthermore, small fissures in the cortical part of the fragment at the trans cortex were often seen in the radiographs already immediately postoperatively. Osteotomies often cause little cracks at the trans cortex. Additionally, as mentioned before, the sheep tibia is very brittle and the screws (designed for human size) were at the upper limit with their diameter. Less fracture lines were detected in TI, maybe because the screw was inserted more slowly by hand and sometimes the surgeon decided to predrill with another screw.

Moreover, radiolucent zones at the cis cortex of the TI screws, where the sleeve was resorbed, were detected. However, this may be expected since resorption of the polymer was ongoing and thus, radioopacity of this area is expected to be increased. The reason could also be due to the micromotion respectively stimulation of the whole bone besides sleeve resorption (more space between bone and screw after resorption). However, in this case resorption would be expected over the entire length of fixation including the trans cortical part of the screws. Also, a more pronounced stimulation of the periost at the screw tip would then be expected. Since this was not the case and the transcortical part of the screws did not show increased radiolucency, it is safe to assume that resorption of the polymer was the reason for this radiological appearance.

In the quantitative radiographic evaluation using the OsiriX program, more callus area in total was detected for TI compared to RI. The TI group showed more callus in all three projections except at the beginning in the posterolateral projection. But both groups were almost equal in the early time points (until four weeks). As mentioned before, this indicates the same behavior of the two screws at earlier time points, when the sleeve of the VFLS was still fully present.
Furthermore, the TI group showed a callus, which was longer in size but less dense compared to the callus of the RI group. This was also confirmed in µCT, indicating that the TI was able to activate the whole bone.

In the µCT, a significantly higher callus volume in TI (17.8 ccm, p=0.004) compared to RI (9.31 ccm) and a higher bone volume was detected for the TI compared to the RI group. At the whole medial longitudinal part of the tibiae, TI built significantly (9.89 ccm, p=0.00028) more callus compared to RI (4.17 ccm). This could also be found at the lateral part of the tibia, but without significant differences (TI: 7.91 ccm; RI = 5.14 ccm).
In the ROI (gap including 3rd and 4th screw hole), TI showed more callus on the medial (4.7 ccm) and lateral side (4.79 ccm) in comparison to RI (medial 2.48 ccm; lateral 3.67 ccm). Comparing the µCT results with the histomorphometric and the semiquantitative radiographic evaluation (TI showed less cis and trans callus), results do not match at first sight. But taking into account that the histomorphometry and the semiquantitative radiographic evaluation are only a 2D view and involve only the medial and lateral

sides, it could be, that RI showed a bigger callus area when only evaluating medial and lateral sides without the anterior and posterior sides.

At the posterior side, which is only included in the µCT, more motion respectively a higher amount of callus can be caused due to muscle contraction and a physiologically higher load on the posterior limb.

In the µCT, the bone volume in the ROI of the TI group was higher compared to the RI group. As shown in the histological evaluation, the TI group had less old bone and more new bone formation. TI showed more callus and bone volume compared to RI in the µ-CT. On the one hand, the threshold plays an important role in the µCT evaluation. It depends, where the threshold was set to recognize old bone and new bone respectively callus. On the other hand, as mentioned before, the radiographic evaluation is a 2D view and endosteal callus or bone formation in the posterior and anterior projection cannot be detected. However, the fact that TI showed less old but more new bone formation could also mean that due to the dynamization of the bone healing process more active remodeling at the osteotomy side had taken place. These results are corroborated with the results of intravital fluorescence staining, where the VFLS showed higher values.

In the semiquantiative radiographic and µCT evaluation, callus and bone density of the whole tibia were significantly higher in RI compared to TI. Due to an activated remodeling process where in the TI group old bone was rebuilt to new bone, the bone density was lower due to a smaller amount of old bone with high density compared to the RI group. The TI group showed significantly more callus volume in the µCT. As the results of the mechanical tests did not detect significant differences between groups in any of the investigated variables. It could be concluded that the development of the large amount of callus in the TI group was still in the physiological mechanical property range leading to successful gap closure.

Furthermore, the callus area of the TI group was much longer compared to the RI group. Another reason to note could be that the RI group has formed a more compact callus, which was smaller and already receding.

The higher polar moment of inertia in all sections of the TI group, indicated more callus around the bone axis which was well distributed proximal and distal to the fracture gap. This is another indication that the entire bone has been activated. Furthermore, the analysis of principal axes showed a higher Imax/Cmax and Imin/Cmin around the segmental defect in the TI group compared to the RI group. This could suggest that torsional stiffness and breaking strength were higher in the TI group.

Biomechanically, the RI and TI group showed almost equal results with slightly higher values for TI. It could be, that the higher amount of endosteal callus in the TI group had an important effect on fracture stabilization. It has been proven that an unstable fixation could cause a larger amount of callus ("irritation callus")[16] and afterwards led to pseudoarthrosis[33]. But in our study, with no significant differences in the mechanical properties, it seems that with the VFLS more callus volume can be built without compromising the tissue resistance (normal callus). The RI group had a denser callus and more concentrated at the trans cortical, resp. lateral sides compared to the TI, which showed a more even distribution between trans and cis cortex. In addition, endosteal callus is usually less dense compared to the cortical callus which is more like a shell and resists better to torsional and shear forces. Nevertheless, the combination of the endosteal and more evenly distributed callus resulted in comparable numbers for the biomechanical tests. For patients with predispositions for fracture failure, a more even distributed and endosteal callus may be favourable meaning more chances to gain complete fracture healing. Histologically, due to the micromotion of the VFLS group, more old bone was resorbed and more new bone was built (total section histomorphometry). When thinking of the human patients predisposed to delayed-union and non-union, such an active process is welcome. In the sectoral histomorphometrical analysis, the TI group showed significantly more endosteal callus ($p=0.012$; TI 43.69%) compared to the RI group (31.3%). The reason for that could be, that the endosteal callus was built to stabilize the fracture during the micromotion.

Compared to the study of Richter et al. testing the DLS, our RI group performed much better compared to the RI group of Richter et al., even under the same conditions as the control group of this study[51]. The reason for this could not be explained except the fact that the mechanical tests were not performed by the same person and that the Instron machine may have been adapted in the mean time (ca. 6 years in between tests). Nevertheless, since results were compared to internal controls the results are validated within the specimens of the same animals and can be accepted.

Overall, under these experimental study conditions, the histological findings demonstrated a good biocompatibility of the VFLS (following test guideline: ISO 10993-6: 2016), in comparison to the RI screw (cis cortex ØTI - ØRI = 8.2 and trans cortex ØTI - ØRI = 2.0). The TI did not induce significant tissue effects. No acute or

chronic-active inflammation and no necrosis/osteolysis or abnormal tissue reaction were observed compared to RI after 9 weeks.

At the cis cortex and in the medullary cavity of TI, a higher amount of macrophages and giant cells was observed due to the degradation of the resorbable sleeve. The free and cell associated (within macrophages and giant cells) foreign material, which was also found at both cortices, is considered to be residuals of the resorbed sleeve, as this material was only found in the TI group. The sleeve degradation led to increased inflammatory infiltration and tissue remodeling response with slightly higher scores for fibrosis and neovascularization. This was expected, as the screw design is such that after sleeve resorption (within the first 3-4 weeks), the fixation of the bone fragments is limited and only provided by the trans cortex to allow micromotion. 5/6 samples of the TI group revealed some fatty infiltration in the screw hole at the cis cortex. With the sleeve positioned in the cis cortex and the bone marrow cavity, some fatty tissue and cells from the bone marrow cavity might have infiltrated the empty space at the cis cortex after sleeve degradation. Additional to the above mentioned increase of inflammatory cells (macrophages, giant cells) and tissue remodeling response, the fatty infiltration contributed to a slightly increased biocompatibility end-score, which resulted in a slight reaction of TI compared to RI at the cis cortex. Differences between TI and RI at the trans cortex did reflect a similar situation, however here, detectable differences were even smaller (minimal reaction).

Metallosis was detected in both groups. These findings were detected in most preclinical investigations performed with locking plates. There are several explanations for the metallosis. On one hand, due to the metal-on-metal friction between screw head and screw hole of the plate, which could trigger metallic particles to loosen, thereby causing metallosis. On the other hand, the particles could come from bending of the plate and screwing in the drill sleeve with drilling the hole. Depuy Synthes has analyzed these particles in previous studies performed by our group using the same titanium plate and drill sleeves and found that the particles consist of steel (of the drill sleeve) and not of titanium (of the screw).

Using the semiquantitave evaluation method, more intense fluorescence depositions were detected in the TI group compared to the RI group. However, this was not the case in the quantitative evaluation, where the RI group revealed more xylenol orange depositions. The quantitative fluorescence evaluation could have many biases, because the threshold was difficult to set and it was a rather subjective view. Fluorescence dyes are markers for bone activation (including bone activation, bone development and bone

resorption) within 48 hours after injection binding to the calcium and being embedded in newly formed bone[62]. Due to the micromotion and the increased resorption of old bone and new bone formation it is clear that in the TI group the bone is more activated and therefore accumulates more fluorescence.

Due to the sleeve resorption, lymph nodes could have been stimulated in the TI group, leading to more structure changes compared to the RI group.
Whereas, the amount of nonlocal cells found in lymph nodes was similar for both, RI and TI group, which indicates a non test-item related system reaction. These findings could also be induced by stress-related immunosuppression (e.g. surgical intervention) and increased sensibility to bacterial infection or parasitic infestation. The appearance of activated foamy (epithelioid-like) macrophages mostly along lymph vessels was detected in both groups, TI and RI. They were interpreted also as non test-item related findings of unspecified origin. No clinical abnormalities or other abnormal findings were observed in any of the twelve operated sheep, so that these findings can be considered having no impact on the study outcome.

5.1 Conclusion

In conclusion, the results of this study confirm that the variable fixation technology using the Variable Fixation Locking Screw has some boosting effects on bone fracture healing. The results of this study also demonstrate that the VFLS is a biocompatible and safe medical device as good as the commercial titanium Locking Screw (RI), as none of the sheep implanted with VFLS showed any signs of abnormal systemic response. The sleeve degradation was as expected.

A new medical device is urgently needed, as population numbers are rising rapidly[7,8] and the expensive costs of fracture healing failure are increasing enormously[6].

Since today, the VFLS would be the first screw on the market, which has a variable strain magnitude and not a constant strain. The activation of the entire bone as an organ, suggest that the VFLS has the potential to increase the success rate of biological osteosynthesis in the target group (older people, predisposed for delayed- and non-union).

However, further clinical studies in human medicine are required to clarify the outcome of VFLS in human patients with predispositions for bone healing failure.

6 References

1. Wang Z, Bhattacharyya T: Trends of non-union and prescriptions for non-steroidal anti-inflammatory drugs in the United States, 1993-2012. Acta Orthop 86:632-637, 2015.
2. Papakostidis C, Grotz MR, Papadokostakis G, et al: Femoral biologic plate fixation. Clin Orthop Relat Res 450:193-202, 2006.
3. Jayakumar P, Jupiter JB: Non-union in forearm fractures. Acta Chir Orthop Traumatol Cech 81:22-32, 2014.
4. Wolinsky PR, McCarty E, Shyr Y, et al: Reamed intramedullary nailing of the femur: 551 cases. J Trauma 46:392-399, 1999.
5. Peter V. Giannoudis RA: Management of long-bone non-unions. Elsevier Injury, Int J Care Injured 38:1-2, 2007.
6. Versicherung SSU: Sammelstelle für die Statistik der Unfallversicherung UVG. 2017.
7. Singer BR, McLauchlan GJ, Robinson CM, et al: Epidemiology of fractures in 15,000 adults: the influence of age and gender. J Bone Joint Surg Br 80:243-248, 1998.
8. Affairs UNDoEaS: Wold Population Ageing 2013. 2013.
9. Klonoff DC: The increasing incidence of diabetes in the 21st century. J Diabetes Sci Technol 3:1-2, 2009.
10. Spanheimer RG, Umpierrez GE, Stumpf V: Decreased collagen production in diabetic rats. Diabetes 37:371-376, 1988.
11. centre WM: Obesity and overweight. 2015.
12. Copuroglu C, Calori GM, Giannoudis PV: Fracture non-union: who is at risk? Injury 44:1379-1382, 2013.
13. Lujan TJ, Henderson CE, Madey SM, et al: Locked plating of distal femur fractures leads to inconsistent and asymmetric callus formation. J Orthop Trauma 24:156-162, 2010.
14. Schell H, Thompson MS, Bail HJ, et al: Mechanical induction of critically delayed bone healing in sheep: radiological and biomechanical results. J Biomech 41:3066-3072, 2008.
15. Rodriguez-Merchan EC, Forriol F: Nonunion: general principles and experimental data. Clin Orthop Relat Res:4-12, 2004.
16. Frolke JP, Patka P: Definition and classification of fracture non-unions. Injury 38 Suppl 2:S19-22, 2007.
17. Liu C, Carrera R, Flamini V, et al: Effects of mechanical loading on cortical defect repair using a novel mechanobiological model of bone healing. Bone 108:145-155, 2018.
18. Thomas P. Rüedi AF: AO Principles of Fracture Management: Vol. 1: Prinicples, Vol. 2: Specific fractures (ed 2nd Edition). Stuttgart, Germany, Thieme Publishing Group, 2007.
19. Claes L: Biologie und Biomechanik der Osteosynthese und Frakturheilung. Orthopädie und Unfallchirurgie up2date 1:329-346, 2006.
20. Perren SM, Fernandez A, Regazzoni P: Understanding Fracture Healing Biomechanics Based on the "Strain" Concept and its Clinical Applications. Acta Chir Orthop Traumatol Cech 82:253-260, 2015.
21. Perren SM: Evolution of the internal fixation of long bone fractures. The scientific basis of biological internal fixation: choosing a new balance between stability and biology. J Bone Joint Surg Br 84:1093-1110, 2002.

22. Schmidt U, Penzkofer R, Bachmaier S, et al: Implant material and design alter construct stiffness in distal femur locking plate fixation: a pilot study. Clin Orthop Relat Res 471:2808-2814, 2013.
23. Lill H, Hepp P, Korner J, et al: Proximal humeral fractures: how stiff should an implant be? A comparative mechanical study with new implants in human specimens. Arch Orthop Trauma Surg 123:74-81, 2003.
24. Kralinger F, Gschwentner M, Wambacher M, et al: Proximal humeral fractures: what is semi-rigid? Biomechanical properties of semi-rigid implants, a biomechanical cadaver based evaluation. Arch Orthop Trauma Surg 128:205-210, 2008.
25. Goodship AE, Cunningham JL, Kenwright J: Strain rate and timing of stimulation in mechanical modulation of fracture healing. Clin Orthop Relat Res:S105-115, 1998.
26. Epari DR, Schell H, Bail HJ, et al: Instability prolongs the chondral phase during bone healing in sheep. Bone 38:864-870, 2006.
27. Cordey SMPuJ: Die Gewebsdifferenzierung in der Frakturheilung. Unfallheilkunde Traumatology Springer-Verlag 1977 80:161-164, 1977.
28. Perren SM: Physical and biological aspects of fracture healing with special reference to internal fixation. Clin Orthop Relat Res:175-196, 1979.
29. Chao EY, Aro HT, Lewallen DG, et al: The effect of rigidity on fracture healing in external fixation. Clin Orthop Relat Res:24-35, 1989.
30. K. A. Egol ENK, E. Fulkerson, F. J. Kummer, K. J. Koval: Biomechanics of Locked Plates and Screws. J Orthop Trauma 18 Number 8:488-493, 2004.
31. Goodship AE, Kenwright J: The influence of induced micromovement upon the healing of experimental tibial fractures. J Bone Joint Surg Br 67:650-655, 1985.
32. Wolf S, Janousek A, Pfeil J, et al: The effects of external mechanical stimulation on the healing of diaphyseal osteotomies fixed by flexible external fixation. Clin Biomech (Bristol, Avon) 13:359-364, 1998.
33. Egol KA, Kubiak EN, Fulkerson E, et al: Biomechanics of locked plates and screws. J Orthop Trauma 18:488-493, 2004.
34. Steiner M, Claes L, Ignatius A, et al: Numerical simulation of callus healing for optimization of fracture fixation stiffness. PLoS One 9:e101370, 2014.
35. Hente R, Lechner J., Füchtmeier B.: Der Einfluss einer zeitlich limitierten kontrollierten Bewegung auf die Frakturheilung. deutsche Gesellschaft der experimentellen Unfallchirurgie C6.1:23-24, 2001.
36. Kenwright J, Richardson JB, Goodship AE, et al: Effect of controlled axial micromovement on healing of tibial fractures. Lancet 2:1185-1187, 1986.
37. Klein P, Schell H, Streitparth F, et al: The initial phase of fracture healing is specifically sensitive to mechanical conditions. J Orthop Res 21:662-669, 2003.
38. Kenwright J, Richardson JB, Cunningham JL, et al: Axial movement and tibial fractures. A controlled randomised trial of treatment. J Bone Joint Surg Br 73:654-659, 1991.
39. Gardner MJ, Nork SE, Huber P, et al: Stiffness modulation of locking plate constructs using near cortical slotted holes: a preliminary study. J Orthop Trauma 23:281-287, 2009.
40. Stoffel K, Dieter U, Stachowiak G, et al: Biomechanical testing of the LCP--how can stability in locked internal fixators be controlled? Injury 34 Suppl 2:B11-19, 2003.
41. Goldstein C, Sprague S, Petrisor BA: Electrical stimulation for fracture healing: current evidence. J Orthop Trauma 24 Suppl 1:S62-65, 2010.

42. Hannemann PF, Mommers EH, Schots JP, et al: The effects of low-intensity pulsed ultrasound and pulsed electromagnetic fields bone growth stimulation in acute fractures: a systematic review and meta-analysis of randomized controlled trials. Arch Orthop Trauma Surg 134:1093-1106, 2014.
43. Deckers MM, van Bezooijen RL, van der Horst G, et al: Bone morphogenetic proteins stimulate angiogenesis through osteoblast-derived vascular endothelial growth factor A. Endocrinology 143:1545-1553, 2002.
44. Konda SR, Christiano A, Fisher N, et al: Femoral Nonunion With Iliac Crest Bone Graft. J Orthop Trauma 31 Suppl 3:S19-S20, 2017.
45. Choi YS, Kim KS: Plate augmentation leaving the nail in situ and bone grafting for non-union of femoral shaft fractures. Int Orthop 29:287-290, 2005.
46. Synthes: Small Fragment Locking Compression Plate (LCP) System. Stainless steel and titanium., 2002.
47. Cronier P, Pietu G, Dujardin C, et al: The concept of locking plates. Orthop Traumatol Surg Res, 2010.
48. Synthes: Dynamic Locking Screw (DLS) System.
For use with locking compression plate (LCP) systems., in Synthes (ed), Vol, 2011.
49. Lagerpusch N: Die Dynamisierung der winkelstabilen Plattenosteosynthese mit Hilfe der „Dynamic Locking Screw“ (DLS) –
Eine experimentelle Studie an Schafen, in Zürich MT (ed), Vol, 2011.
50. Dobele S, Horn C, Eichhorn S, et al: The dynamic locking screw (DLS) can increase interfragmentary motion on the near cortex of locked plating constructs by reducing the axial stiffness. Langenbecks Arch Surg 395:421-428, 2010.
51. Richter H, Plecko M, Andermatt D, et al: Dynamization at the near cortex in locking plate osteosynthesis by means of dynamic locking screws: an experimental study of transverse tibial osteotomies in sheep. J Bone Joint Surg Am 97:208-215, 2015.
52. Administration FFaD: Class 2 Device Recall Dynamic Locking Screw System (DLS) 3.7mm & Dynamic Locking Screw (DLS) 5.0mm, in FDA (ed), Vol. http://www.accessdata.fda.gov, 2015.
53. Zimmer®: Zimmer® MotionLoc® Screw for the Periarticular Locking Plate System, in, Vol, 2015.
54. Doornink J, Fitzpatrick DC, Madey SM, et al: Far cortical locking enables flexible fixation with periarticular locking plates. J Orthop Trauma 25 Suppl 1:S29-34, 2011.
55. Bottlang M, Lesser M, Koerber J, et al: Far cortical locking can improve healing of fractures stabilized with locking plates. J Bone Joint Surg Am 92:1652-1660, 2010.
56. Martini L, Fini M, Giavaresi G, et al: Sheep model in orthopedic research: a literature review. Comp Med 51:292-299, 2001.
57. Nunamaker DM: Experimental models of fracture repair. Clin Orthop Relat Res:S56-65, 1998.
58. Pearce AI, Richards RG, Milz S, et al: Animal models for implant biomaterial research in bone: a review. Eur Cell Mater 13:1-10, 2007.
59. Ravaglioli A, Krajewski A, Celotti GC, et al: Mineral evolution of bone. Biomaterials 17:617-622, 1996.
60. Willie BM, Bloebaum RD, Bireley WR, et al: Determining relevance of a weight-bearing ovine model for bone ingrowth assessment. Journal of Biomedical Materials Research Part A 69a:567-576, 2004.

61. Leow JM, Clement ND, Tawonsawatruk T, et al: The radiographic union scale in tibial (RUST) fractures: Reliability of the outcome measure at an independent centre. Bone Joint Res 5:116-121, 2016.
62. van Gaalen SM, Kruyt MC, Geuze RE, et al: Use of fluorochrome labels in in vivo bone tissue engineering research. Tissue Eng Part B Rev 16:209-217, 2010.

7 Appendix

7.1 Tables

7.1.1 Material and Methods

Tab. 7.1: Overview of the groups with animal ID, Side of the operated limb, weight (kg) with mean and STD, Age (years) with mean and STD. Animals, 84.04 and 84.14 were excluded from the study.

Group	Animal ID	Side	Weight (kg)	Mean_ STD	Age (years)	Mean_STD	State
RI	84.01	right	74.6	75.0 ± 3.96	3.0	3.0 ± 0.0	included
	84.03	right	73.8		3.0		included
	84.05	right	71.9		3.0		included
	84.08	left	79.5		3.0		included
	84.10	left	80.0		3.0		included
	84.11	left	70.3		3.0		included
TI	84.02	left	72.8	75.0 ± 3.47	3.0	3.0 ± 0.0	included
	84.13	left	74.8		3.0		included
	84.06	left	71.1		3.0		included
	84.07	right	74.7		3.0		included
	84.09	right	75.5		3.0		included
	84.12	right	81.3		3.0		included
	84.04	left	77.1		3.0		excluded
	84.14	right	83.5		3.0		excluded

Tab. 7.2: Semiquantitative radiographic evaluation – scoresystem for the three projections over 9 weeks: ap = anteroposterior (0°) and two angled planes: anterior = anterolateral (275°) and posterior = posterolateral (265°).

M SRU 0084
Sheep: 84.__

M SRU Vetsuisse Faculty

Universität Zürich[UZH]

Callus area			Score	0w	3w	4w	5w	6w	7w	8w	9w	Notes
ap	Cortical callus formation	no callus noted	0									
		callus not reaching into the defect	1									
		callus bridging the defect < 50%	2									
		Callus bridging the defect >50% but <100 %	3									
		Callus bridging the defect completely	4									
	RUST Score	a) fracture with a fracture line and no callus formation	1									
		b) a fracture with callus formation and a fracture line	2									
		c) a fracture with bridging callus, but the fracture line is still visible across both cortices	3									
		d) complete bridging of the callus with no evidence of fracture line	4									
	cis-cortex	no callus noted	0									
		callus not reaching into the defect	1									
		callus reaching into the defect, fracture line in callus visible	2									
		callus reaching into the defect, fracture line in callus less visible	3									
		callus reaching into the defect, fracture line in callus not visbile	4									
	trans-cortex	no callus noted	0									
		callus not reaching into the defect	1									
		callus reaching into the defect, fracture line in callus visible	2									
		callus reaching into the defect, fracture line in callus less visible	3									
		callus reaching into the defect, fracture line in callus not visbile	4									
anterior	Within osteotomy/ cortical gap: Fracture ends											
		no callus noted	0									
		callus not reaching into the defect	1									
		callus reaching into the defect, fracture line in gap visible	2									
		callus reaching into the defect, fracture line in gap less visible	3									
		callus reaching into the defect, fracture line in gap not visbile	4									
posterior	Within osteotomy/ cortical gap: Fracture ends											
		no callus noted	0									
		callus not reaching into the defect	1									
		callus reaching into the defect, fracture line in gap visible	2									
		callus reaching into the defect, fracture line in gap less visible	3									
		callus reaching into the defect, fracture line in gap not visbile	4									
Callus opacity			**Score**	**0w**	**3w**	**4w**	**5w**	**6w**	**7w**	**8w**	**9w**	
ap	Callus maturity/radiopacity realtive to normal cortical opacity	soft tissue opacity	0									
		<50% of normal	1									
		>50-100% of normal	2									
		> 100% (superimposition)	3									
Bone activation			**Score**	**0w**	**3w**	**4w**	**5w**	**6w**	**7w**	**8w**	**9w**	
		Callus around screwtip										

Tab. 7.3: Thin section –score system for the biocompatibility (screw hole). 1. Inflammation and 2. Tissue response.

Biocompatibility (Screw hole)

1. Inflammation: Scoring scheme for inflammatory cells

Cell type/response	Score				
	0	1	2	3	4
Polymorphonuclear cells	0	Rare, 1-5/phf[a]	5-10/phf	Severe infiltrate	Packed sheets
Eosinophils	0				
Lymphocytes	0				
Plasma cells	0				
Macrophages	0				
Giant cells	0	Rare, 1-2/phf	3-5/phf		
Necrosis	0	Minimal	Mild	Moderate	Severe

[a] phf per high-powered field (400x)

2. Tissure response: Scoring scheme for tissue reactions

Response	Score				
	0	1	2	3	4
Neovascularization	0	Minimal Capillary Proliferation, focal, 1-3 buds	Groups of 4-7 capillaries with supporting fibroblastic structures	Broad band of capillaries with supporting fibrotic structures	Extensive band of capillaries with supporting fibroblastic structures
Fibrosis	0	Narrow band	Moderately thick band	Thick band	Extensive band
Fatty infiltrate	0	Minimal amount of fat associated with fibrosis	Several layers of fat and fibrosis	Elongated and broad accumulation of fat cells about the implant side	Extensive fat completely surrounding the implant

Tab. 7.4: Thin section –score system for the additional observations (screw hole). Traumatic necrosis and foreign debris (biomaterial parameters).

Additional observations (Screw hole)

Traumatic necrosis

Traumatic nectosis due to surgery	
0	no
1	yes

Foreign debris: Scoring scheme for biomaterial parameters

Biomaterial parameters	Score			
	Not present / not fragmented	Free	Cell associated (macrophage)	Free and cell associated
Foreign residuals (fragmentation/debris)	0	1	2	3

" granulated finely stippled material free and cell associated

* metallosis

Tab. 7.5: Thin section –score system for defect area: Amount of osteoclasts, bone activity and defect unitiy.

Defect healing (Defect area)

Osteoclasts: Scoring scheme osteoclasts

Score	Percentage of cells per microscopic field [%]
0	none
1	rare 1-5 cells/hpf
2	moderate amount, 6-10 cells/ hpf
3	abundant amount >11 cells/hpf

Bone activity: Bone remodeling (bone resorption br versus bone formation bf)

Level		Definition/Score
br>bf	increased bone resorption compering to formation , negative remodeling (bone resporption)	bone resorption/R
br=bf	same level/ static	static/S
bf>br	increased boneformation compering to resorption , positive remodeling (bone formation)	formation/F

Defect unitiy: Scoring scheme for Defect unity (healing process)

Response	Score				
	0	1	2	3	4
Defect united in %	0	<15% not united	16-50% united	51-75%united	76-100% united

Tab. 7.6: Lymph nodes –score system including structure changes, nonlocal cells, presence of foreign material, amount of extracellular foreign material if present and amount of cells with intracellular foreign material only if present.

Evaluation criteria of lymph nodes MSRU0084

Structure changes	Score	Lymph node
none	0	-
mild abnormalities	1	secondary follicle activation, cortex vascular lesions (dilation of blood and/or lymphatic vessels)
moderate abnormalities	2	Localized: Secondary follicle hyperplasia/ follicular depletion (atrophy), lymphatic sinus ectasia,medullar and cortex vascular lesions (dilation of blood and/or lymphatic vessels), macrophage hyperplasia (Histiocytosis-cortical-sinus)
severe abnormalities	3	Whole organ (Cortex, Paracortex, Medulla): Secondary follicle Hyperplasia/ Follicular depletion (atrophy), lymphatic sinus ectasia,medullar and cortex vascular lesions (dilation of blood and/or lymphatic vessels), macrophage hyperplasia (cortical and medullary sinus)

Nonlocal Cells (inflammatory/hypersensitivity cells)	Score	
none	0	-
mild abnormalities	1	inflammatory cells focal/single cells
moderate abnormalities	2	inflammatory cells multifocal/several cells
severe abnormalities	3	inflammatory cells multifocal to confluent/high amount

Presence of foreign material	Score
none	0
macrophage bound	1
free	2
free and macrophage bound	3

Amount of extracellular foreign material only if present!	Score
none	0
some (focal)	1
moderate amount (scattered foci)	2
abundant amount (multifocal to coalescing)	3

Amount of cells with intracellular foreign material only if present!	Score
none	0
1 to 5	1
6 to 10	2
more than 10	3

Structure changes: deviation from physiological organ structure

7.1.2 Results

Tab. 7.7: Sacrifice results of both Groups, TI and RI. Fibrosis, callus around screw hole, amount of unlocked screw, removal torque of each screw and mean.

Group	Animal	Schrew hole	Fibrosis	Total fibrosis	Callus around screw hole	Total callus around screw hole	Unlocked screw	Total unlocked screw	Removal torque	Mean removal torque	Total fibrosis	Total callus around screw hole	Total unlocked screw	Mean removal troque
Reference Item	84.01	1	-	0	-	0	-	0	2.4	2.82	0.00	0	none	2.79
		2	-		-		-		1.75					
		3	-		-		-		4.5					
		4	-		-		-		2.25					
		5	-		-		-		4.25					
		6	-		-		-		1.75					
	84.03	1	-	0	-	0	-	0	3.25	2.7				
		2	-		-		-		3.25					
		3	-		-		-		2					
		4	-		-		-		2.3					
		5	-		-		-		NA					
		6	-		-		-		2.7					
	84.05	1	-	0	-	0	-	0	3.5	2.77				
		2	-		-		-		3.5					
		3	-		-		-		3.5					
		4	-		-		-		1.25					
		5	-		-		-		1.75					
		6	-		-		-		3.1					
	84.08	1	-	0	-	0	-	0	3.37	2.93				
		2	-		-		-		3.3					
		3	-		-		-		3.94					
		4	-		-		-		2.55					
		5	-		-		-		2.54					
		6	-		-		-		1.89					
	84.10	1	-	0	-	0	-	0	3.14	2.75				
		2	-		-		-		2.9					
		3	-		-		-		2.79					
		4	-		-		-		3.22					
		5	-		-		-		NA					
		6	-		-		-		1.68					
	84.11	1	-	0	-	0	-	0	3.79	2.80				
		2	-		-		-		4.67					
		3	-		-		-		1.92					
		4	-		-		-		3.18					
		5	-		-		-		1.17					
		6	-		-		-		2.04					
Test Item	84.02	1	-	0	-	3	-	0	1	1.27	6.00	10	none	2.01
		2	-		-		-		0.9					
		3	-		+++		-		2.3					
		4	-		-		-		1					
		5	-		-		-		1.4					
		6	-		-		-		1					
	84.06	1	-	0	-	0	-	0	1.75	1.61				
		2	-		-		-		2.6					
		3	-		-		-		0.5					
		4	-		-		-		0.80					
		5	-		-		-		2					
		6	-		-		-		2					
	84.07	1	-	0	+	3	-	0	3.79	2.86				
		2	-		+		-		1.46					
		3	-		+		-		2.51					
		4	-		-		-		3.45					
		5	-		-		-		3.25					
		6	-		-		-		2.67					
	84.09	1	-	0	-	4	-	0	1.92	2.36				
		2	-		-		-		2.49					
		3	-		+++		-		1.7					
		4	-		+		-		1.82					
		5	-		-		-		2.77					
		6	-		-		-		3.43					
	84.12	1	-	0	-	0	-	0	2.15	2.03				
		2	-		-		-		3.47					
		3	-		-		-		2.32					
		4	-		-		-		1.31					
		5	-		-		-		1.61					
		6	-		-		-		1.33					
	84.13	1	+	6	-	0	-	0	1.17	1.95				
		2	+		-		-		2.32					
		3	+		-		-		2.2					
		4	+		-		-		2.21					
		5	+		-		-		2.63					
		6	+		-		-		1.18					

not present (-), minimal amount (+), moderate amount (++), high amount (+++)

Tab. 7.8: Cortical callus formation -in the semiquantitative radiologic evaluation

Group	Measured Parameter: Cortical Callus Formation							
	0w	3w	4w	5w	6w	7w	8w	9w
TI	x	2.17 ± 1.33	2.33 ± 0.52	2.67 ± 0.82	2.67 ± 0.82	2.75 ± 0.88	2.92 ± 0.8	2.75 ± 0.88
RI	x	1.75 ± 0.88	2.58 ± 0.8	2.67 ± 0.92	3.08 ± 0.92	3.5 ± 0.63	3.42 ± 0.92	3.67 ± 0.41
Legend: TI = Test Item, RI = Reference Item								

Tab. 7.9: RUST score -in the semiquantitative radiologic evaluation

Group	Measured Parameter: RUST Score							
	0w	3w	4w	5w	6w	7w	8w	9w
TI	x	1.92 ± 0.67	2 ± 0	2.33 ± 0.52	2 ± 0	2.33 ± 0.52	2.25 ± 0.42	2.25 ± 0.42
RI	x	2 ± 0.55	2.25 ± 0.61	2.5 ± 0.55	2.58 ± 0.67	2.58 ± 0.67	2.75 ± 0.42	2.75 ± 0.42
Legend: TI = Test Item, RI = Reference Item								

Tab. 7.10: Callus area cis-cortex -in the semiquantitative radiologic evaluation

Group	Measured Parameter: Callus Area Cis-Cortex							
	0w	3w	4w	5w	6w	7w	8w	9w
TI	x	0 ± 0	1.08 ± 0.92	1.17 ± 0.82	1.17 ± 0.93	2.17 ± 1.17	2 ± 0.9	2.42 ± 0.49
RI	x	0.17 ± 0.26	1.17 ± 0.98	1.75 ± 0.88	2 ± 0	2.25 ± 0.76	2.51 ± 0.45	2.83 ± 0.41
Legend: TI = Test Item, RI = Reference Item								

Tab. 7.11: Callus area trans-cortex -in the semiquantitative radiologic evaluation

Group	Measured Parameter: Callus Area Trans-Cortex							
	0w	3w	4w	5w	6w	7w	8w	9w
TI	x	0 ± 0	1.08 ± 0.8	1.33 ± 0.52	1.17 ± 0.75	1.83 ± 1.03	1.75 ± 0.69	2.08 ± 1.12
RI	x	1.17 ± 0.68	1.83 ± 0.75	1.59 ± 0.49	2.17 ± 0.41	2.5 ± 0.55	2.5 ± 0.84	2.67 ± 0.52
Legend: TI = Test Item, RI = Reference Item								

Tab. 7.12: Callus area cranial cortical gap -in the semiquantitative radiologic evaluation

Group	Measured Parameter: Callus Area Cranial Cortical Gap							
	0w	3w	4w	5w	6w	7w	8w	9w
TI	x	0.2 ± 0.45	1 ± 0.63	1.33 ± 0.52	1 ± 0.63	1.09 ± 1.2	1.75 ± 0.76	1.58 ± 1.02
RI	x	0.42 ± 0.49	1.17 ± 0.75	1.75 ± 0.99	1.75 ± 0.42	1.42 ± 0.86	1.83 ± 0.98	1.83 ± 0.98
Legend: TI = Test Item, RI = Reference Item								

Tab. 7.13: Callus area caudal cortical gap -in the semiquantitative radiologic evaluation

Group	Measured Parameter: Callus Area Caudal Cortical Gap							
	0w	3w	4w	5w	6w	7w	8w	9w
TI	x	0.33 ± 0.52	1.25 ± 0.42	1.75 ± 0.42	1.75 ± 0.88	1.58 ± 1.16	2.25 ± 0.61	1.92 ± 1.12
RI	x	0.58 ± 0.59	1.75 ± 0.42	1.91 ± 1.02	2.33 ± 0.52	2.08 ± 0.67	2.5 ± 0.78	2.42 ± 0.67
Legend: TI = Test Item, RI = Reference Item								

Tab. 7.14: Callus opacity -in the semiquantitative radiologic evaluation

Group	Measured Parameter: Callus Opacity							
	0w	3w	4w	5w	6w	7w	8w	9w
TI	x	0.75 ± 0.42	1 ± 0	1.08 ± 0.21	1.25 ± 0.42	1.5 ± 0.55	1.25 ± 0.27	1.33 ± 0.41
RI	x	0.83 ± 0.26	1.17 ± 0.41	1.33 ± 0.52	1.42 ± 0.49	1.5 ± 0.55	2 ± 0.63	1.67 ± 0.41
Legend: TI = Test Item, RI = Reference Item								

Tab. 7.15: Bone activation: callus around screw tips -in the semiquantitative radiologic evaluation

Group	Measured Parameter: Bone Activation							
	0w	3w	4w	5w	6w	7w	8w	9w
TI	x	1.75 ± 0.53	3.08 ± 0.86	3.67 ± 1.03	2.83 ± 0.68	3.01 ± 0.8	2.75 ± 0.76	2.67 ± 0.52
RI	x	0.75 ± 0.76	1.5 ± 0.9	2.1 ± 1.28	1.67 ± 0.82	1.75 ± 0.61	1.92 ± 1.02	1.92 ± 0.74
Legend: TI = Test Item, RI = Reference Item								

Tab. 7.16: Quantitative radiologic evaluation: Mean callus area [cm²] for every sheep (84.01-84.14) of all three projections over 9 weeks: anteroposterior (0°) and two angled planes: anterolateral (275°) and posterolateral (265°).

Animal	Mean CallusArea [cm2]							
	0w	3w	4w	5w	6w	7w	8w	9w
84.01	NA	2.384	4.643	5.267	5.399	6.103	6.12	5.845
84.02	NA	2.466	4.606	5.956	8.043	8.682	9.153	8.54
84.03	NA	0.163	0.577	0.731	1.34	1.451	1.916	1.711
84.05	NA	1.538	3.296	4.047	4.77	5.476	5.341	5.037
84.06	NA	0.098	1.65	2.584	3.464	4.303	4.986	4.778
84.07	NA	1.345	3.45	4.955	7.267	6.629	6.747	5.616
84.08	NA	0.718	1.931	2.697	3.978	3.687	4.075	4.402
84.09	NA	0.98	2.567	4.515	6.136	8.536	6.43	6.432
84.10	NA	3.225	5.419	7.25	8.421	9.365	9.202	7.738
84.11	NA	0.858	2.325	4.577	5.511	6.349	6.497	7.482
84.12	NA	2.081	3.366	5.18	6.433	5.975	7.832	6.926
84.13	NA	1.365	2.051	3.511	4.716	5.13	4.811	5.321

Tab. 7.17: Quantitative radiologic evaluation: Mean callus area [cm²] of all three projections over 9 weeks: anteroposterior (0°) and two angled planes: anterolateral (275°) and posterolateral (265°).

Group	Measured Parameter: Mean Callus Area in all three Projections							
	0w	3w	4w	5w	6w	7w	8w	9w
TI	NA	1.39 ± 0.76	2.95 ± 0.98	4.45 ± 1.11	6.01 ± 1.53	6.54 ± 1.63	6.66 ± 1.52	6.27 ± 1.24
RI	NA	1.48 ± 1.05	3.03 ± 1.64	4.09 ± 2.03	4.90 ± 2.10	5.41 ± 2.44	5.53 ± 2.24	5.37 ± 2.03
Legend: TI = Test Item, RI = Reference Item								

Tab. 7.18: Quantitative radiologic evaluation: Mean callus area in ap (anteroposterior, 0°) projection over 9 weeks.

Group	Measured Parameter: Mean Callus Area in AP Projection							
	0w	3w	4w	5w	6w	7w	8w	9w
TI	NA	0.72 ± 0.45	1.36 ± 0.51	2.15 ± 0.51	2.95 ± 0.81	2.85 ± 0.50	2.92 ± 0.67	2.97 ± 0.55
RI	NA	0.52 ± 0.40	1.18 ± 0.75	1.55 ± 0.93	1.99 ± 1.04	2.30 ± 1.33	2.38 ± 1.18	2.28 ± 1.00
Legend: TI = Test Item, RI = Reference Item								

Tab. 7.19: Quantitative radiologic evaluation: Mean callus area in anterolateral (275°) projection over 9 weeks.

Group	Measured Parameter: Mean Callus Area in anterolateral Projection							
	0w	3w	4w	5w	6w	7w	8w	9w
TI	NA	0.21 ± 0.15	0.62 ± 0.40	1.00 ± 0.48	1.38 ± 0.47	1.71 ± 0.69	1.61 ± 0.82	1.57 ± 0.83
RI	NA	0.24 ± 0.20	0.61 ± 0.52	0.87 ± 0.65	1.24 ± 0.76	1.09 ± 0.82	1.19 ± 0.84	1.17 ± 0.84
Legend: TI = Test Item, RI = Reference Item								

Tab. 7.20: Quantitative radiologic evaluation: Mean callus area in posterolateral (265°) projection over 9 weeks.

Group	Measured Parameter: Mean Callus Area in posterolateral Projection							
	0w	3w	4w	5w	6w	7w	8w	9w
TI	NA	0.46 ± 0.30	0.97 ± 0.48	1.30 ± 0.46	1.68 ± 0.72	1.99 ± 0.88	2.13 ± 0.64	1.73 ± 0.62
RI	NA	0.72 ± 0.54	1.24 ± 0.57	1.67 ± 0.66	1.67 ± 0.61	2.02 ± 0.62	1.95 ± 0.65	1.92 ± 0.47
Legend: TI = Test Item, RI = Reference Item								

Tab. 7.21: Biomechanical results for TI and RI: Peak torque, apparent stiffness, yiel point, energy to failure and rotation to failure.

Group	Measured Parameter [%of contr.]				
	Peak Torque	App. Stiffness	Yiel Point	Energy to Failure	Rotation to Failure
TI	85.2 ± 13.4	91.1 ± 13.0	64.2 ± 27.8	47.2 ± 16.2	71.4 ± 8.7
RI	54.9 ± 11.3	89.9 ± 8.4	63.8 ± 25.9	43.0 ± 10.8	69.3 ± 7.9
Legend: RI = Reference Item, TI = Test Item					

Tab. 7.22: Histomorphometry of total section including measurement of old bone, new bone and non-bone

Group	Measured Parameter		
	Old bone	New bone	Non-bone
TI	26.86 ± 2.77	34.02 ± 2.94	39.12 ± 3.64
RI	30.28 ± 3.11	30.61 ± 3.18	39.12 ± 3.22
Legend: RI = Reference Item, TI = Test Item			

Tab. 7.23: Histomorphometry of sectoral section including measurement of callus endosteal, callus at cis cortex and callus at trans cortex.

Group	Measured Parameter		
	Callus endosteal	Callus cis	Callus trans
TI	43.69 ± 7.55	12.42 ± 4.00	43.90 ± 10.15
RI	31.30 ± 6.47	15.67 ± 7.69	53.04 ± 11.55
Legend: RI = Reference Item, TI = Test Item			

Tab. 7.24: Fluorescence evaluation inclunding amount measurements of calcein green, xylenol orange and oxytetracycline

Group	Measured Parameter		
	Calcein green	xylenol orange	oxytetracycline
TI	4.55 ± 1.72	1.38 ± 1.11	5.62 ± 3.08
RI	3.69 ± 2.18	2.1 ± 1.46	3.79 ± 0.7
Legend: RI = Reference Item, TI = Test Item			

Tab. 7.25: Results of thin section evaluation for screw hole and defect area at cis cortex (light grey labeled animals TI group).

	Evaluation:	Cis cortex											
	Test item:	VFLS Variable Fixation Locking Screw											
	Reference Item:	Locking Screw Synthes											
		Test item						**Reference Item**					
	Animal ID	84.02 TL	84.06 TL	84.07 TR	84.09 TR	84.12 TR	84.13 TL	84.01 TR	84.03 TR	84.05 TR	84.08 TL	84.10 TL	84.11 TL
Biocompatibility	**1. Inflammation**												
	Polymorphonuclear	0	0	0	0	0	0	0	0	0	0	0	0
	Eosinophils	0	0	0	0	0	0	0	0	0	0	0	0
	Lymphocytes	0	0	0	1	0	1	0	0	0	0	0	0
	Plasma cells	0	0	0	0	0	0	0	0	0	0	0	0
	Macrophages	3	3	3	2	2	2	2	1	2	1	2	1
	Giant cells	1	2	1	1	1	1	0	0	0	0	0	0
	Necrosis/ osteolysis	0	0	0	0	0	0	0	0	0	0	0	0
	SUB-TOTAL	4	5	4	4	3	4	2	1	2	1	2	1
	SUB-TOTAL (x2)	8	10	8	8	6	8	4	2	4	2	4	2
	2. Tissue response												
	Neovascularisation	2	2	1	1	1	1	0	1	0	0	0	0
	Fibrosis	2	2	1	1	1	1	0	1	0	0	0	0
	Fatty infiltrate	1	1	1	0	1	1	0	0	0	0	0	0
	F.2 SUB-TOTAL	5	5	3	2	3	3	0	2	0	0	0	0
	TOTAL (1.+2.)	13	15	11	10	9	11	4	4	4	2	4	2
	GROUP TOTAL	69						20					
	Average (Ø)	11,50						3,33					
	Ø TI - Ø RI [1]	8,17											
additional observations	Traumatic necrosis	0	0	0	0	0	0	0	0	0	0	0	0
	Foreign debris (*: metallosis; "granulated, finely stippled material free and cell associated)	3" *	3"	3" *	3" *	3" *	3" *	3*	3*	3*	3*	3*	3*
Bone remodeling	Osteoclasts	2	2	1	0	1	1	1	1	1	1	1	1
	Bone activity	S	S	S	S	S	S	F	F	S	S	S	S
	Defect unity (thick section)	4	4	4	4	4	4	4	4	4	4	4	4

[1] Used to determine irritant ranking shown below as the conclusion. A negative difference is recorded as zero.

Conclusion: Under the conditions of this study, the Test Item was considered to demonstrate the following:

___ minimal or no reaction (0.0 up to 2.9);

_x_ slight reaction (3.0 upt to 8.9);

___ moderate reaction (9.0 upt to 15.0);

___ severe reaction (>15.1)

to the tissue as compared to the Reference Item.

Tab. 7.26: Results of thin section evaluation for screw hole and defect area at trans cortex (light grey labeled animals TI group).

	Evaluation:	Trans cortex											
	Test item:	VFLS Variable Fixation Locking Screw											
	Reference Item:	Locking Screw Synthes											
		Test item						**Reference Item**					
	Animal ID	84.02 TL	84.06 TL	84.07 TR	84.09 TR	84.12 TR	84.13 TL	84.01 TR	84.03 TR	84.05 TR	84.08 TL	84.10 TL	84.11 TL
Biocompatibility	**1. Inflammation**												
	Polymorphonuclear	0	0	0	0	0	0	0	0	0	0	0	0
	Eosinophils	0	0	0	0	0	0	0	0	0	0	0	0
	Lymphocytes	0	0	0	0	0	0	0	0	0	0	0	0
	Plasma cells	0	0	0	0	0	0	0	0	0	0	0	0
	Macrophages	1	2	1	2	2	2	2	0	0	0	0	0
	Giant cells	0	2	0	1	0	1	1	0	0	0	0	0
	Necrosis/ osteolysis	0	0	0	0	0	0	0	0	0	0	0	0
	SUB-TOTAL	1	4	1	3	2	3	3	0	0	0	0	0
	SUB-TOTAL (x2)	2	8	2	6	4	6	6	0	0	0	0	0
	2. Tissue response												
	Neovascularisation	1	1	0	1	1	1	1	0	0	0	0	0
	Fibrosis	1	1	0	1	1	1	1	0	0	0	0	0
	Fatty infiltrate	0	0	0	0	0	0	0	0	0	0	0	0
	F.2 SUB-TOTAL	2	2	0	2	2	2	2	0	0	0	0	0
	TOTAL (1.+2.)	4	10	2	8	6	8	8	0	0	0	0	0
	GROUP TOTAL	38						8					
	Average (Ø)	6,33						4,33					
	Ø TI - Ø RI [1]	2,00											
additional observations	Traumatic necrosis	0	0	0	0	0	0	0	0	0	0	0	0
	Foreign debris (*: metallosis; "granulated, finely stippled material free and cell associated)	3"	3"	3"	3"	3"	3"	3*	0	0	3*	3*	0
Bone remodelling	Osteoclasts	1	2	1	2	1	1	1	1	1	1	1	1
	Bone activity	F	S	S	S	S	S	F	S	S	F	S	S
	Defect unity (thick section)	4	1	4	3	4	4	4	0	4	3	4	4

[1] Used to determine irritant ranking shown below as the conclusion. A negative difference is recorded as zero.

Conclusion: Under the conditions of this study, the Test Item was considered to demonstrate the following:

__x__ minimal or no reaction (0.0 up to 2.9);

___ slight reaction (3.0 upt to 8.9);

___ moderate reaction (9.0 upt to 15.0);

___ severe reaction (>15.1)

to the tissue as compared to the Reference Item.

Tab. 7.27: Lymph nodes score results of structure changes, nonlocal cells, presence foreign material, amount of extracellular foreign material and amount of cells with intracellular foreign material.

Group	Animal ID	Side	Structure changes				Nonlocal cells (inflammatory/hypersensitivity cells)				Presence foreign material				Amount of extracellular foreign material				Amount of cells with intracellular foreign material			
			Inn popliteal		Inn inguinales		Inn popliteal		Inn inguinales		Inn popliteal		Inn inguinales		Inn popliteal		Inn inguinales		Inn popliteal		Inn inguinales	
			treated	non-treated	treated	non-treated	treated	non-treated	treated	non-treated	treated	non-treated	treated	non-treated	treated	non-treated	treated	non-treated	treated	non-treated	treated	non-treated
TI	84.02	le	1		1		1		1		0***		0***		0		0		0		0	
		ri		1		1		0		0		0***		0***		0		0		0		0
	84.06	le	0		1		0		1		0*		0*		0		0		0		0	
		ri		1		1		0		1		0*		0*		0		0		0		0
	84.07	le		0		1		1		1		0*		0*		0		0		0		0
		ri	0		1		1		1		0***		0***		0		0		0		0	
	84.09	le		0		1		1		1		0*		0*		0		0		0		0
		ri	1		1		1		1		0*		0*		0		0		0		0	
	84.12	le		0		1		1		1		0*		0*		0		0		0		0
		ri	0		1		1		0		0**		0**		0		0		0		0	
	84.13	le	1		0		1		1		0***		0***		0		0		0		0	
		ri		0		0		0		1		0*		0*		0		0		0		0
TI	Mean score		0.5	0.33	0.83	0.83	0.83	0.5	0.83	0.83	0	0	0	0	0	0	0	0	0	0	0	0
RI	84.01	le		1		1		1		1		0**		0**		0		0		0		0
		ri	1		1		1		0		0*		0*		0		0		0		0	
	84.03	le		0		0		1		0		0*		0*		0		0		0		0
		ri	0		0		1		1		0		0*		0		0		0		0	
	84.05	le		0		0		1		1		0***		0***		0		0		0		0
		ri	0		0		1		0		0*		0**		0		0		0		0	
	84.08	le	0		0		0		0		0*		0*		0		0		0		0	
		ri		0		0		0		1		0*		0*		0		0		0		0
	84.10	le	0		0		0		1		0*		0**		0		0		0		0	
		ri		1		0		1		1		0***		0*		0		0		0		0
	84.11	le	0		0		1		1		0*		0*		0		0		0		0	
		ri		1		0		1		1		0		0*		0		0		0		0
RI	Mean score		0.17	0.5	0.17	0.17	0.67	0.83	0.67	0.83	0	0	0	0	0	0	0	0	0	0	0	0

7.2 Figures

7.2.1 Material and Methods

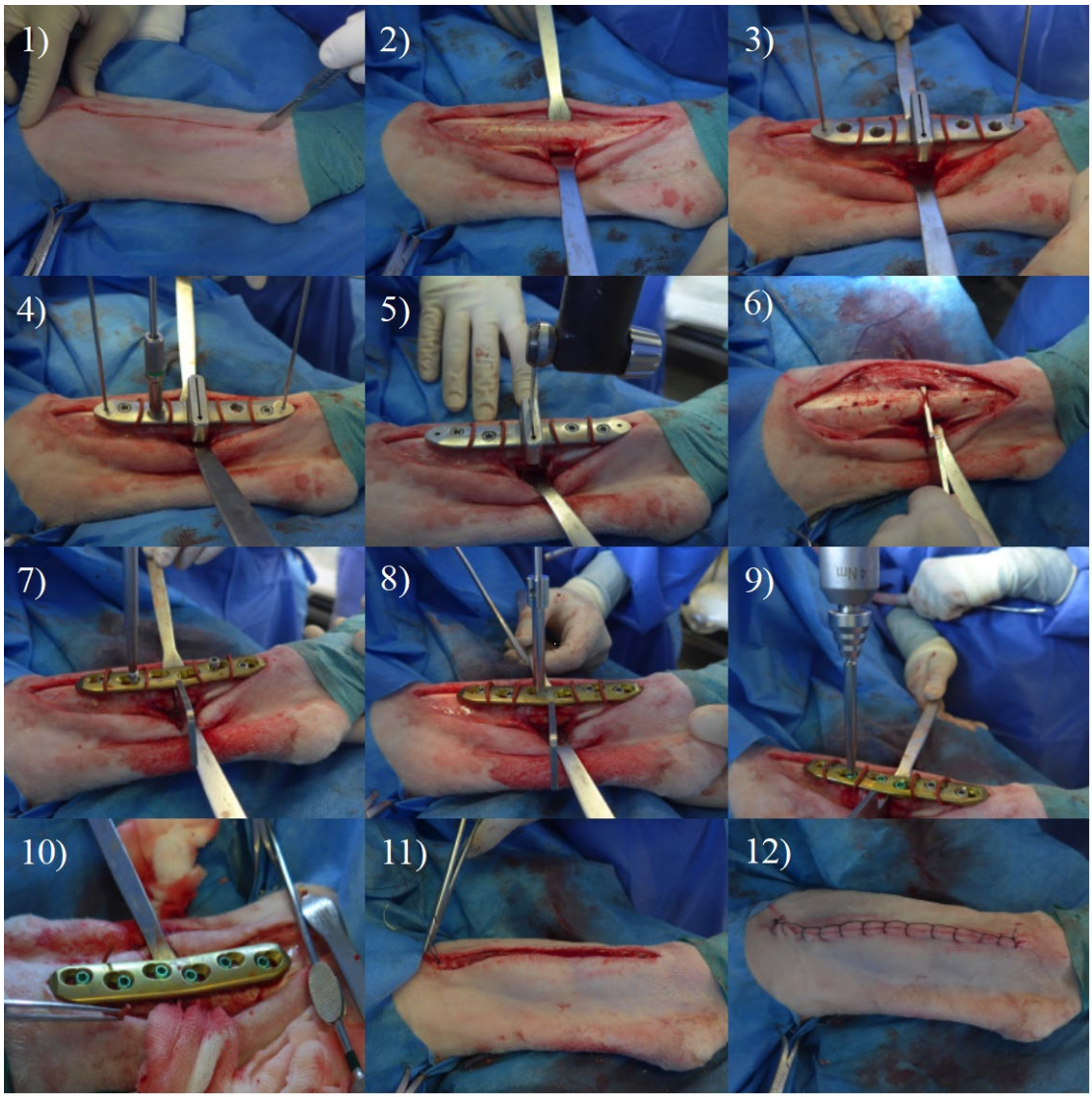

Fig. 7.1: Surgical procedure step by step. Detailed explanation for 1) till 12) see chapter 3.4.1 surgical procedure.

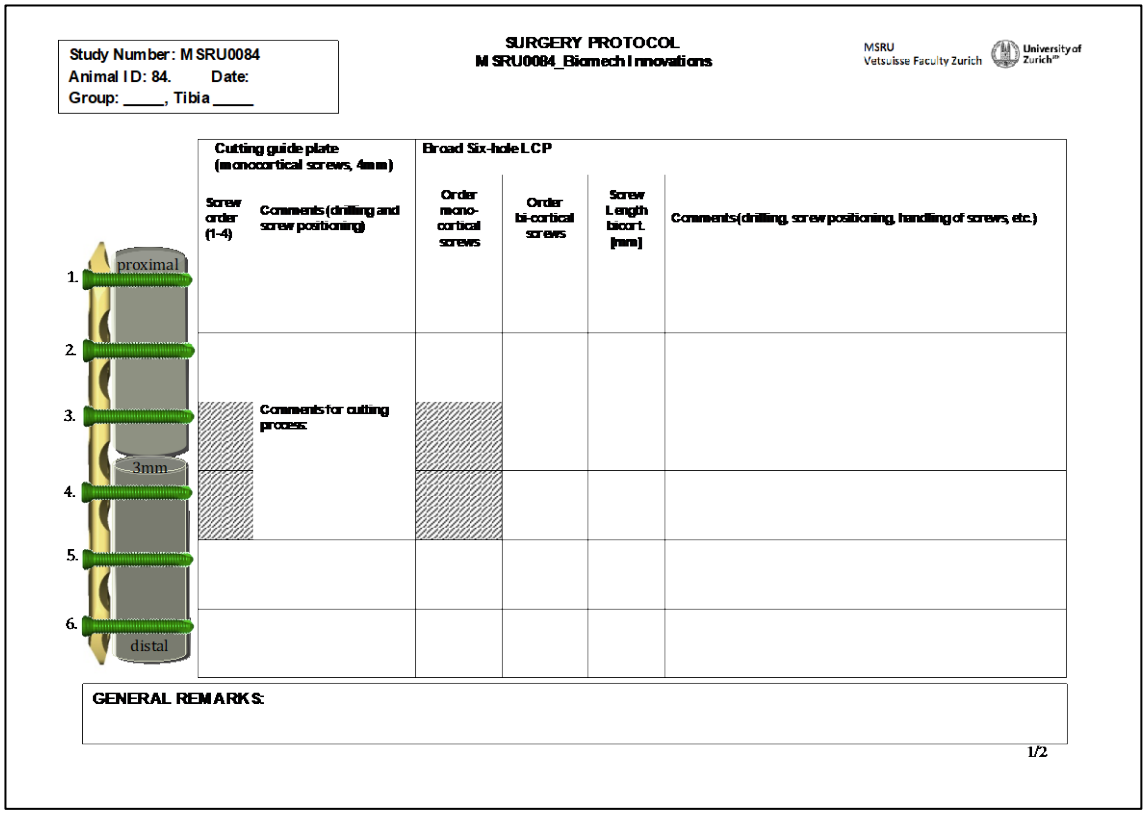

Study Number: MSRU0084
Animal ID: 84. Date:
Group: _____, Tibia _____

SURGERY PROTOCOL
MSRU0084_Biomech Innovations

MSRU Vetsuisse Faculty Zurich — University of Zurich

	Cutting guide plate (monocortical screws, 4mm)		Broad Six-hole LCP			
	Screw order (1-4)	Comments (drilling and screw positioning)	Order mono-cortical screws	Order bi-cortical screws	Screw Length bicort. [mm]	Comments (drilling, screw positioning, handling of screws, etc.)
1.						
2.						
3.		Comments for cutting process:				
4.						
5.						
6.						

proximal
3mm
distal

GENERAL REMARKS:

1/2

Fig. 7.2: Surgery Protocol page 1: For screw 1-6 the screw order, screw length and comments have been noted.

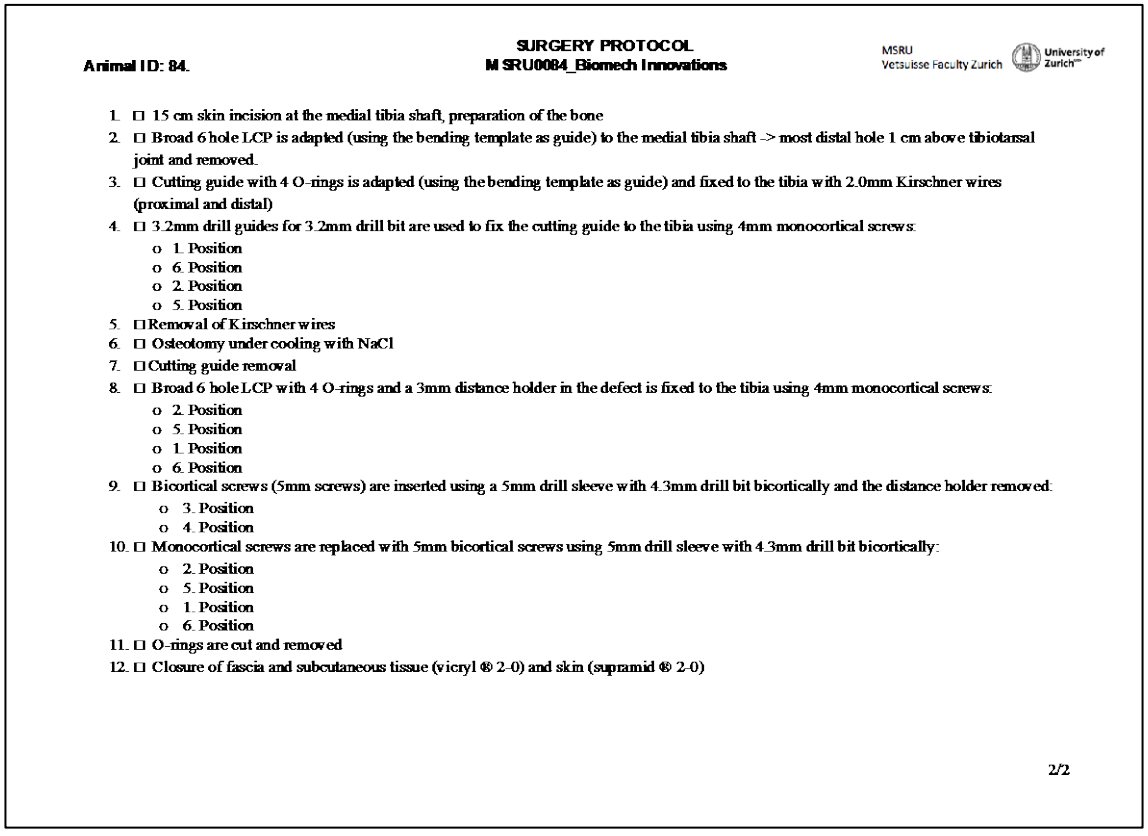

Animal ID: 84.

SURGERY PROTOCOL
MSRU0084_Biomech Innovations

MSRU Vetsuisse Faculty Zurich — University of Zurich

1. ☐ 15 cm skin incision at the medial tibia shaft, preparation of the bone
2. ☐ Broad 6 hole LCP is adapted (using the bending template as guide) to the medial tibia shaft -> most distal hole 1 cm above tibiotarsal joint and removed.
3. ☐ Cutting guide with 4 O-rings is adapted (using the bending template as guide) and fixed to the tibia with 2.0mm Kirschner wires (proximal and distal)
4. ☐ 3.2mm drill guides for 3.2mm drill bit are used to fix the cutting guide to the tibia using 4mm monocortical screws:
   - o 1. Position
   - o 6. Position
   - o 2. Position
   - o 5. Position
5. ☐ Removal of Kirschner wires
6. ☐ Osteotomy under cooling with NaCl
7. ☐ Cutting guide removal
8. ☐ Broad 6 hole LCP with 4 O-rings and a 3mm distance holder in the defect is fixed to the tibia using 4mm monocortical screws:
   - o 2. Position
   - o 5. Position
   - o 1. Position
   - o 6. Position
9. ☐ Bicortical screws (5mm screws) are inserted using a 5mm drill sleeve with 4.3mm drill bit bicortically and the distance holder removed:
   - o 3. Position
   - o 4. Position
10. ☐ Monocortical screws are replaced with 5mm bicortical screws using 5mm drill sleeve with 4.3mm drill bit bicortically:
    - o 2. Position
    - o 5. Position
    - o 1. Position
    - o 6. Position
11. ☐ O-rings are cut and removed
12. ☐ Closure of fascia and subcutaneous tissue (vicryl ® 2-0) and skin (supramid ® 2-0)

2/2

Fig. 7.3: Surgery Protocol page 2: Detailed check-list for the surgery procedure.

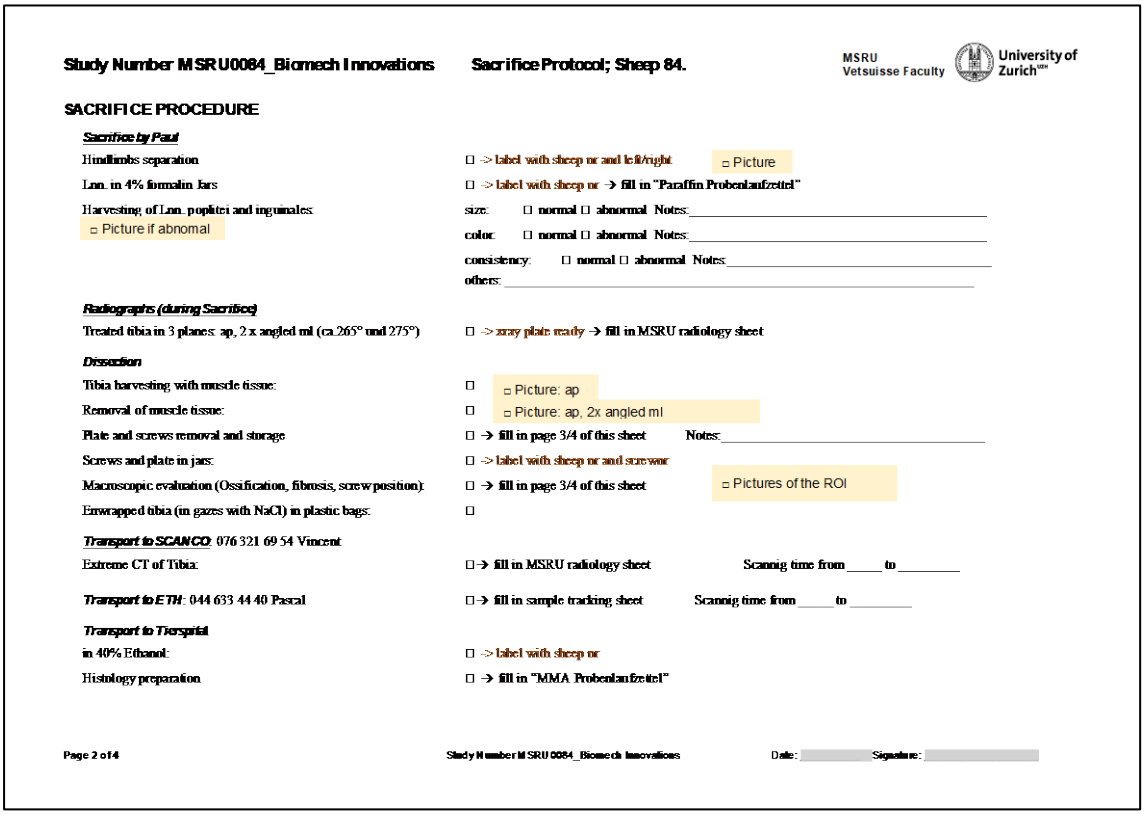

Study Number MSRU0084_Biomech Innovations **Sacrifice Protocol; Sheep 84.**

MSRU Vetsuisse Faculty — University of Zurich

SACRIFICE PROCEDURE

Sacrifice by Paul

Hindlimbs separation	☐ -> label with sheep nr and left/right ▫ Picture
Lnn. in 4% formalin Jars	☐ -> label with sheep nr → fill in "Paraffin Probenlaufzettel"
Harvesting of Lnn. poplitei and inguinales: ▫ Picture if abnomal	size: ☐ normal ☐ abnormal Notes:_____
	color: ☐ normal ☐ abnormal Notes:_____
	consistency: ☐ normal ☐ abnormal Notes:_____
	others:_____

Radiographs (during Sacrifice)

Treated tibia in 3 planes: ap, 2 x angled ml (ca.265° und 275°)	☐ -> xray plate ready → fill in MSRU radiology sheet

Dissection

Tibia harvesting with muscle tissue:	☐ ▫ Picture: ap
Removal of muscle tissue:	☐ ▫ Picture: ap, 2x angled ml
Plate and screws removal and storage	☐ → fill in page 3/4 of this sheet Notes:_____
Screws and plate in jars:	☐ -> label with sheep nr and screw nr
Macroscopic evaluation (Ossification, fibrosis, screw position):	☐ → fill in page 3/4 of this sheet ▫ Pictures of the ROI
Enwrapped tibia (in gazes with NaCl) in plastic bags:	☐

Transport to SCANCO: 076 321 69 54 Vincent

Extreme CT of Tibia:	☐→ fill in MSRU radiology sheet Scannig time from _____ to _____

Transport to ETH: 044 633 44 40 Pascal

	☐→ fill in sample tracking sheet Scannig time from _____ to _____

Transport to Tierspital

in 40% Ethanol:	☐ -> label with sheep nr
Histology preparation	☐ → fill in "MMA Probenlaufzettel"

Page 2 of 4 — Study Number MSRU 0084_Biomech Innovations — Date: Signature:

Fig. 7.4: Sacrifice procedure from the beginning (slaughtering by Paul) till histology preparation

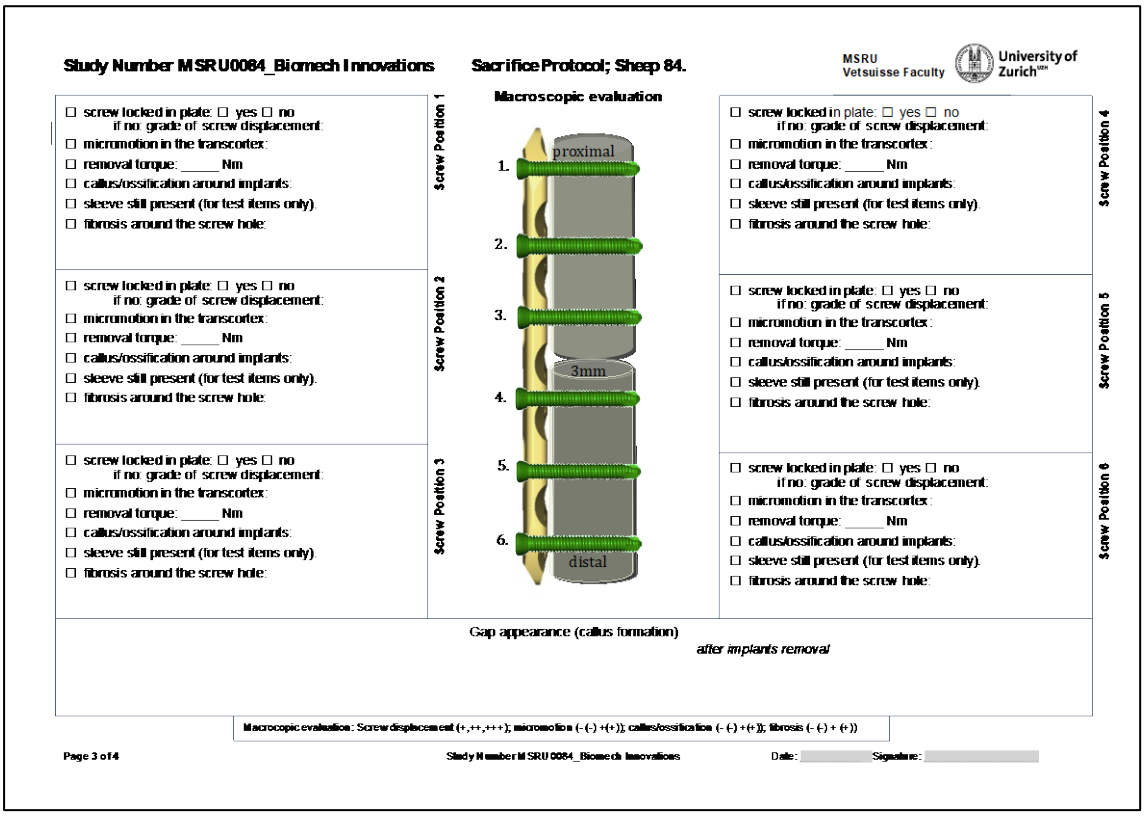

Study Number MSRU0084_Biomech Innovations **Sacrifice Protocol; Sheep 84.**

MSRU Vetsuisse Faculty — University of Zurich

Macroscopic evaluation

Screw Position 1
☐ screw locked in plate: ☐ yes ☐ no
if no: grade of screw displacement:
☐ micromotion in the transcortex:
☐ removal torque: _____ Nm
☐ callus/ossification around implants:
☐ sleeve still present (for test items only):
☐ fibrosis around the screw hole:

Screw Position 2
☐ screw locked in plate: ☐ yes ☐ no
if no: grade of screw displacement:
☐ micromotion in the transcortex:
☐ removal torque: _____ Nm
☐ callus/ossification around implants:
☐ sleeve still present (for test items only):
☐ fibrosis around the screw hole:

Screw Position 3
☐ screw locked in plate: ☐ yes ☐ no
if no: grade of screw displacement:
☐ micromotion in the transcortex:
☐ removal torque: _____ Nm
☐ callus/ossification around implants:
☐ sleeve still present (for test items only):
☐ fibrosis around the screw hole:

Screw Position 4
☐ screw locked in plate: ☐ yes ☐ no
if no: grade of screw displacement:
☐ micromotion in the transcortex:
☐ removal torque: _____ Nm
☐ callus/ossification around implants:
☐ sleeve still present (for test items only):
☐ fibrosis around the screw hole:

Screw Position 5
☐ screw locked in plate: ☐ yes ☐ no
if no: grade of screw displacement:
☐ micromotion in the transcortex:
☐ removal torque: _____ Nm
☐ callus/ossification around implants:
☐ sleeve still present (for test items only):
☐ fibrosis around the screw hole:

Screw Position 6
☐ screw locked in plate: ☐ yes ☐ no
if no: grade of screw displacement:
☐ micromotion in the transcortex:
☐ removal torque: _____ Nm
☐ callus/ossification around implants:
☐ sleeve still present (for test items only):
☐ fibrosis around the screw hole:

Gap appearance (callus formation)
after implants removal

Macrocopic evaluation: Screw displacement (+,++,+++); micromotion (-(-) +(+)); callus/ossification (-(-) +(+)); fibrosis (-(-) + (+))

Page 3 of 4 — Study Number MSRU 0084_Biomech Innovations — Date: Signature:

Fig. 7.5: Sacrifice protocol for each screw: Control of locking state, micromotion, removal torque, callus/ ossification around the implants, sleeve absence and fibrosis around screw hole. Including empty space for comments and notes.

Fig. 7.6: Radiographs in three projections, week 9. On the left: animal 84.01 (RI, right tibia) and on the right: animal 84.09 (TI, right tibia).

84.05 8w_ap 84.01 8w_cranial 84.01 8w_caudal

Fig. 7.7: Quantitative radiologic evaluation of the callus area (green line) measured with Osirix.

Fig. 7.8: Biomechanical testing at ETH: Preparation of the tibia (Picture left), potted distal part of the tibia (picture middle), set up (picture right).

7.2.2 Results

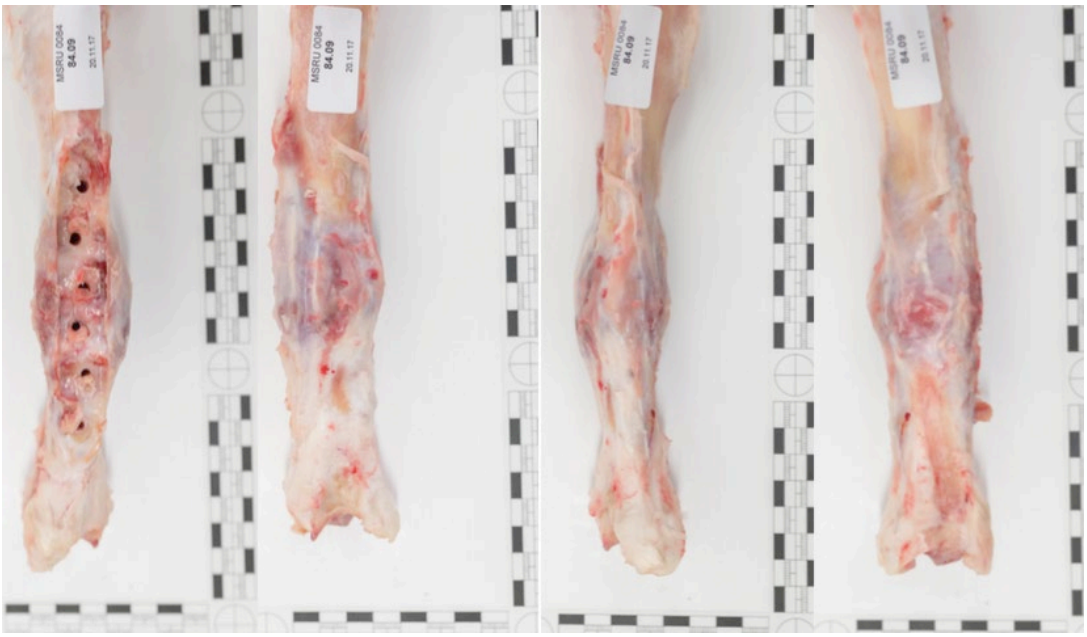

Fig. 7.9: Sacrifice pictures of a right sheep tibia (TI, animals 84.09)

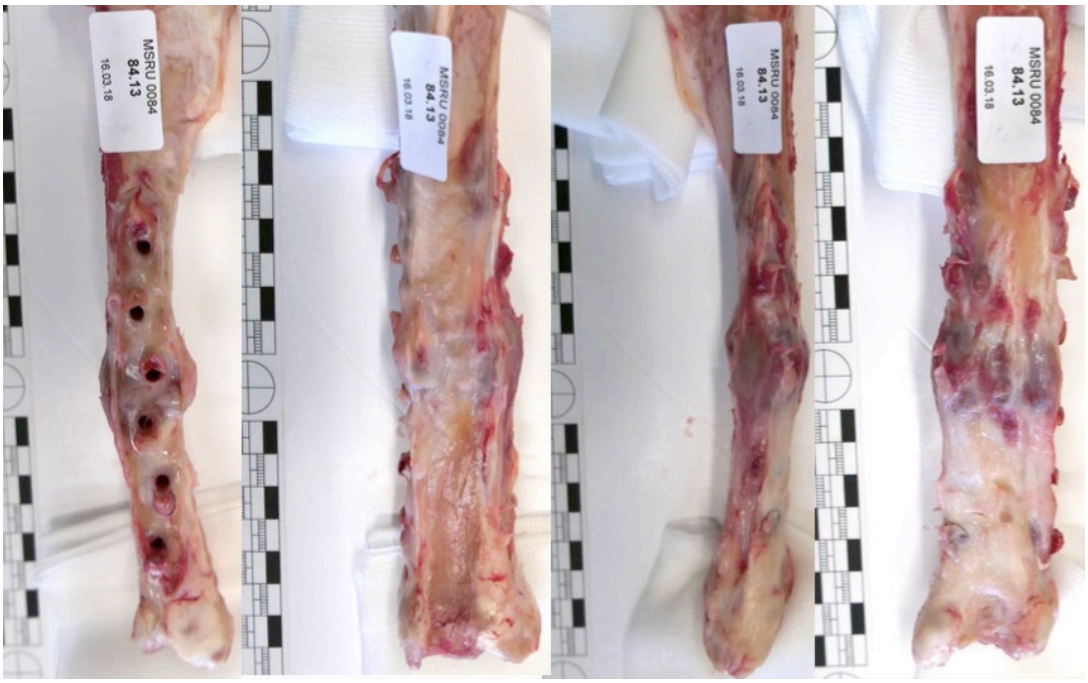

Fig. 7.10: Sacrifice pictures of a left sheep tibia (TI, animal 84.13)

Fig. 7.11: Sacrifice pictures of a right sheep tibia (RI, animal 84.05)

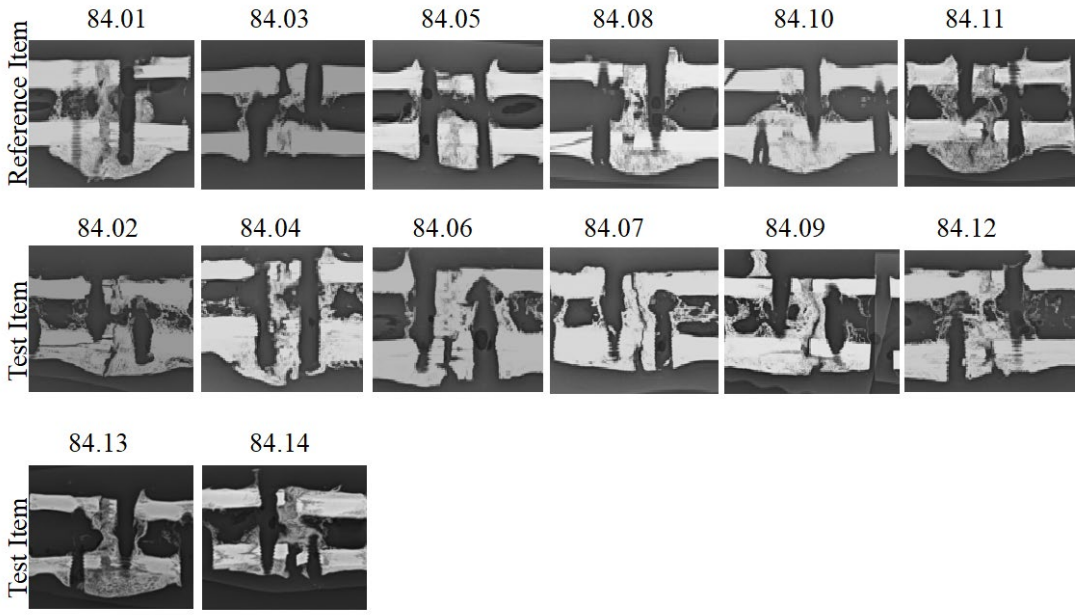

Fig. 7.12: Microradiographs of all animals

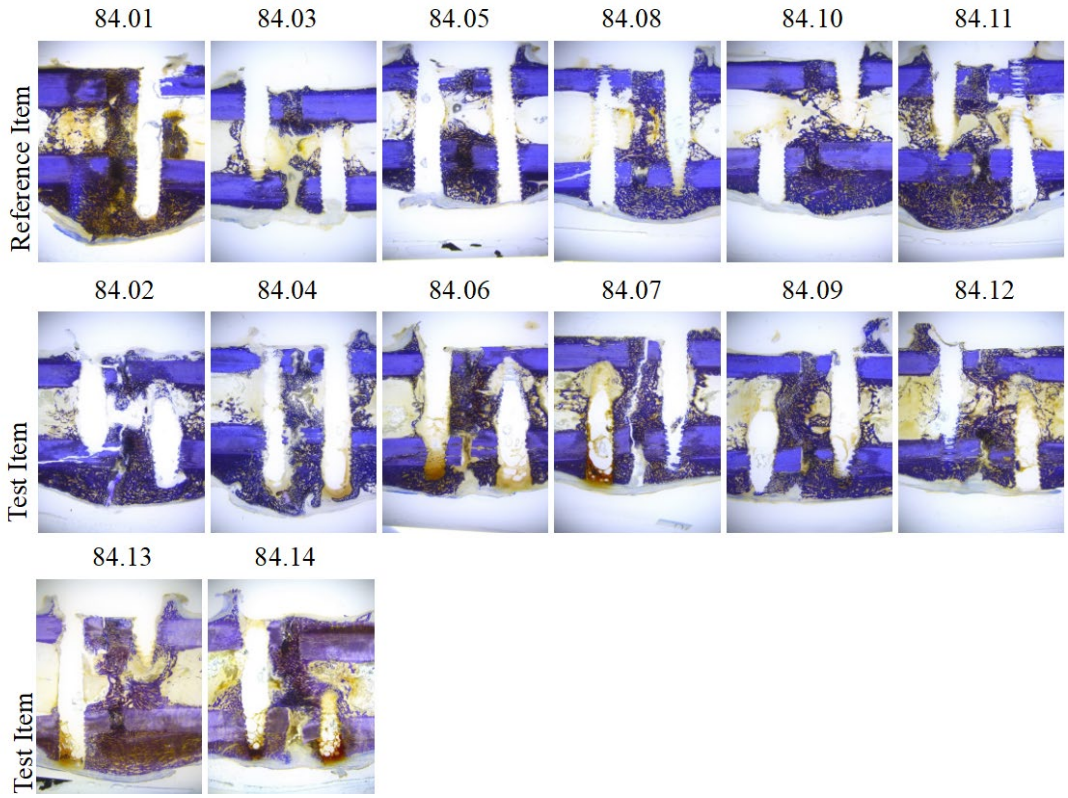

Fig. 7.13: Histology Slides Toluidineblue

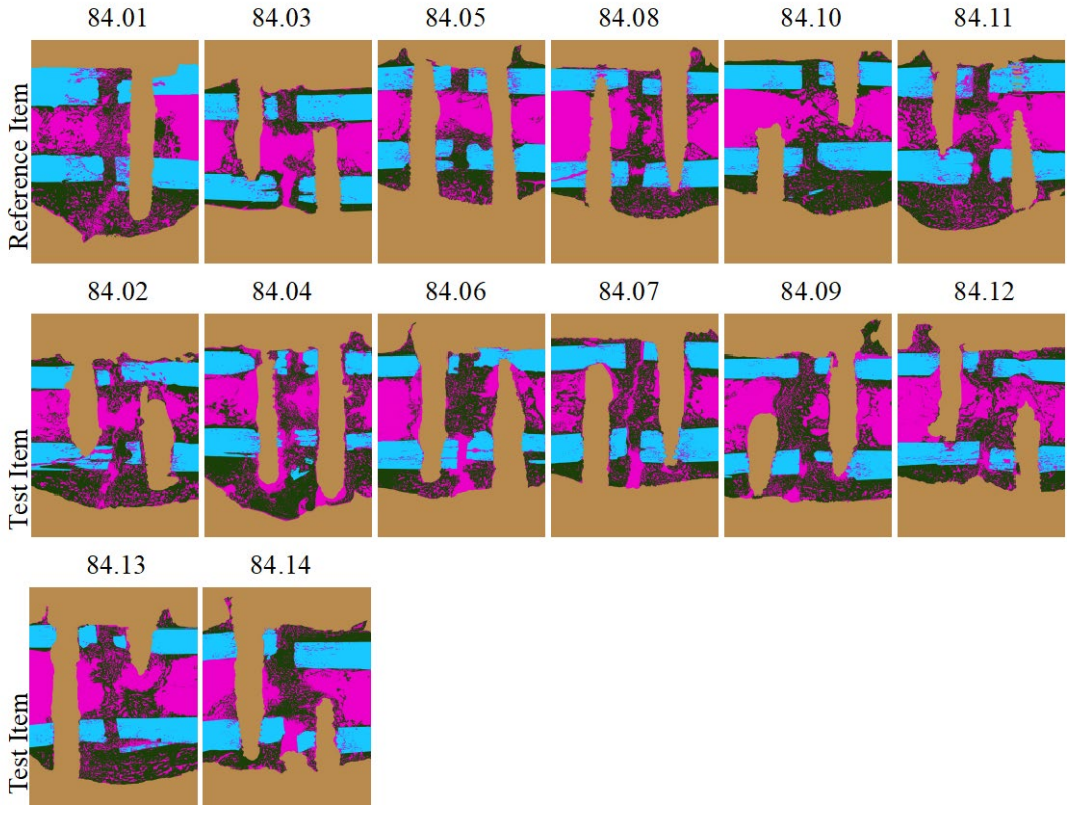

Fig. 7.14: Histomorphometry total section analysis

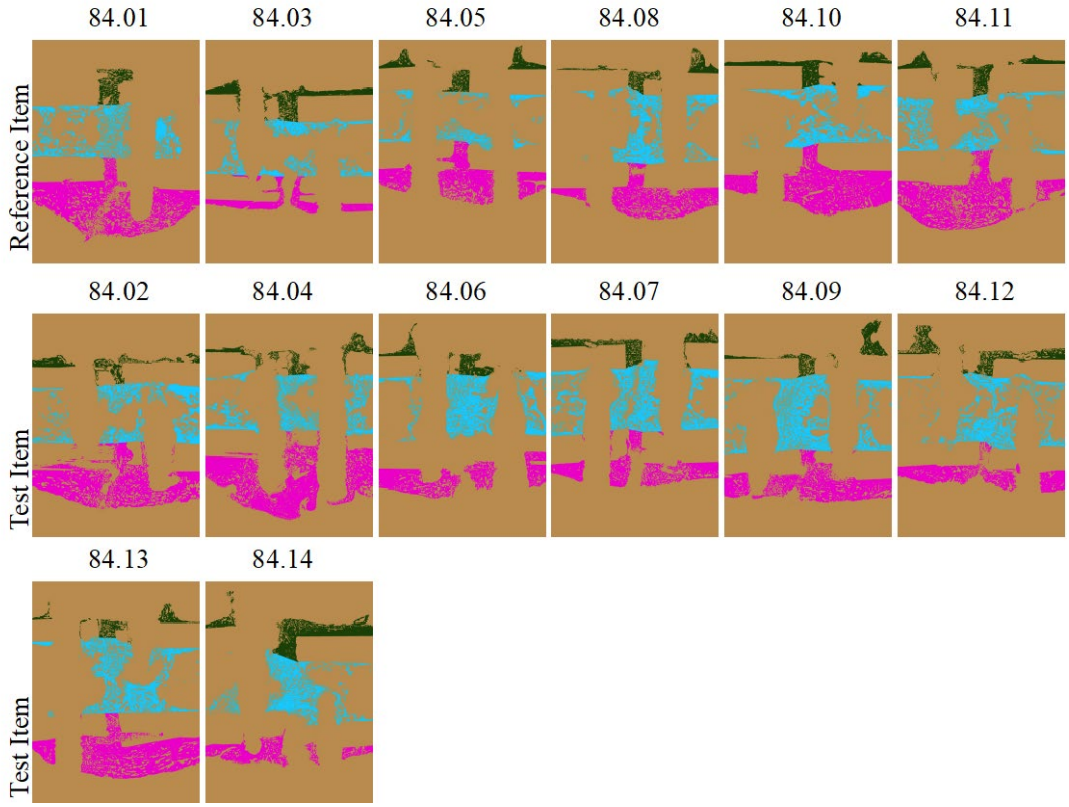

Fig. 7.15: Histomorphometry sectoral analysis

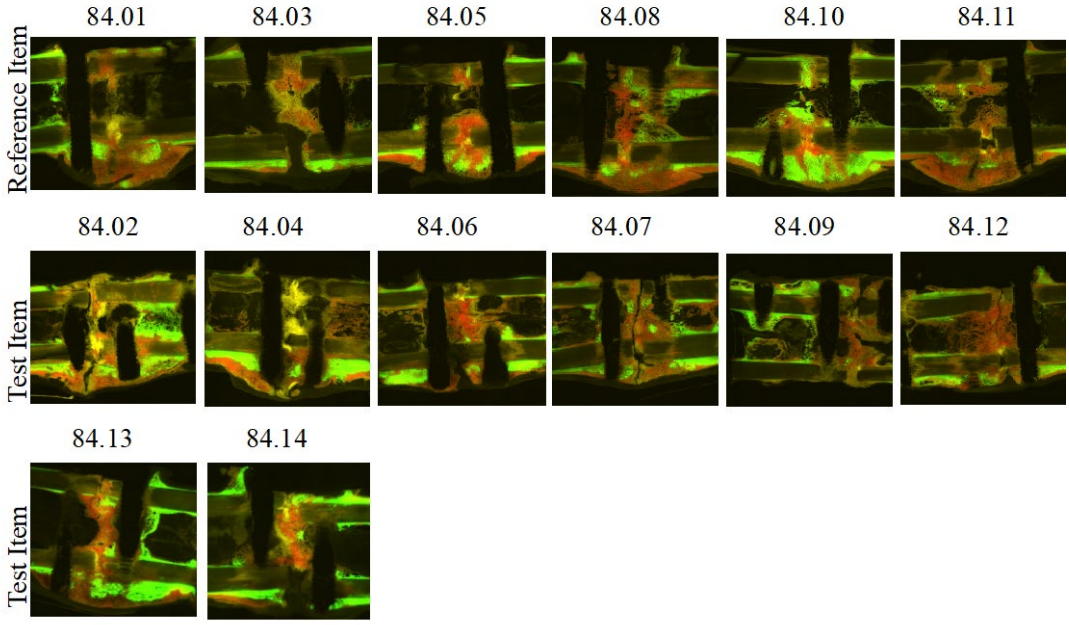

Fig. 7.16: Fluroescence overlay (calcein green, xylenol orange, oxytertracycline)

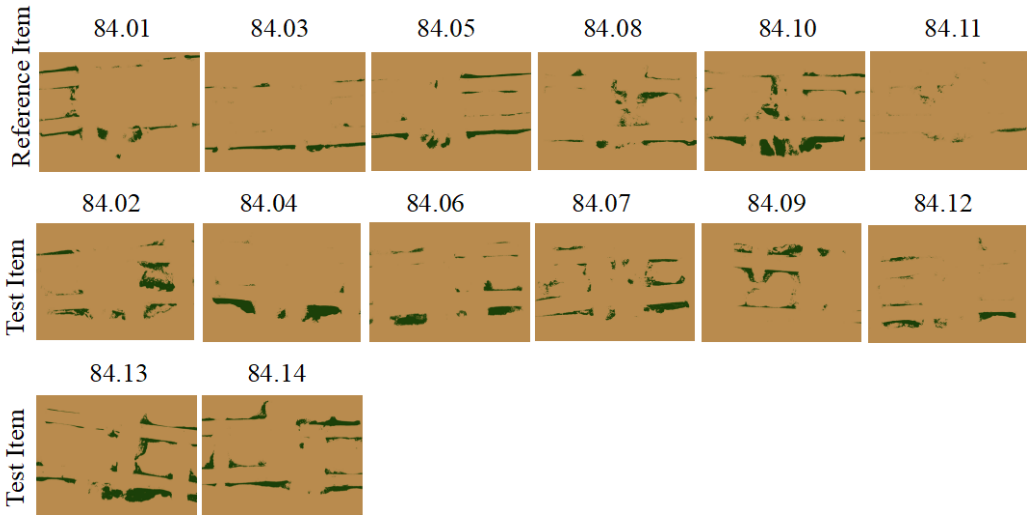

Fig. 7.17: Histomorphometry calcein green

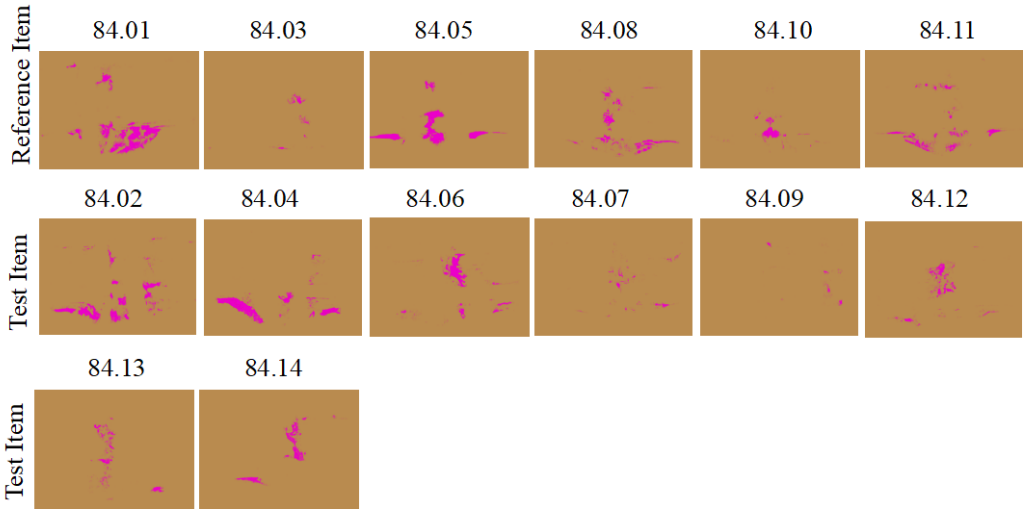

Fig. 7.18: Histomorphometry xylenol orange

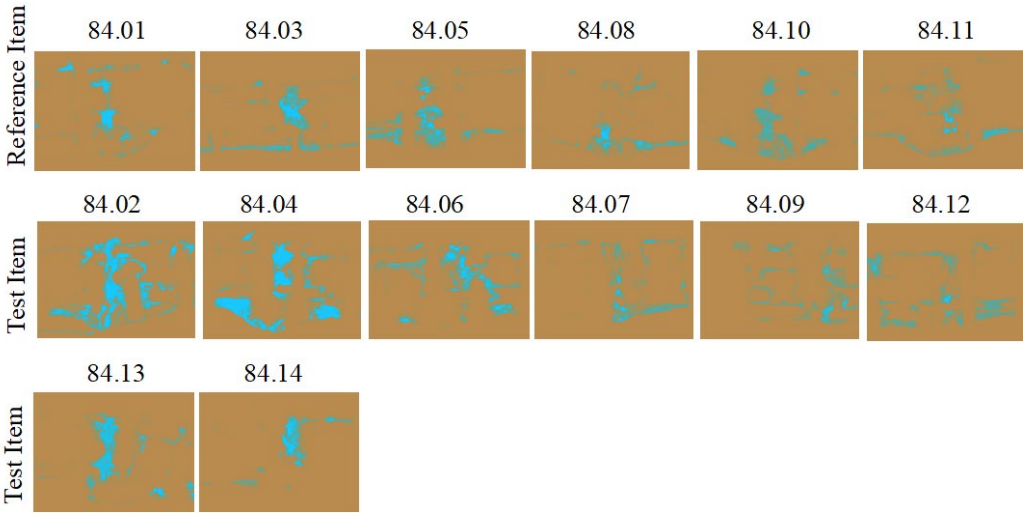

Fig. 7.19: Histomorphometry oxytetracycline

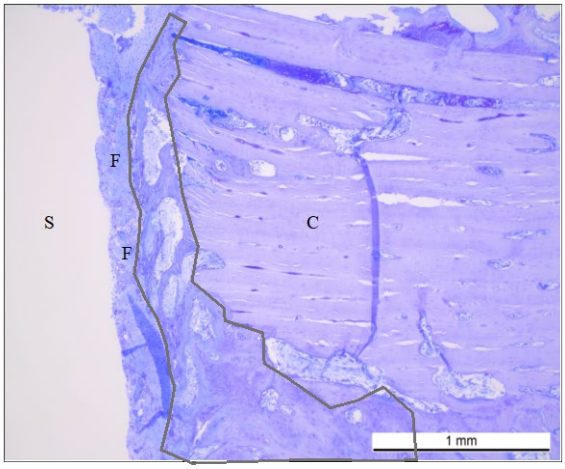

Fig. 7.20: Animal 84.02 TI, cis cortex (C) with area of resorbed sleeve, overview picture, toluidine blue staining, 45x magnification: screw hole (S) visible with fibrous tissue (F) next to newly formed bone (marked in grey), in the fibrous tissue area macrophages with residuals of sleeve material as well as giant cells detected.

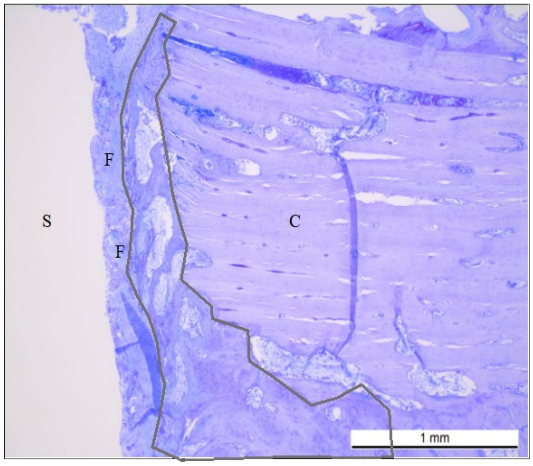

Fig. 7.21: Animal 84.10 RI, cis cortex (C) with screw hole, overview picture, toluidine blue staining 45x magnification: screw hole clearly visible (S), newly formed bone (marked in grey) no fibrosis.

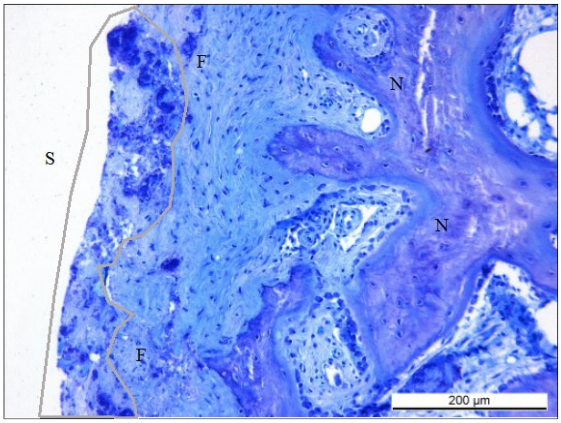

Fig. 7.22: Animal 84.02 TI, cis cortex with area of resorbed sleeve, toluidine blue staining, 100x magnification: Screw hole (S) with fibrous tissue (F), residuals of sleeve material (finely stippled) free and cell associated in macrophages (area marked in grey), newly formed bone with thick osteoid seam (N) and active osteoblasts next to the fibrous tissue.

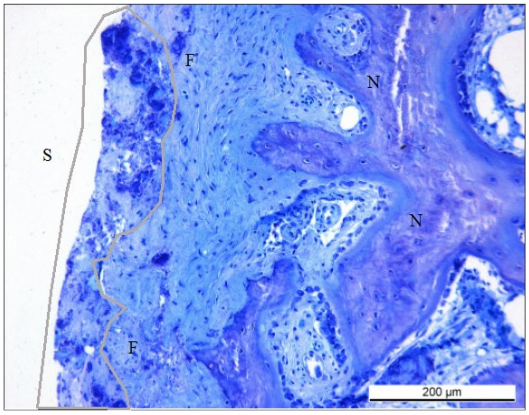

Fig. 7.23: Animal 84.02 TI, cis cortex with area of resorbed sleeve, toluidine blue staining, 200x magnification: Screw hole (S) visible with fibrous tissue (F), residuals of sleeve material (finely stippled) free (orange arrow) and cell associated in macrophages (black arrows).

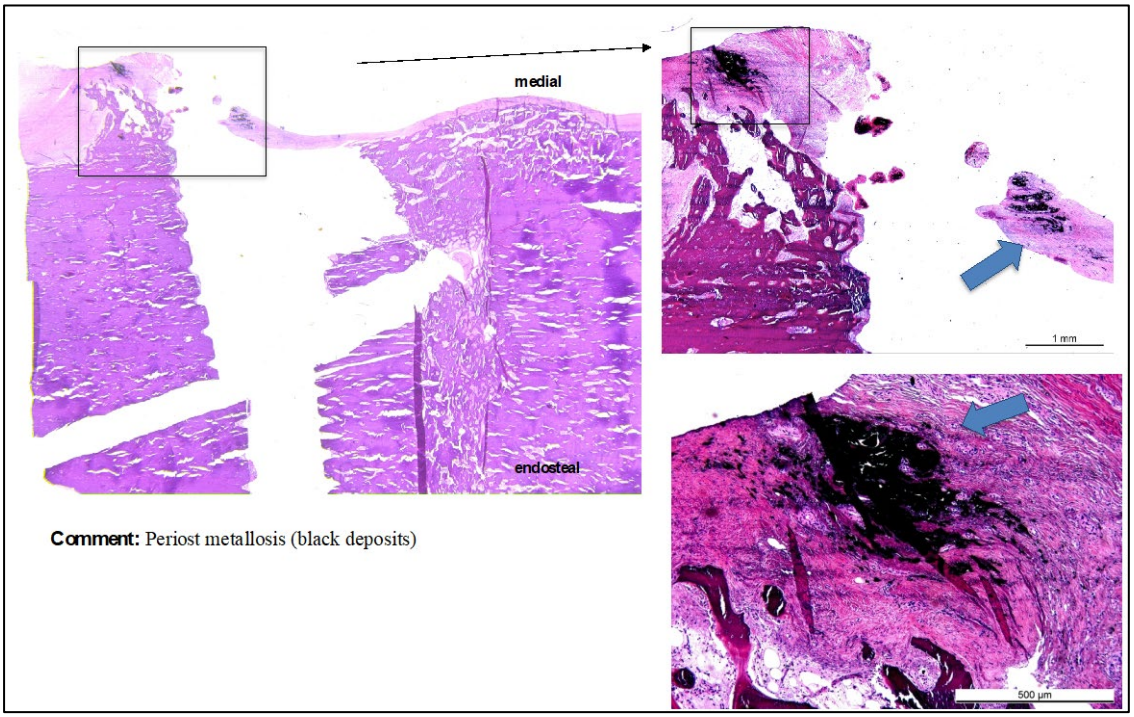

Fig. 7.24: Screw hole (RI, animal 84.01 cis/medial), example of metallosis (conglomerates of black foreign material) in soft tissue. HE staining.

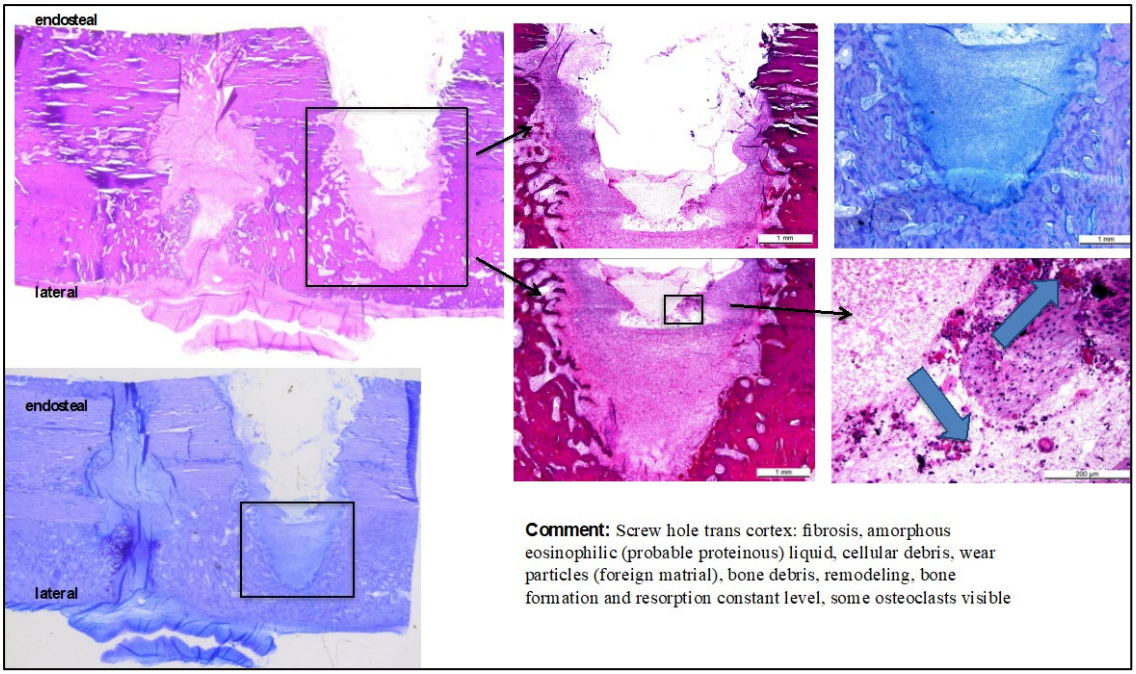

Fig. 7.25: Screw hole trans cortex (TI, animal 84.06 trans/lateral), example of some fluid accumulation, presence of foreign material (blue arrows) and fibrosis. HE staining and Toluidine blue staining.

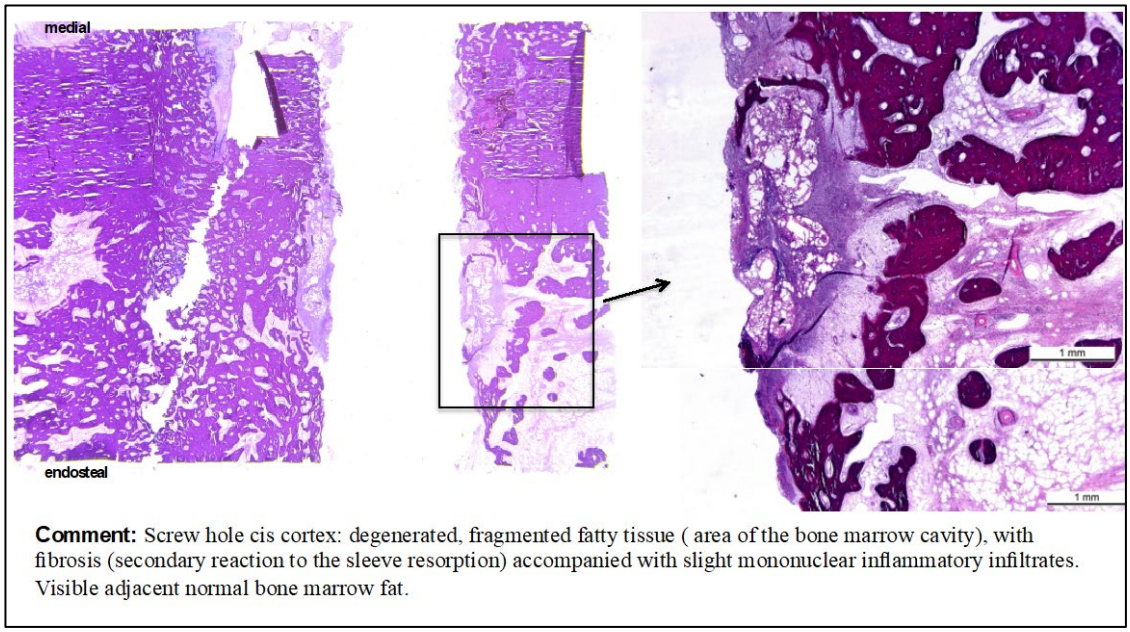

Fig. 7.26: Screw hole (TI, animal 84.07 cis/medial), example of fatty infiltrate from the bone marrow. HE staining

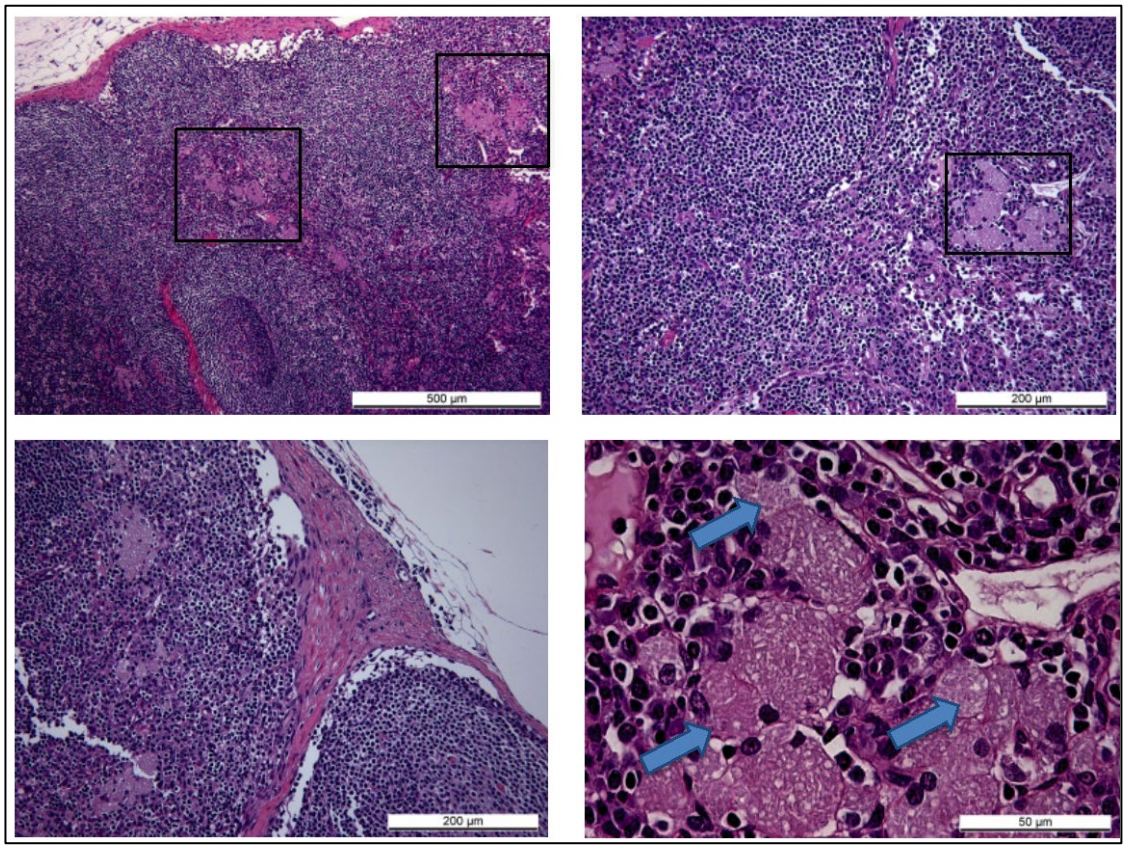

Fig. 7.27: Inguinal right lymph node, animal 84.02, TI group. Visible foamy (epitheloid-like) macrophage aggregates with brownish-beige containing small particles (1-3µm) foreign residuals (blue arrow), which does not polarize, groups located mostly along the lymp vessels within the cortex.

Danksagung

Mein grösster Dank geht an Frau **Prof. Dr. med. vet. Brigitte von Rechenberg.** Für die Möglichkeit eine Dissertation bei der MSRU schreiben zu dürfen und für die Unterstützung, wie für die spannenden und lehrreichen Diskussionsrunden danke ich ganz besonders.

Herr **Prof. Dr. Stephen Ferguson** danke ich für die Übernahme des Korreferats.

Ein grosses Dankeschön geht an **PhD Dr. med. vet. Karina Klein**. Sie hat mich immer sehr gut unterstützt und mir bei der ganzen Studie und beim Anfertigen der Dissertation geholfen. Sie war immer mit einem Lächeln anzutreffen und mit ihr hat die Arbeit sehr viel mehr Freude gemacht.

Meinem Projekt Partner **PhD Dr. med. vet. Stefano Brianza** bedanke ich mich herzlich für seine geniale Idee und für die tolle Zusammenarbeit.

Dr. med. Michael Plecko bedanke ich mich, dass er den weiten Weg von Graz nach Zürich auf sich genommen hat, um zu operieren. Mit seiner präzisen Chirurgie und mit seinem enormen Wissen hat er uns sehr bereichert. Er war immer sehr zuvorkommend und hat mit seiner positiven Art und Weise für ein gutes Arbeitsklima gesorgt.

Prof. Dr. med. vet. Mark Flückiger danke ich für die Mithilfe beim Auswerten der Radiologiebilder.

Bei all meinen Doktorandengspändlis bedanke ich mich ganz fest für die tolle Zeit, die wir im und auch außerhalb des Büros zusammen verbringen durften: **Raphael Arz, Konrad Finck, Anna Geks, Vanessa Graf, Isabel Heckel, Martina Heygen, Anna Kaczmarek, Claudia Michaelis, David Michalik, Alina Renner, Katharina Siwy, Alina Steigerwald und Christina Wiezorek**.

Ohne unsere Anästhesistin wären unsere Operationen gar nicht möglich gewesen. Deshalb geht ein grosses Dankeschön an **Dr. med. vet. Dagmar Verdino**, die immer mit Kaffee am frühen Morgen für gute Laune sorgte.

Dr. med. vet. Myrna Gunning war fast immer an meiner Seite beim Casten und Röntgen. Ebenso danke ich ihr auch für die sprachliche Unterstützung bei dieser Arbeit.

Rosita Walther danke ich für den immerwährend guten Überblick beim Sacrifice und auch für die Hilfe beim Bearbeiten der Histologieproben.
Ich danke **Aymone Lenisa** für die Unterstützung im Labor und für die sorgfältige Arbeit.

Dr. med. vet. Aga Agnieszka Karol danke ich für die spannenden Auswertungen der Dünnschnitte und Lymphknoten.

Bei **Silvana Ressegatti, Käthi Kämpf** und der **Familie Knüsel** bedanke ich mich für die Pflege und die gute Fürsorge der Schafe.

Meinen Eltern und **meinen Freunden** danke ich für die mentale Unterstützung.

Curriculum Vitae

Vorname Name	Katrin Planzer
Geburtsdatum	10.09.1991
Geburtsort	Altdorf UR
Nationalität	Schweizerin
Heimatort	Bürglen UR
8/1998 – 7/2004	Primarschule, Ettiswil LU, Schweiz
8/2004 - 6/2010	Kantonsschule Willisau LU, Schweiz
Juni 2010	Matura, Kantonsschule KSW, Willisau, Schweiz
9/2010 – 8/2011	Biologiestudium, Universität Zürich, Schweiz
9/2011 – 12/2016	Bachelor- und Masterstudium Veterinärmedizin, Universität Zürich, Schweiz
Januar 2017	Abschlussprüfung vet. med. Universität Zürich, Schweiz
6/2017 – 9/2018	Anfertigung der Dissertation unter Leitung von Prof. Dr. med. vet. Brigitte von Rechenberg am Institut für Molekulare Mechanismen bei Krankheiten der Vetsuisse-Fakultät Universität Zürich Direktor Prof. Dr. med. vet. et phil. II Michael Hottiger
1/2019 - dato	Internship, Bessy's Kleintierklinik, Regensdorf, Schweiz